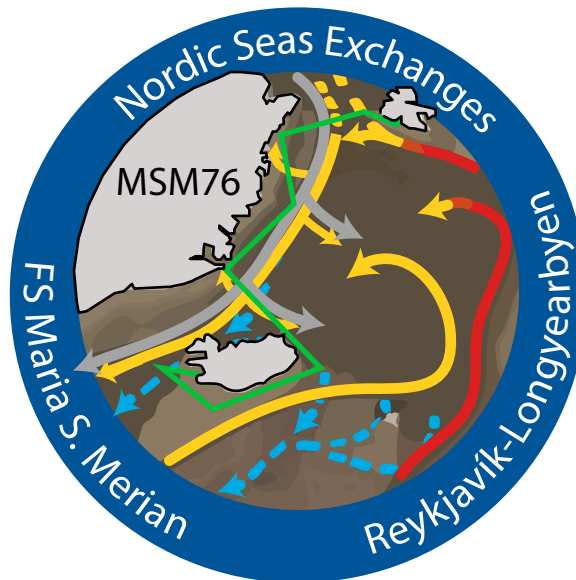


Nordic Seas Exchanges **Cruise No. MSM 76**

August 11 – September 11, 2018

Port of Sailing: Reykjavik (Iceland)
Port of Arrival: Longyearbyen (Norway)



Authors: L. von Albedyll, F. Benz, C. Ellmer, T. Kanzow,
S. Kritsotalakis, J. Lauber, A. Mubashir, M. Muchow,
A. Münchow, S. Trace-Kleeberg, E. Werner

Chief Scientist: Torsten Kanzow

Alfred-Wegener- Institut
Helmholtz-Zentrum für Polar- und Meeresforschung

1. Summary	4
2. Participants	5
3. Research Program	6
4. Narrative of the Cruise	7
5. Preliminary Results	14
5.1 Lowered CTD	14
5.1.1 System and Operation	14
5.1.2 CTD Calibration	15
5.1.3 CTD Oxygen Calibration	18
5.1.4. Sampling water for $\delta^{18}\text{O}$ -Analysis	22
5.1.5 Preliminary Results	22
5.2. Lowered Acoustic Doppler Current Profilers (LADCP)	26
5.2.1. System and Operation	26
5.2.2 Processing	27
5.2.3 Preliminary Results	31
5.3 Vessel-mounted acoustic Doppler current profiler (VmADCP) Measurements	34
5.3.1 Instrument setup and configuration	34
5.3.2 Navigation Data	35
5.3.3 Processing	36
5.3.4 Calibration	37
5.3.5 Preliminary Results	39
5.4 Profiling Microstructure (Chipod)	41
5.4.1 System and operation	41
5.4.2 Raw data	42
5.5: Surface Current Measurements using the Wave Monitoring System	43
5.5.1 System Operations	43
5.5.2 Preliminary Findings	44
5.5.3 Data Management	48
5.5.4 References	49
5.6 Hydrographic underway measurements	49
5.6.1 System operation and preliminary results	49
5.7. Moorings	51
5.7.1 Recoveries	51
5.7.2 Deployments	52
5.7.3 Mooring Casualties	53
5.7.4 Preliminary results from Denmark Strait recoveries	54
5.7.5 MicroCAT sensor calibration	58
5.8 Bathymetry	60
5.8.1 System and Operations	61
5.8.2 Preliminary results	63
5.8.3 Data management	64
6. Ship's meteorological station	64
6.1 System Operation	64
6.2 Preliminary Results	65
7. Station List	66

8. Data and Sample Storage and Availability	107
9. Acknowledgement	108
10. Reference List	108

1. Summary

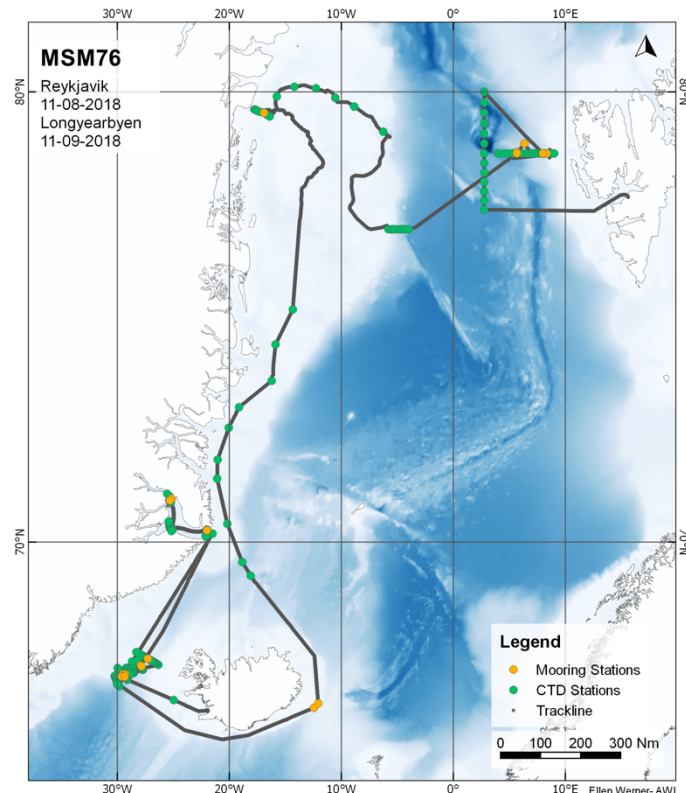


Abb. 1.1: Fahrverlauf (graue Linien) und CTD Stationen (grüne Punkte) sowie Verankerungsstationen (orangene Punkte) der Expedition MSM 76.

Fig. 1.1: Cruise track (grey lines) and CTD stations (green dots) as well as mooring stations (orange dots) during the expedition MSM 76.

The R/V Maria S. Merian cruise MSM76 was carried out jointly by the Alfred-Wegener-Institut Bremerhaven and the Institut für Meereskunde at the Centre for Marine and Atmospheric Sciences of Hamburg University. Scientists and technicians from Universities of Delaware and Bremen also participated in the cruise. During the expedition we (1) continued the monitoring of the Denmark Strait overflow (DSO) transport at the sill of Demark Strait using moorings; (2) carried out a process study in the region of intense mixing downstream of Denmark Strait, and (3) studied the subsurface circulation of warm Atlantic Water on the shelf of Northeast Greenland and its impact on marine terminating glaciers in East Greenland - focusing on Scoresby Sund the 79°N Glacier, and (4) continued to monitoring of the circulation of Atlantic Water in the West Spitsbergen Current at the transition between the Nordic Seas and the Arctic Ocean in Fram Strait. Together, the data will contribute to ongoing and planned projects (RACE II, EU NAACLIM, TRR 181, SPP Sea Level, FRAM, GROCE) on the variability of the overflows and the Atlantic Water circulation and hence the exchanges between the Atlantic and Arctic basins.

A multi-platform approach was taken to achieve the goals, based on moorings, as well as lowered and vessel-mounted observations. From these platforms, measurements of temperature, salinity, dissolved oxygen, current velocity, and temperature microstructure, were obtained. Altogether, **16** moorings were deployed, and **14** moorings were recovered, including two PIES. In addition, **202** CTD / LADCP casts were taken, **127** of which had additionally been equipped with a profiling microstructure temperature probe. Along with this, underway data of surface hydrography and current velocity were collected throughout the cruise.

Die R/V Maria S. Merian Kreuzfahrt MSM76 wurde gemeinsam vom Alfred-Wegener-Institut Bremerhaven und dem Institut für Meereskunde am Zentrum für Marine und Atmosphärenwissenschaften der Universität Hamburg durchgeführt. Wissenschaftler und Techniker der Universitäten Delaware und Bremen nahmen ebenfalls an der Expedition teil. Während der Expedition setzten wir 1.) mit Hilfe von Verankerungen die Überwachung des Transports des Denmark Strait Overflow (DSO) an der Schwelle der Demark Strait fort; 2.) führten wir eine Prozessstudie in der Region der intensiven Vermischung stromabwärts der Dänemarkstraße durch und untersuchten 3.) die unterirdische Zirkulation von warmem Atlantikwasser auf dem Schelf von Nordostgrönland und seine Auswirkungen auf die maritimen Gletscher in Ostgrönland - mit Schwerpunkt auf den Scoresby Sund, dem 79°N-Gletscher. Außerdem führten wir 4.) die Überwachung der Zirkulation von Atlantikwasser im West-Spitzbergen-Strom am Übergang zwischen dem Nordmeer und dem Arktischen Ozean in der Framstraße fort. Zusammen werden die Daten zu laufenden und geplanten Projekten (RACE II, EU NAACLIM, TRR 181, SPP Sea Level, FRAM, GROCE) über die Variabilität der Überläufe und der atlantischen Wasserkreisläufe und damit den Austausch zwischen dem atlantischen und dem arktischen Becken beitragen.

Um die Ziele zu erreichen haben wir verschiedene Methoden benutzt, welche auf Verankerungen, vertikale Stations-Profilen, und kontinuierlichen Beobachtungen von schiffsmontierten Sensoren beruhen. Von diesen Plattformen wurden Messungen von Temperatur, Salzgehalt, gelöstem Sauerstoff, Strömungsgeschwindigkeit und Temperaturmikrostruktur durchgeführt. Insgesamt wurden 16 Verankerungen ausgebracht, 14 geborgen, darunter zwei PIES. Zusätzlich wurden 202 CTD / LADCP Schnitte gemacht, von denen 127 zusätzlich mit einer profilierenden Mikrostruktur-Temperatursonde ausgestattet wurden. Darüber hinaus wurden während der gesamten Fahrt Daten zur Oberflächenhydrographie und zur Strömungsgeschwindigkeit erhoben.

2. Participants

Name / Name	Task	Institut/Institute
1. Prof. Dr. Torsten Kanzow	Fahrtleiter / Chief Scientist	AWI
2. Stylianos Kritsotalakis	Verankerungsmessungen / Mooring Data	UHB
3. Dr. Andreas Münchow	Schiffsmessungen / vessel-based data	UDEL
4. Luisa von Albedyll	Leiterin CTD Wache / CTD Watch Leader	AWI
5. Julius Lauber	CTD Wache / CTD Watch	UHH
6. Alena Zippel	CTD Wache / CTD Watch	AWI
7. Ali Mubashshir	CTD Wache / CTD Watch	AWI
8. Sunke Trace-Kleeberg	CTD Wache / CTD Watch	AWI
9. Mara Muchow	CTD Wache / CTD Watch	UHH
10. Frederike Benz	Sauerstoffmessung / Oxygen sampling	UHH
11. Simon Wett	Leiter Sauerstoffmessung / Leader Oxygen sampling	UHH
12. Andreas Welsch	CTD Technik / CTD Technology	UHH
13. Ulrich Drübbisch	Verankerungen / Moorings	UHH
14. Cassandra Elmer	Verankerungen / Moorings	UDEL
15. Dragonfly Leathrum-Simons	Schiffsmessungen / vessel-based data	UDEL
16. Matthias Monsees	Verankerungen / Moorings	AWI
17. David Kuhlmeier	Verankerungen / Moorings	AWI
18. Ellen Werner	Bathymetry	AWI

3. Research Program

Torsten Kanzow

During the expedition four main goals were pursued, which are subsequently explained.

Goal 1: *Survey of the dense water distribution along the descending Denmark Strait Overflow pathway*

The entrainment of ambient water into the Denmark Strait Overflow (DSO) exiting the Nordic Seas has been found to be most effective within the first 100 – 200 km downstream of the Greenland-Scotland Ridge, where warm Atlantic Water and cold East Greenland shelf waters are mixed into the plume. Neither the processes and locations of intense mixing, nor the pathways of dense water on the Greenland shelf have been well-captured by observations so far. The first objective of the cruise was to obtain a spatially high-resolution hydrographic and current data set from vessel operated systems (CTD/LADCP, vm-ADCP) covering the sill section at DS, as well as at sections downstream of the DSOW pathway in the region of enhanced entrainment. The survey served to the define locations of vigorous water mass modification (see goal 2). Besides the survey activity, the DSO long-term monitoring array

maintained by Hamburg University at the sill of Denmark Strait was service serviced successfully, such that the time series of DSO volume transport established in 1996 is continued.

Goal 2: *Yoyo stations / mooring deployments at entrainment hot spots in the DSO plume*

During R/V Merian cruise MSM21-1b an extremely local mixing hot spot was identified in the DSO plume. During MSM76 we targeted the entrainment in hot spots with yoyo stations of hydrography, current measurements and repeated microstructure profiling. Furthermore, short-term moorings were deployed (and successfully recovered) in order to obtain time series with probably high entrainment rates associated with eddying flows and strong dissipation in the DSO plume. These measurements shall serve to improve our understanding of the time and space scale involved in the different entrainment processes in the overflow plume.

Goal 3: *Recording long-term changes in the Atlantic Water at the transition between the Nordic Seas and the Arctic Ocean in Fram Strait.*

During the cruise, the moorings of AWI's long-term oceanographic mooring array in the West Spitsbergen Current (WSC) have been serviced. For the past 17 years, the array has been capturing the oceanic exchanges of heat and fresh water between the Nordic Seas and the Arctic Ocean - revealing a 1°C temperature increase in the Atlantic Water layer in the WSC since starting the time series in 1996. The moorings are part of the HGF infrastructure FRAM.

Goal 4: *Ocean Glacier interaction in East Greenland*

There is a widespread retreat and acceleration of marine terminating glaciers around Greenland, which drain the Greenland Ice Sheet, with several studies suggesting that the warming Atlantic Waters might be a major driver of these changes. During the cruise, we focused on ocean-glacier interaction through carrying out CTD/LADCP surveys in the Scoresby Sund-Nordvest Fjord system and near the 79N Glacier. At both locations moorings for the study of Atlantic Water transport toward the glaciers were deployed. These activities support the BMBF GROCE and DFG SPP Sea Level programs on the shelf of Northeast Greenland.

4. Narrative of the Cruise

Torsten Kanzow

In the early afternoon of 11 August the research vessel Maria S. Merian left the port of Reykjavik to start the MSM 76 expedition "Nordic Seas Exchanges". On board there were scientists from the Alfred-Wegener-Institute for Polar and Marine Research, and from the Universities of Hamburg, Delaware (USA) and Bremen. Our work area included Denmark Strait between Iceland and Greenland, the shelf of East Greenland and Fram Strait at the transition from the Nordic Seas and the Arctic Ocean.

In the early morning of 12 August, we arrived in the Denmark Strait area. During the day, we were able to conduct a survey across the deep overflow plume at the continental slope of Greenland. Here we observed current velocities within the plume of up to 3 knots. The survey served us to define positions at which mooring were supposed to be deployed within the plume. In the evening of that day already three of a total of six moorings were deployed successfully. They will remain in the ocean for 2 weeks to measure continuously velocities and temperatures within the cold overflow plume.

On 13 August we started deploying successfully the remaining three moorings, with which we will observe for the duration of at least two weeks the turbulent circulation patterns that are important for the properties and the strength of the “Denmark Strait Overflow Plume” - the deep current flowing over the Greenland-Iceland Ridge. Strong winds and poor visibility due to fog accompanied our work. We succeeded in recovering a mooring in Denmark Strait, that had acquired measurements of the overflow for the duration of twelve months. After servicing the instruments, we re-deployed the mooring at the same location. This way we accomplished to continue the measurements in this key location of the Atlantic Meridional Overturning Circulation that have been operated quasi-continuously since 1996. Unfortunately, an attempt to recover a second, single current meter mooring by dragging was not successful.

For the largest part of the week we then conducted a survey of the spatial distribution of the overflow plume along the continental slope of Greenland downstream of Denmark Strait. For this purpose, the vessel successfully covered 90 stations during which data of the vertical distributions of temperature, salinity, dissolved oxygen and current velocity were collected throughout the entire water column by means of a lowered sensor system (CTD / LADCP). The data show, that the overflow plume sinks to greater depths with increasing distance from Denmark Strait. We will use these observations to calculate to what extent this important current gains in strength by entraining ambient waters along the way. Valuable measurements of the bathymetry (depth soundings by a swath echosounder) completed the observations.

Toward the second half of the week the winds calmed down and the sun re-appeared, allowing for occasional sightings of whales and icebergs floating by in the distance. By Saturday we had completed the survey and conducted an 18 hour-long time series station, in order to investigate the turbulent mixing processes of relatively warm, ambient waters into the cold plume. In spite of strong, variable currents the nautical staff of R/V Maria S. Merian managed skillfully to keep the vessel in position over the entire period.

After leaving the first work area southeast of Denmark Strait we arrived in the evening of 20 August after a one day-long transit across the shelf of East Greenland at the mouth of Scoresby Sund. The latter represents the largest fjord system worldwide, into which many glaciers terminate, thereby continuously injecting icebergs into the fjord. The increase transport of glacier ice into the oceans has led to a marked rise of the global sea level in the last 20 years.

After one week's work in Denmark Strait the sighting through the fog of the rocky coastline framing the mouth of Scoresby Sund represented a spectacular moment. Along the mouth, we conducted a survey of the water mass structure and the ocean currents. Overnight, the lights of the exposed settlement Ittoqqortoormiit on the northern shore became visible.



Figure 4.1: View of an iceberg at the transition between Scoresby Sund and Nordvest Fjord. Photo: Dragonfly Leathrum-Simons.

We continued our voyage into Scoresby Sund, and arrived at the transition to the narrow Nordvest Fjord framed by steep cliffs in the afternoon of 21 August. This transition represented a focus of our work, as we expected to find here a concentrated inflow of Atlantic Water. In order to choose meaningful locations for our oceanographic measurements, we began to carry out an echosounder survey of the water depths. The results suggested the existence of two possible passages for the throughflow of Atlantic Water. Based on this, in the midst of a breathtaking scenery of small rocky islands, icebergs extending up to 40 m above the sea surface, and steep cliffs we undertook a survey of the water mass and oceans currents. The analysis proved our assumption right – we found a swift inflow of Atlantic Water into Northvest Fjord near the sea floor.

In the afternoon of 22 August, we deployed two moorings (one in each passage), in order to continuously observe the characteristics of the inflow for the duration of one year. Subsequently, we carried out a short hydrographic survey of Viking Bay, a few miles wide and long embayment into which Brede Glacier terminates. Next morning, we headed back to the mouth of Scoresby Sund, where we deployed a third mooring for the continuous observation of the Atlantic Water circulation. After another one-day transit we returned to Denmark Strait. Here we successfully recovered two moorings deployed on the deep overflow plume one year ago. On August 25 we first failed to recover a third mooring, while later in the afternoon and during the subsequent morning all six moorings deployed during the first days of our expedition were recovered successfully. Our spectacular and successful working week ends with the conduction of continuous water mass and ocean current surveys at an isolated rise located right in the flow path of the overflow plume. Here we expect to find elevated levels of entrainment of warm ambient waters into the cold plume.



Figure 4.2: View of the hangar of R/V Maria S. Merian. Scientists download sensor data and take water samples from the CTD / LADCP system used for the water mass and ocean current surveys. Photo: Dragonfly Leathrum-Simons.

On Monday, 27 August, we finally left our working area southwest of Denmark Strait. Strong winds and swell accompanied our two day-long transit at first along the south coast and then along the east coast of Iceland toward the Iceland-Faroe Ridge. The latter is - just like the sill in Denmark Strait – a part of a ridge system that marks the boundary from the subpolar North Atlantic to the Nordic Seas.



Fig. 4.3: View of the coast of Iceland. (Photo: Dragonfly Leathrum-Simons).

One year earlier two bottom moorings (so-called PIES) has been deployed on the Iceland-Faroe Ridge in order to observe a possible pathway of overflow of dense water from the Nordic Seas toward the Atlantic. On 29 August we successfully recovered both PIES. Subsequently we continued our way across the Iceland Sea toward the shelf of Greenland. On the way we conducted lowered hydrographic measurements, in order to calibrate sensors, that we had previously recovered. The fairly uniform water mass properties of the deep Greenland Sea are ideal for this exercise.

Much of our time in this week, that was characterized by extended transits, was spent on first analyses of the observational data. We investigated the performance of the sensors of the lowered CTD system, visualized the data sets recovered from the moored sensors, evaluated their plausibility. Based on this first analyses regarding the circulation in Denmark Strait were carried out, for which also underway measurements of ocean currents, surface temperature and meteorological parameters are taken into account. Overall, we are very pleased by the high degree of both data return and quality.



Fig. 4.4: A grapnel is used for the recovery of a mooring. Photo: Dragonfly Leathrum-Simons

In the early morning of 31 August we reached the shelf of Greenland near the latitude of the mouth of Scoresby Sund. Since then we moved toward the North with partly spectacular views of the Greenlandic coast. The shelf exhibits deep troughs that extend eastward from the large fjord systems on the coast toward the shelf edge. The troughs are regarded as possible conduits along which Atlantic Water may penetrate from the open ocean into the fjords where it may interact with marine terminating glaciers. In the troughs and at selected shallower sites we conducted hydrographic measurements. These are regions in which historically only very few measurements have been taken. On 1 September the measurements were completed, and R/V Merian moved further north, through sea ice and fog. Our target was the embayment in front of the 79°N glacier – one of the largest marine terminating glaciers in Northeast Greenland. Together with a neighboring glacier, it drains the ice masses of the Northeast Greenland Ice

Stream (NEGIS) into the sea, with NEGIS comprising 15% of the area of the entire ice shelf of Greenland.

After R/V Merian sailed past larger areas covered by fast ice on the shelf of Northeast Greenland, we reached the entry to the embayment of the 79°N Glacier on 3 September. The day before, strong northerly winds had set the sea ice in motion and had moved large ice floes into the bay, such that there was no possibility for us to move further onshore.

One of our goals had been to recover a mooring deployed a year ago right at the calving front of the glacier. With good visibility of the rocky shores of Greenland we repeated a hydrographic survey across Windwind Trough (located just outside of the bay) instead that had been covered two years ago by R/V Polarstern. First analyses showed a marked temperature increase within the subsurface layer of relatively warm Atlantic Water. It is this water mass that flows into the 80 km-long cavity underneath the floating ice tongue of the 79°N glacier, causing large meltrates at the ice base.

Over the course of the day, the winds calmed down. Yet, no improvement of the sea ice conditions in the bay were seen, such that we had to give up our ambition to get closer to the glacier. We deployed a mooring at the entry to Westwind Trough, that shall observe continuously the circulation changes of the Atlantic Water for the duration of one year.



Fig. 4.5: View of the Greenland coast close to the 79°N Glacier (Photo: Dragonfly Leathrum-Simons).

Subsequently, we sailed across the shallow shelf in an easterly direction toward the shelf edge. The latter was clearly visible as a narrow belt of ice floes, that moved southward out of the Arctic Ocean, carried along by the East Greenland Current. This current represents the most important export pathway of sea ice and low-salinity ocean waters from the Arctic Ocean. Swell and poor visibility due to snowfall forced us to steam southward along the ice belt on the shelf until favorable sea ice condition on 5 September allowed us to conduct a survey of the strength and hydrographic structure of the East Greenland Current.

In the afternoon of 6 September we began our work on the eastern side of Fram Strait in the area of the West Spitsbergen Current. The latter represents the northward extension of the Gulf Stream-North Atlantic Current pathway, along which warm, saline waters from the subtropical North Atlantic are carried toward the Arctic Ocean. Since 1997 the Alfred-Wegener-Institute has been operating a long-term observatory in the West Spitsbergen Current based on a moored array running along 79°N latitude line across the continental slope of Spitsbergen.

In the following days, moorings were serviced during daytime and hydrographic measurements were conducted during nighttime. We succeeded in recovering three moorings that had been sampling the strength and structure of the West Spitsbergen Current at an hourly resolution continuously for two years. Regrettably, a fourth mooring at the shelf break could not be recovered. In order maintain the observatory, in the following four moorings were re-deployed which shall be serviced again in two years-time.



Fig. 4.6: Deployment of a mooring in the West Spitsbergen Current over the stern of Merian (Photo: Dragonfly Leathrum-Simons).

After completion of the mooring and hydrographic work along the 79°N section we steamed toward the position 80°00' N and 002°45' E. It is along this meridian that we conducted as the last work package of the expedition a hydrographic survey in the center of Fram Strait in a southerly direction over a distance of 120 nautical miles. Here our aim was to capture the part of the warm waters that – coming from the West Spitsbergen Current – do not flow further to the north into the Arctic Ocean but instead recirculate within Fram Strait, only to move back southward along the shelf edge of Greenland.

We are thus targeting the main supply pathway of the warm Atlantic Water, that over the course of this expedition we repeatedly encountered on the shelf of Greenland, in Scoresby Sund and near the 79°N Glacier.

On 11 September our expedition came to an end in the port of Longyearbyen. I am looking back with joy on a successful expedition. Our time on board has been highly enjoyable owing to both the spirit and professionalism of all parts of the crew of R/V Maria S. Merian and to the impressive engagement and solidarity among the scientific participants.

5. Preliminary Results

5.1 Lowered CTD

Luisa von Albedyll , Julius Lauber , Mara Muchow, Torsten Kanzow

5.1.1 System and Operation

During the expedition, hydrographic measurements were conducted using a standard CTD SBE 911+ System. In total, 202 CTD casts were carried out. Measurements were taken in four main working areas, Denmark Strait, Scoresby Sund, at the Greenland Shelf and at 79°N covering the West Spitsbergen Current. A SBE 9 plus CTD unit, provided by the University of Hamburg was mounted on a rosette with three 5 litre bottles attached for water sampling. Water was sampled at most stations (see Table 7.1) for calibration of salinity and oxygen sensors and a $\delta^{18}\text{O}$ study.

The CTD was equipped with dual sensors for temperature and conductivity (one mounted at the top of the frame and the other at the bottom), as well as one sensor for oxygen and pressure. Details of the sensors with serial numbers and calibration dates can be found in Table 5.1.1. In addition, ocean currents were measured using two ADCPs attached to the CTD frame, one upward and the other downward looking (see section 5.2). A downward looking altimeter with a range of about 100 m measured the distance to the bottom for safe handling of the CTD. During 127 profiles the frame was additionally equipped with a Chi-Pod for high-frequency measurements of temperature, the time derivative of temperature and acceleration (see section 5.4).

For data logging and triggering of the water samplers, the vessel's CTD deck unit was used. Data was recorded and displayed in the SeasaveV7 software. Time and ship's location were taken from the ship's navigational system (NMEA). Processing was conducted using the ManageCTD processing software maintained by Gerd Rohardt (AWI). The program uses the SBE Data Processing software that carries out the following routines: (1) Data Management – (2) WildEdit – (3) Bottle Summary – (4) Split – (5) Translate – (6) Translate – (7) Cell Thermal Mass – (8) Loop Edit – (9) Bin averaging (pressure). Between step 5 and 6, the operator needs to manually pick the start time and the end depth of the profile. Furthermore, the software was used to produce header files that contain information on depth, longitude, latitude and station number extracted from the ship's action log.

CTD file naming convention included the cruise identifier (MSM76), the station number (XXX, three digits) and cast (YY, two digits), leading to MSM76_XXX_YY. All CTD stations and the samples taken at the respective stations are listed in Chapter 7 (Table 7.1).

Special stations

At station 103, a YOYO-CTD cast was conducted lasting for 18 hours and consisting of 26 individual casts. While the ship held its position, the CTD was moved from the surface to the bottom (at 960 m). When the CTD was at the surface again, a new file was started, counting with upwards running cast numbers (MSM76_103_YY).

At stations 154, 158 and 159 towed CTDs were carried out. This involved lowering and lifting the CTD from the bottom to 300m above it while the ship sailed with a maximum speed of 0.5 knots. The bottom depth changed during the drift as we were crossing a seamount (100-200 m high). When reaching the upper end of one cast (300m above the sea floor), a new file with a different cast number was started. Station 154 lasted 8 hours (31 casts), Station 158 for 7 hours (20 casts) and Station 159 for 4 hours (13 casts). Note: for the towed CTDs, the action log of the ship does not provide detailed information on the different casts.

At the stations 53, 162, 163 and 227 Microcat SBE37 sensors that were deployed or recovered during the cruise were attached to the CTD. During the casts the rosette was stopped at two or three different depths featuring low temperature and salinity gradients for 7 minutes to calibrate the MicroCATs (see section 5.7.4).

	Type	SN and calibration date
CTD	SBE 911+	S/N 09P6395-0285
CTD-Sensors	Frequency 0 Temperature 1	1526, cal.date 11-Apr-17 Bottom sensor
	Frequency 1 Conductivity	1222, cal.date 12-Apr-17 Bottom sensor
	Frequency 2 Pressure, Digiquartz with TC	0285, cal.date 03-Dec-14
	Frequency 3 Temperature 2	5456, cal.date 11-Apr-17 Top sensor
	Frequency 4, Conductivity, 2	3960 cal.date 12-Apr-17 Top sensor
	Oxygen	SBE43
Altimeter	Benthos PSA916	885
Rosette	SBE Carousel	12 bottles á 5L; 3 mounted

Table 5.1.1: Serial numbers and calibration dates of all CTD sensors attached to the rosette

5.1.2 CTD Performance

5.1.2.1 Assessment of sensor stability

Since there are two pairs of sensors for temperature and conductivity attached to the rosette, we compared their measurements to each other to test for sensor drifts, etc. Since one pair was attached on the top and the other one on the bottom of the rosette, differences at depths are expected at which large vertical temperature and salinity gradients are found. To avoid comparisons at such locations, comparisons are only done at the bottle stops during the upcast. The bottles were only fired at depths showing low vertical gradients.

In Figure 5.1.1 the temporal evolution of the differences between the two temperature and salinity values of the two sensor pairs is shown. For temperature, we find a standard deviation of $0.030\text{ }^{\circ}\text{C}$ around the mean value of $-0.001\text{ }^{\circ}\text{C}$. For conductivity, the behavior looks very similar with a mean of 0.002 mS/cm and a standard deviation of 0.03 mS/cm . The salinity differences yield a standard deviation of 0.0121 psu around the mean difference of -0.0009 psu . There is slight evidence of a positive trend in the salinity differences – though not exceeding 0.003 psu throughout the entire cruise.

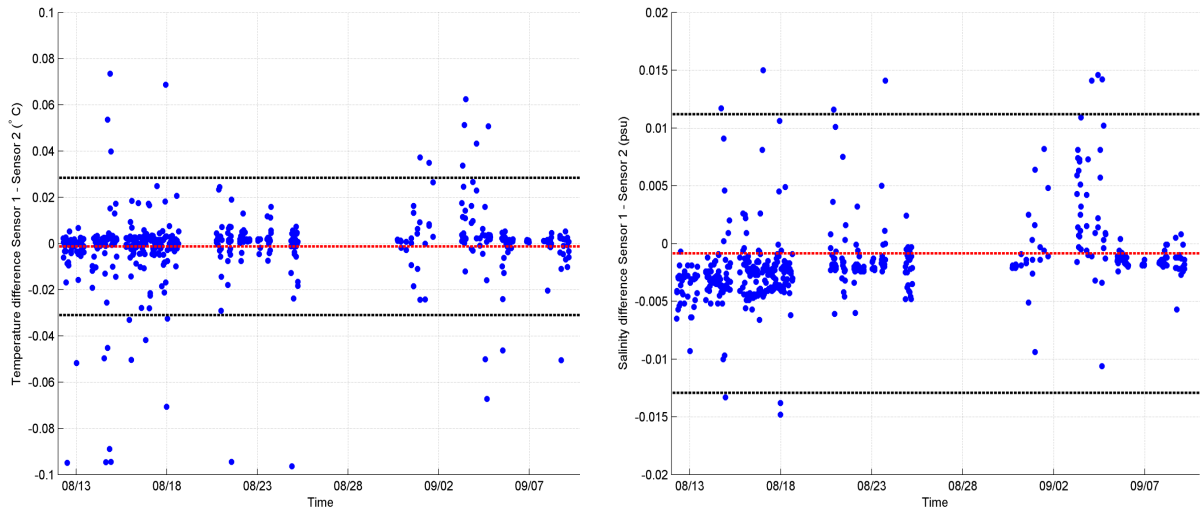


Figure 5.1.1: Temporal evolution of the temperature (left) and salinity (right) differences between sensor 1 and 2. The red dashed lines are the mean differences and the black dashed lines represent the standard deviations around the mean.

In Figure 5.1.2 the behavior of the salinity difference of the two sensors is shown as a function of depth. It is visible that the largest differences appear at depths smaller than 300 m. Especially at small depths, the profiles might have exhibited some systematic vertical gradients that affected the comparisons at the bottle stops (creating biases). Note that this is not a sign of limited quality of the sensor measurements, but a result of the sensor setup (one pair being at the top and the other at the bottom of the CTD frame). Down to 1500 m the differences stay quite constant (with a mean difference between the sensors of around 0.002 psu) as visible by the red curve. This depth dependence is also similar for temperature and conductivity.

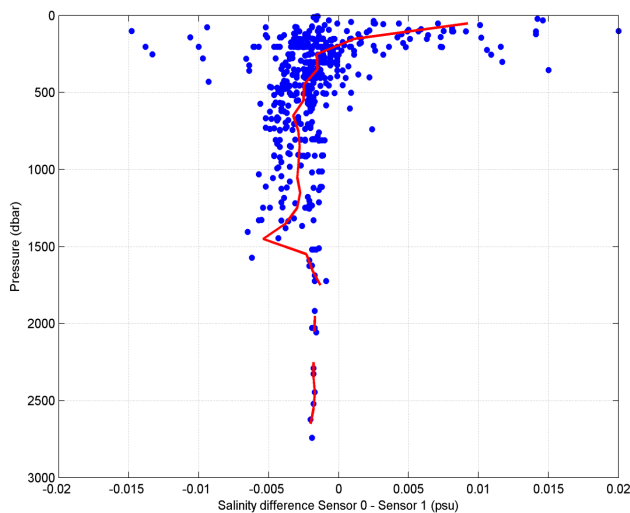


Figure 5.1.2: Depth-dependence of the salinity difference between sensor 1 and 2. The red line shows the mean for 100 m depth bins. Very low and large values are not shown.

5.1.2.2 Salinity Calibration with water samples from the CTD

It is ultimately important to calibrate the conductivity sensors by comparing its values to the salinity of water samples taken during CTD casts. Therefore, during the whole cruise three Niskin bottles were attached of the rosette. At every station, we took water samples close to the sea floor and at two other depths, where the salinity gradients were weak. While closing the Niskin bottles, the Seabird CTD operating software created the so-called bottle-files, which store the CTD values at the sampling points, which were then used for the subsequent comparison. The actual calibration of the conductivity sensors was not carried out during the cruise, therefore here we only report on the preliminary comparison between CTD and bottle-derived values (the latter having been measured using the onboard Autosal salinometer). There are values from each of the two sensor pairs (T, C), which have been converted to salinity (SAL1 and SAL2). The latter are then compared to the respective bottle values. During the cruise a „sal_raw.csv“ file was composed, which contains the data from both the salinometer and from the bottle-files, including the station number.

For the subsequent comparison, the salinity anomalies, S_{a_i} , for each sample were calculated in the following way:

$$S_{a_i} = S_{SALI} - S_{CTD_i}$$

where S_{SALI} is a the salinometer-derived salinity for each water sample and S_{CTD_i} represents the corresponding salinity value derived from the CTD (with the index $i=1$ referring to sensor pair 1 and $i = 2$ to pair 2).

For both S_{a_1} and S_{a_2} the mean, median and standard deviation was calculated to compare them. The results are shown in Table 5.1.2. (see also the differences of the two salinity sensors In the previous subchapter).

	S_{a_1} / psu	S_{a_2} / psu
Median	-0.0007	-0.0029
Mean	-0.0014	-0.0022
Stand. Dev.	0.0049	0.0047

Table 5.1.2.: The median, mean and standard deviation of S_{a_1} and S_{a_2} .

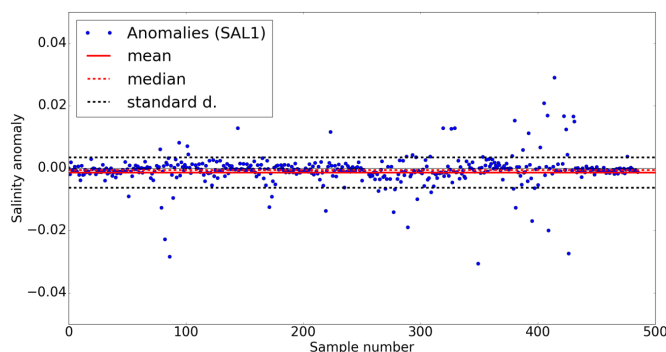


Figure 5.1.3.: The anomaly of the sensor SAL1 with the mean, median and standard deviation.

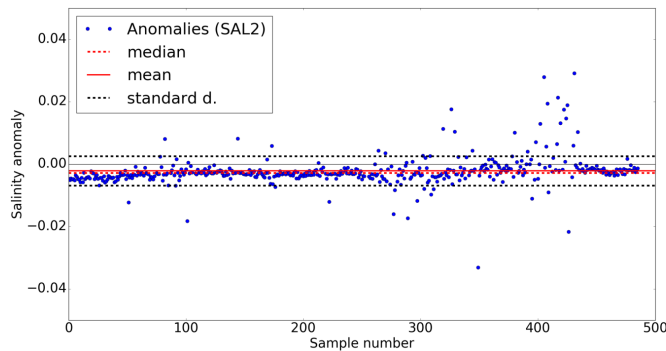


Figure 5.1.4.: The anomaly of the sensor SAL2 with the mean, median and standard deviation.

In the Figs. 5.1.3 and 5.1.4 the anomalies S_{a_1} and S_{a_2} are displayed. It is noticeable that S_{a_1} and S_{a_2} are highly correlated, meaning that the individual CTD sensors pairs did not create large individual outliers. By comparing Figure 5.1.3. and 5.1.4 is also noticeable (as seen in Table 5.1.2), that there is a mean offset between the two sensor pairs. However, neither S_{a_1} nor S_{a_2} seem to exhibit any noticeable trend. It should be noted that the final processing and calibration (i.e. correction of the CTD derived salinities applying the salinometer-derived salinities) was carried out after the cruise by Andreas Wisotzki (AWI). This step is therefore not part of the cruise report. Here we can note that the sensors work stably and at high accuracy throughout the cruise.

[5.1.3 CTD Oxygen Calibration](#)

In order to calibrate the oxygen sensor of the CTD probe, oxygen samples were taken from the Niskin bottles attached to the CTD frame on a regular basis. The oxygen concentration was determined using the Winkler titration method. In the beginning of the cruise, 3 to 4 oxygen samples were taken from every station. Due to the limited amount of chemicals this was reduced to every second station from station 8 onwards. In every CTD watch team there was one person responsible for the oxygen sampling, so with just a few exceptions the oxygen sampling was always done by the same three persons. After the sampling, the bottles were stored in the dark for several minutes. The titration was performed within 12 hours after the sampling. In total 364 samples were taken from 97 CTD stations, including 97 double samples for an estimate of the quality of the sampling and titration procedure. In total 9 samples were flagged as bad data due to leaking Niskin bottles or incidences during the sampling or titration procedure. Those data were not taken into account for the analysis.

[5.1.3.1 System and Operation](#)

The reagents used for the sampling are a Manganese(II)Chloride solution $MnCl_2$, that was prepared by dissolving 200 g of $MnCl_2$ in 500 ml distilled water and the alkaline solution $NaOH+KI$, that was prepared by dissolving 180 g $NaOH$ and 75 g KI in 500 ml distilled water. For the titration sulfuric acid, H_2SO_4 , 46-47% (manufacturer Bernd Kraft, Duisburg, Germany) was added to the samples and sodium thiosulfate, $Na_2S_2O_3$, with a concentration of 0.01 N from readymade vials (manufacturer Merck KGaA, Darmstadt, Germany and Th. Geyer GmbH & Co. KG, Renningen, Germany) was used as a titer. For the titer standard, a potassium iodad solution, KIO_3 , from readymade vials (Merck KGaA, Darmstadt, Germany) was used as well as a potassium iodid solution, KI , that was prepared by dissolving 50 g of KI in 500 ml distilled water. The sampling and titer standard procedure will be described in more detail in the following.

The Niskin bottles from which the oxygen samples were taken were closed in depths where the oxygen concentration showed small gradients. To avoid contamination with atmospheric oxygen the oxygen samples were always taken from the bottles before any other samples were taken. For the sampling procedure the Winkler flasks were carefully filled from the Niskin bottles with a silicone tube that was inserted completely in the flask. The Winkler flasks were rinsed with the seawater that was let overflow approximately two times the volume of the flask. During this procedure it was always made sure that no air bubbles remained in the flask. Directly after the sampling 0,5 ml of NaOH+KI and MnCl₂ respectively was added to the sample which was then shaken until all the dissolved oxygen was bound. After the sampling the Winkler flasks were stored in the dark until the titration.

In order to determine the oxygen concentration of the samples the Winkler titration method was used. This was done using the automated Metrohm 848 Titrino Plus system (s/n 10304277) equipped with a Metrohm Pt Titrode (s/n 01290932) which was set to a Dynamic Equivalence Method. The oxygen concentration in the sample was determined by the amount of titer (thiosulfate, Na₂S₂O₃) that was needed to reach the endpoint. In order to check the quality of the titer, a standard was performed every day at which titrations were done and whenever a new thiosulfate solution was prepared. For the standard, in this order, 1 ml KIO₃, 1 ml H₂SO₄, and 5 ml KI were dissolved in 100 ml distilled water. With this solution the usual titration was run and the amount of consumed thiosulfate was noted. This was repeated three times and then divided by 10 ml, the amount of thiosulfate, theoretically needed to titrate 1 ml KIO₃, yielding the titer factor t .

5.1.3.2 Preliminary Calibration

In order to calibrate the CTD oxygen sensor with the values determined from the titration the difference between the oxygen concentration measured by the CTD oxygen sensor, when the bottle was fired and the titration-derived value are displayed separately for every sample in Figure 5.1.5 (a).

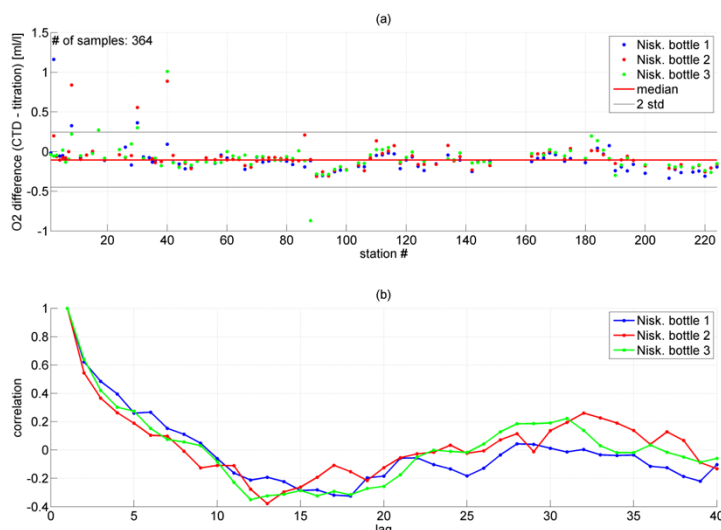


Figure 5.1.5: Difference between the CTD probe oxygen sensor and the oxygen concentration determined from the samples by Winkler titration (a). Autocorrelation of the timeseries for the single bottles on the rosette (b) as a function of station lag.

From this, it is visible that until station 40 the variability in the oxygen difference is higher than after station 40. This is probably due to inaccurate measurement of the volume of the chemicals during the sampling due to clogged dispensers. Afterwards the dispensers were cleaned regularly and the variability decreased. However, a limit of two standard deviations around the median was applied to the data and all values outside this range were neglected. So, from the 364 samples displayed in Figure 5.1.5, 10 are not used in the calibration. The figure does not show any evidence of a trend (drift) in the oxygen difference. However, any possible dependence of the oxygen concentration difference on other variables

such as pressure, temperature, salinity and oxygen concentration remains can't be inferred from this analysis.

In order to test such dependencies, further analyses were conducted. Figure 5.1.6 (a) shows the pressure dependency of the difference between the CTD oxygen sensor values and those derived by Winkler titration. A linear fit of this dependency is displayed as a solid black line. Most of the samples were taken from depths shallower than 500 m, so this might induce a bias to the fit. The difference values were then corrected for the pressure dependence by subtracting the linear fit from them. The resulting data were then plotted against temperature (blue dots in Figure 5.1.6b, red dots show the uncorrected values). To these data the same linear fitting procedure was applied, with the fit subsequently subtracted and this repeated also for salinity and oxygen dependencies (Fig. 5.1.6 c and d, respectively). The values in the lower left corner always show the standard deviation of the corrected values. This value slightly reduces from Figure 5.1.6a to Figure 5.1.6b (pressure correction) but afterwards it remains almost constant. This shows, that the linear dependency of the CTD oxygen measurements, O_{CTD} , on the single variables (P, T, S and O_2) is very small and can be neglected in a first, preliminary calibration approach.

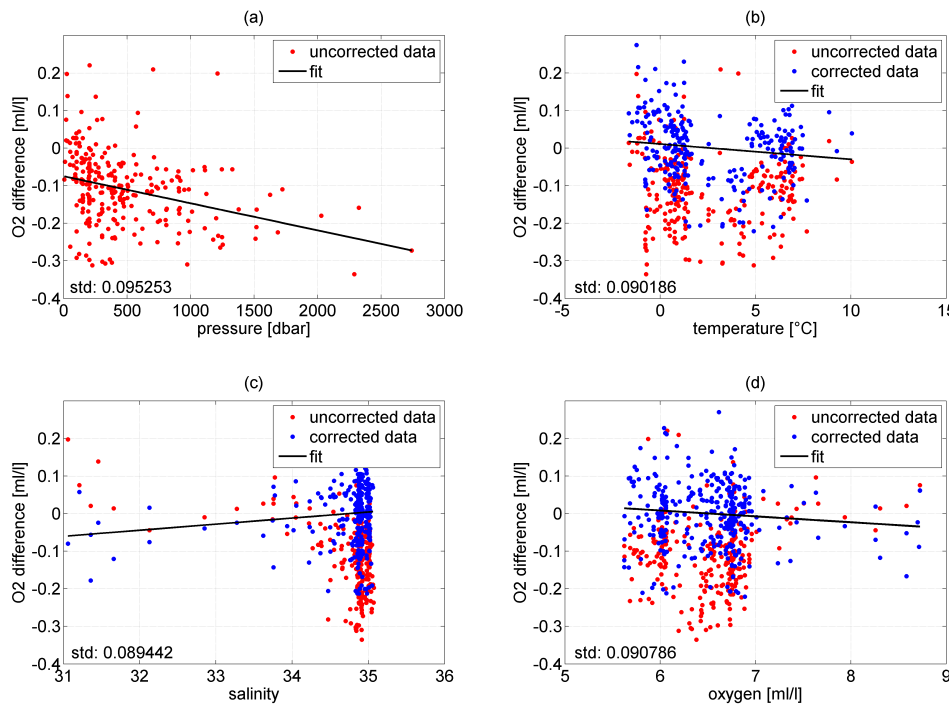


Figure 5.1.6: Iterative fitting and correction of the oxygen difference (sensor value minus titration value) against other variables measured by the CTD probe, namely pressure (a), temperature (b), salinity (c) and oxygen concentration (d).

Instead the median of the oxygen difference between the CTD oxygen sensor and the titration measurements of 0.10 ml/l is taken as a correction for the CTD probe oxygen measurements (O_{CTD}) as follows

$$O_{corrected} \left[\frac{ml}{l} \right] = O_{CTD} \left[\frac{ml}{l} \right] + 0.10 \left[\frac{ml}{l} \right]$$

The uncertainty of this preliminary calibration is assessed by the error of the median value of the oxygen difference. The standard error of the median, σ_E , is calculated via the following formula

$$\sigma_E = \frac{\sigma_S}{\sqrt{F}}$$

where σ_S is the standard deviation of the whole timeseries shown in Fig. 5.1.5a. Here $F = N/M$ is the relationship between the degrees of freedom, F , the total number of elements in the timeseries, N , and the lag, M , at which the zero-crossing of autocorrelation of the timeseries occurs (Figure 5.1.5 b). This is the case for a lag of 9 or 10 stations for the different Niskin bottles. Here, the standard error is calculated separately for each bottle and then averaged. This yields values of $\sigma_{E1} = 0.049$, $\sigma_{E2} = 0.047$ and $\sigma_{E3} = 0.051$ ml/l for the error of the median of the single bottles. This averages to $\sigma_E = 0.05$ ml/l. The uncertainty σ_E of the offset is acceptably lower than the offset itself of 0.10 ml/l.

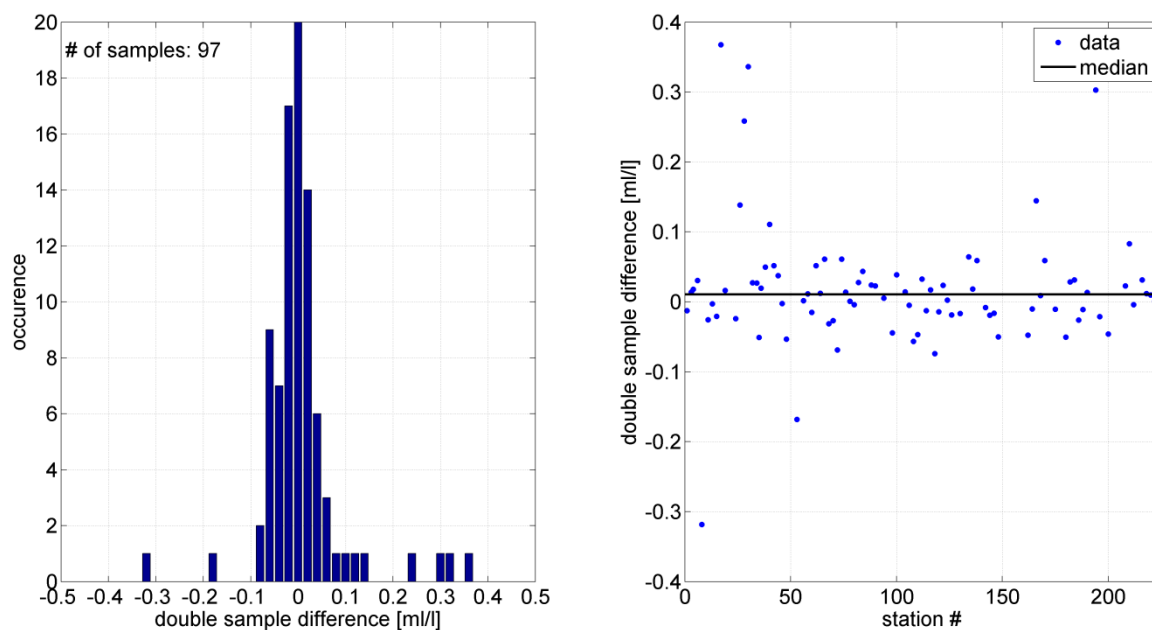


Figure 5.1.7 Double sample accuracy. Histogram of the difference between the single double samples (a). Development of the difference of the single double samples over time (b).

Also, the difference of the double samples (Figure 5.1.7) supports the above results, that an acceptable accuracy of the titration has been achieved. Figure 5.1.7a shows the histogram of the difference between the individual double samples. The shape of this histogram suggests a standard distribution of the differences in the double samples around the mean of 0.016 ml/l with a standard deviation of 0.087 ml/l. Figure 5.1.7 shows that the difference between the double samples, like the difference between the CTD values and the titration (see Fig. 5.1.5a), decreased after station 40 due to the change in the cleaning procedure of the dispensers. Apart from this no other time dependency of the double sample difference is visible. This suggests that the method of the Winkler titration here yielded stable results.

It should be noted that the final processing and calibration (i.e. correction of the CTD derived dissolved oxygen by applying the titration-derived values) was carried out after the expedition by Andreas Wisotzki (AWI). The final calibration is therefore not part of the cruise report.

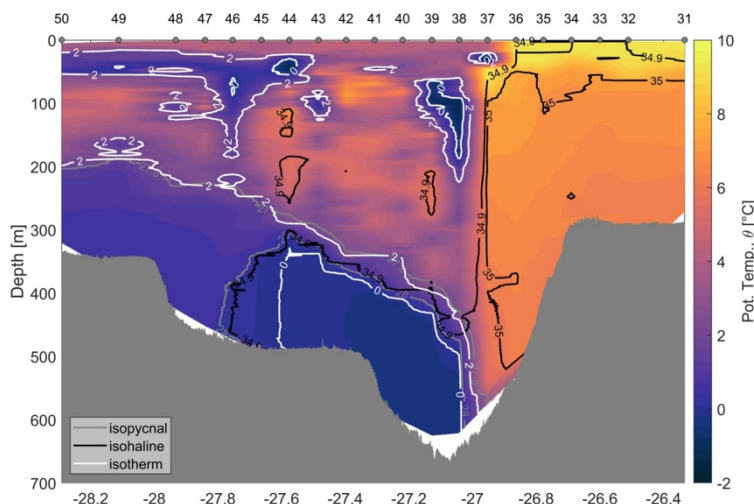
5.1.4. Sampling water for $\delta^{18}\text{O}$ -Analysis

For the analysis of $\delta^{18}\text{O}$ we took water samples on every second CTD station. The sample bottles were provided by Dr. Gilles Reverdin (I¹OCEAN, France). For every sample the sample bottle was rinsed two times (including the cap). The samples were stored on the vessel and shipped to Dr. Gilles Reverdin after the expedition to conduct laboratory measurements.

5.1.5 Preliminary Results

5.1.5.1. Working Area 1: Denmark Strait

Hydrographic work in Denmark Strait (DS) focused on a survey of the dense waters descending into the Atlantic Ocean from the Denmark Strait sill. By means of densely spaced hydrographic lines located perpendicular to the pathway of the cascading plume between 65°N and 66°30'N and 25° and 29°W, the entrainment of ambient waters into the plume was targeted. Repetition of the hydrographic lines up to three times and a YOYO-CTD of 18 hours conducted in the center of the entrainment area were carried out to add knowledge on the temporal variability of the overflow.



In addition, entrainment processes close to a hot spot of local mixing at a seamount were studied in detail by three towed CTD stations. Furthermore, the hydrographic measurements were placed around and at the deployment positions of four short term moorings (see section 5.7). These will help place mooring observations into a broader spatial context.

Figure 5.1.8: Section over the sill of Denmark Strait from West (left, Greenlandic shelf) to East (right, Icelandic shelf). Locations of stations are marked by a dot and a number at the top.

At the DS sill, warm, northward flowing water from the Icelandic branch of the Irminger Current is found over the Icelandic continental shelf (Fig. 5.1.8). It is separated by a sharp front (characterized by the 34.9 psu isohaline) from southward moving waters exiting from the Nordic Seas. In the deepest channel passing the sill, the core of the overflow waters, characterized by cold (-1.5 to 0 °C), saline (> 34.9) and dense waters ($\sigma_0 > 28 \text{ kg/m}^3$) is located. Towards the slope of the Greenland shelf, the thickness of the plume decreases, and it freshens. The 27.8 kg/m^3 isopycnal - that is often used to characterize the upper boundary of overflow waters - follows closely the near-bottom 2 °C isotherm. At 300 m water depth on the Greenlandic shelf, the 27.8 kg/m^3 isopycnal still indicates a plume thickness of about 130 m.

In the upper water column, on the Greenland shelf, a lens of colder waters (temperatures than 2°C) is found between at depths shallower than 100 m, which is characterized by low salinities. In between those colder, subsurface waters and the dense plume, one finds patches of increased temperature and salinity, corresponding possibly to diluted, recirculating branches of the warm Irminger waters.

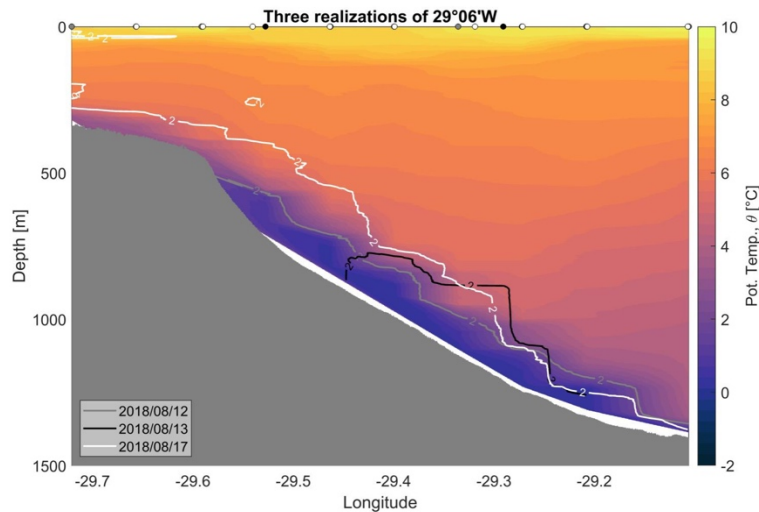


Figure 5.1.9: Temperature section as measured on the 12/08/2018. The 2°C isotherm is given in grey. During two repetitions of the line (on 13/08 and 17/08), the location of the 2°C isotherm substantially changed in horizontal and vertical extent.

Moving downstream, the plume incorporates ambient water, i.e. freshens and warms, but also increases in thickness. The hydrographic line shown in Figure 5.1.9 extends across the plume from $29^{\circ}06'W / 65^{\circ}21'N$ to $29^{\circ}43'W/65^{\circ}39'N$ (see also Figure 5.1.10 for an overview). It is oriented along the main axis of the short-term mooring array (see Fig. 5.7.1). The section shows the temperature field from the first realization of this section on 12 August 2018 (start date), whereas the isotherms superimposed as black and white lines are taken from two more realizations on 13 August and 17 August 2018, respectively. On 12 August, cold waters ($< 2^{\circ}\text{C}$) are found at the Greenlandic shelf slope with a rather constant thickness of 100 m above ground. The cold water fades out towards the Greenland shelf and is not found above 520 m water depth. On 13 August, the cold and dense water seems to have retreated from the upper part of the slope and instead increased in magnitude on the lower part. Water colder than 2°C was not present above 780 m water depth, but the thickness of the cold core below 800 m water depth increased to up to 300 m. During the third realization at the 17 August, the largest spatial extent of plume waters was observed, with the 2° isotherm reaching up all the way to the shelf break to 280 m water depth. Compared to 12 August, the core of the cold water seemed to be shifted upslope, with a maximum thickness of 330 m located at the 890 m isobath, whereas it appears have thinned at isobaths exceeding 1200 m. Overall, the fundamental change observed in the plume geometry on time scale as short as days matches favorably with the temporal changes of the plume observed both during the yo-yo CTD (see Fig. 5.1.11) and the short-term mooring-based velocity measurements (Fig. 5.7.5).

Preliminary plume transport calculations at all CTD stations are displayed in Figure 5.1.10. The overflow waters were characterized by temperatures lower than 2°C and a potential density anomaly of $\sigma_0 > 28 \text{ kg m}^{-3}$. By extracting the thickness of the plume and velocity in this layer, a volume transport at each site was estimated. Figure 5.1.10 shows that in general the overflow waters gain in volume while descending by entraining ambient waters (see also Fig. 5.7.6). However, the repeat sections indicate a large temporal variability. Consequently, as the measurements were taken over a time period of several days, caution is needed when interpreting the volume estimates in the context of spatial changes in transport along the plume axis.

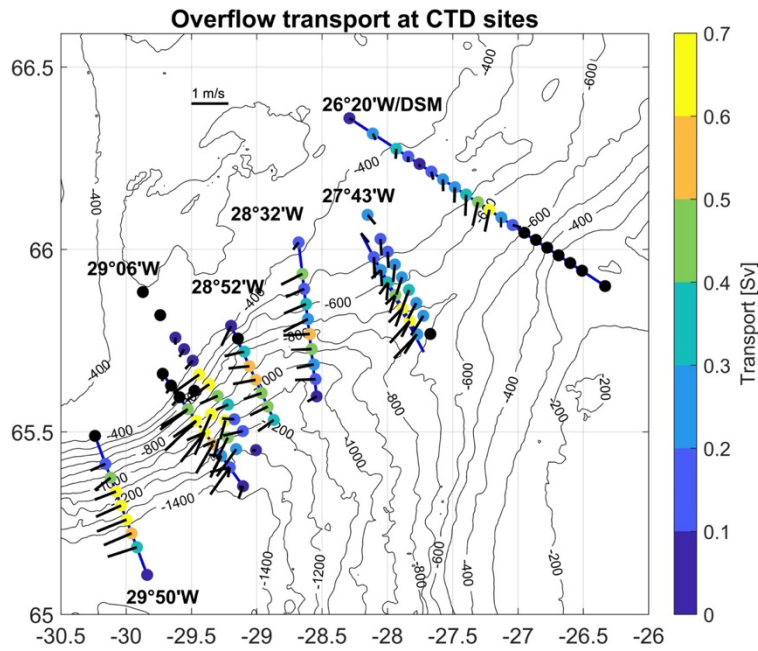


Figure 5.1.10: Transport (color coded) of overflow waters are displayed at each CTD station. When there was more than one station per location, the second (third) realization was plotted slightly shifted to the Northeast. In the calculations, the overflow was defined as those waters exhibiting both a potential temperature below 2 °C and a potential density anomaly of $\sigma_\theta > 28 \text{ kg m}^{-3}$. The black lines indicate the magnitude and direction of the flow velocity of the overflow plume layer.

A YoYo station was conducted between the 18th and the 19th of August 2018 at the center of the main mooring site ~140km downstream of Denmark Strait. The station was comprised of 26 repeated CTD casts (with a duration of 40 min. per cast) at the same location for a total duration of 17 hours. The goal was to i. capture the passage of the overflow at high vertical and temporal resolutions and ii. combine these data with simultaneous temperature microstructure measurements as well data from the surrounding moorings. At the start of the YoYo station, no overflow waters were present (Fig. 5.1.11) with temperatures exceeding 3°C at the sea floor. Temperatures dropped below the 2 °C limit around 8 hours after the start of the station (at 3:30 UTC on 19 August). After that the plume gradually increased its height, reaching a thickness of 150 m at the end of the operations.

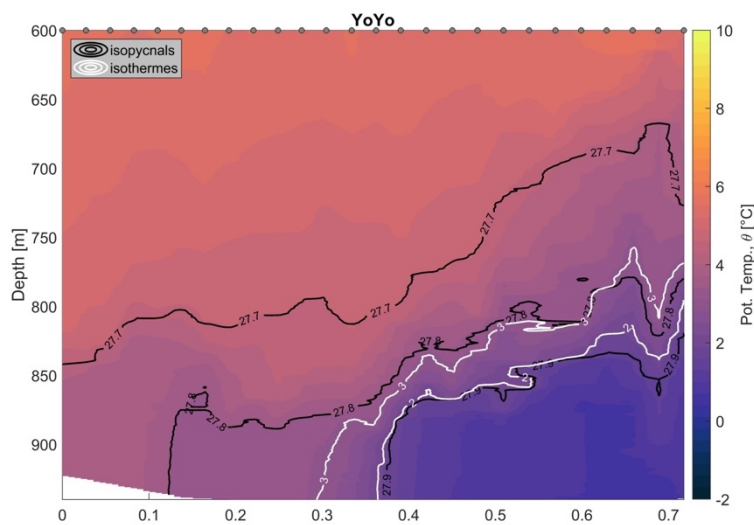


Figure 5.1.11: Potential temperature (°C) measured during the YoYo station as a function of decimal days (x-axis) and depth (y-axis). The 2 °C and 3°C isotherms are given in grey and isopycnals are marked with black. The overflow is characterized by waters with temperature smaller than 2 °C and a potential density of $\sigma_\theta > 27.8 \text{ kg m}^{-3}$.

An indirect way to infer vertical mixing is by characterizing turbulent overturns in density profiles throughout the water column utilizing CTD data. In this method, called Thorpe scales analysis, the unstable parts of observed, vertical density profiles are re-sorted into synthetic, stable ones. The root-mean-square vertical displacement of water particles resulting from the

re-sorting is then used as the scale of turbulent overturns (referred to as Thorpe scales) which linearly scale with the Ozmidov scale (the scale of the largest possible turbulent overturns) – with the latter depending explicitly on dissipation of turbulent kinetic energy and stratification. Thorpe scales were calculated for all casts of the YoYo station for the lower-most 600m of the water column. The results shown in Figure 5.1.12 are preliminary as they still lack several criteria for overturn exclusion. For instance, Thorpe scales in the bottom mixed layer may be unreliable as very small changes in density can create large quite large displacements. Nevertheless, the results clearly indicate a linear increase in time of the depth above the bottom where overturns are first detected (red arrow Fig. 5.1.12) - starting on 19 August 2018 at around 03.30 UTC. This onset of increased number of overturns coincides with the arrival of the plume and its subsequent height increase over time (see Fig. 5.1.11).

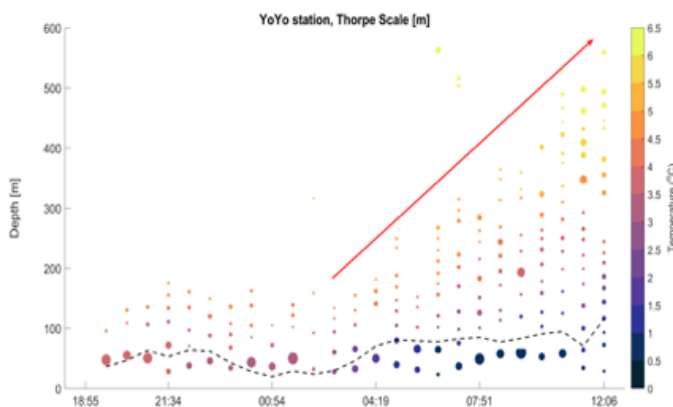


Figure 5.1.12: Scatter plot of Thorpe Scales (width of dots in metres) during the YoYo station for a total number of 26 casts as a function of time (UTC) and water depth. Temperature (°C) is color-coded and the height of the mixed layer is represented with the black dashed line.

5.1.5.2 Working area 2: Scoresby Sund

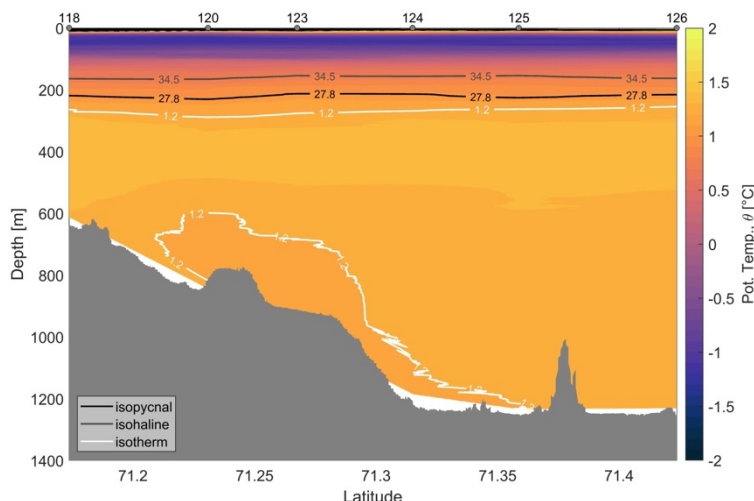


Figure 5.1.13: Transition from outer Scoresby Sund into Nordvestfjord (from South to North), following stations along the grey points with numbers indicating the station numbers.

In Scoresby Sund, CTD work focused on the pathways of warm water of Atlantic origin towards the large glaciers within the fjord system. A section at the fjord’s mouth showed flow into the fjord of waters with temperatures of up to 1.5 °C, located at 300 m depth. Those waters were tracked by hydrographic measurements to the entrance of Nordvestfjord, a narrow fjord system that connects the outer Scoresby Sund to the Daugaard-Jensen glacier. At the conjunction of Scoresby Sund and Nordvestfjord, a complex bathymetry with two islands splits the fjord into three possible gateways for the deep, warm waters (see chart in Fig. 5.8.2).

Temperature, salinity and velocity measurements indicated that the main route of Atlantic Water inflow into Nordvestfjord is located towards the western side of the fjord. Figure 5.1.13 displays the hydrographic properties along this pathway descending from outer Scoresby Sund into the extremely deep Nordvestfjord. The temperature maximum of 1.38 °C is located between 330 and 350 m, while the vertical temperature gradients are very weak below 500 m at the stations located further into the fjord. This results in a thick layer of warm waters we expect to be, if present further in the fjord, in direct contact with the Daugaard-Jensen glacier.

5.1.5.3 Working area 3: Fram Strait

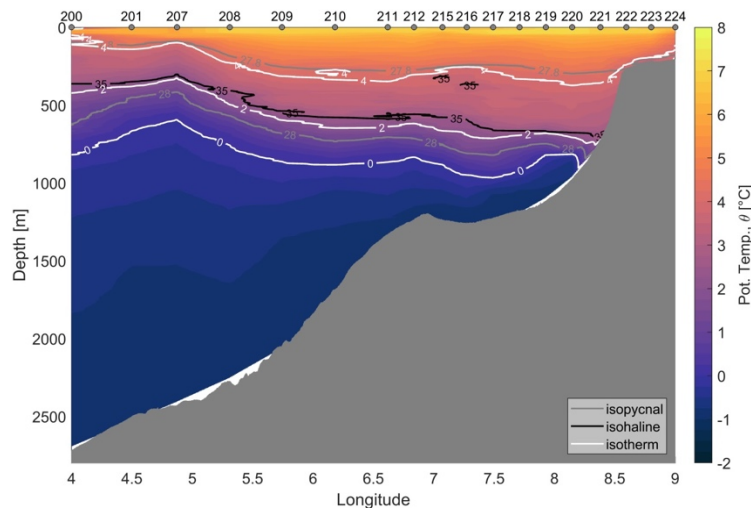


Figure 5.1.14: Potential temperature (color coded) section of the West Spitzbergen Current. Isopycnals, isotherms and isohalines are overlaid. Gray dots and station numbers indicate the position of the CTD stations.

The work in Fram Strait is part of AWI's long-term monitoring programme relying on mooring-based measurements covering the West Spitzbergen Current since 1996. The supporting CTD work consisted of a densely spaced hydrographic line along the mooring line at 79°N extending from 4°E to 9°E (Figure 5.1.14). The warm, saline waters present in the upper 300 m of the water column (temperatures exceeding 4 °C) at the eastern site of Fram Strait close to Svalbard are associated with the West Spitzbergen Current. To the west, their signature fades out, with the upper-ocean isotherms sloping downward to the east indicating a vertically sheared, northward geostrophic flow within the WSC, superimposed by eddy-variability.

5.2. Lowered Acoustic Doppler Current Profilers (LADCP)

Cassandra Ellmer

5.2.1. System and Operation

For the station-based current velocity measurements during MSM76, a pair of 307kHz Lowered Acoustic Doppler Current Profilers (LADCPs) was used, mounted on the CTD rosette. Both instruments run with CPU firmware version 50.40 and have convex heads with 4 beams at 20° angles from the vertical. One instrument, with serial number 22763 (master), was oriented downward-looking. The other, with serial number 22762 (slave), was upward-looking. This configuration was used to survey the entire water column in 8m bins. Power was supplied by an external battery pack mounted on the CTD rosette. This pack was changed after stations 64 and 118. Data collection began anew with each station. After the rosette was back aboard, data

collection was stopped, data was downloaded to a logging computer, and then was immediately uploaded to the server using a memory stick. The system operated as designed on all casts without any issues. Tables 5.2.1 and 5.2.2 show the configuration files for master and slave, respectively.

Table 5.2.1. MASTER configuration file

CR1	Reset to factory settings
WM15	L-ADCP mode
EX11111	Coordinate Transformation
SM1	set to master
SA001	send pulse before water ping
SB0	disable hardware-break detection
SI0	Synchronization interval
SW75	Synchronization delay
TE00:00:01.00	Time per ensemble
TP00:01.00	Time between pings
LP00001	Pings per ensemble
LN014	Number of depth cells
LS0800	Depth Cell size
LF0176	Blank after transmit
LV175	Ambiguity velocity
LW1	Bandwith Control
EZ0111111	Sensor source
CF11101	Flow control
CK	Keep parameters

Table 5.2.2. SLAVE configuration file

CR1	Reset to factory defaults
WM15	L-ADCP mode
EX11111	Coordinate transformation
SM2	Set to slave
SA001	wait for pulse before water ping
SB0	Disable hardware-break detection
ST0300	Slave time out in sec
TE00:00:00.00	Time per ensemble
TP00:00.00	Time between pings
LP00001	Pings per ensemble
LN014	Number of depth cells
LS0800	Depth Cell size
LF0176	Blank after transmit
LV175	Ambiguity velocity
LW1	Bandwith controll (narrow)
EZ0111111	Sensor source
CF11101	Flow control
CK	Keep parameter

[5.2.2 Processing](#)

Each cast was processed with LDEO Software Version IX-13 from <ftp://ftp.ldeo.columbia.edu/pub/LADCP>. It reads the standard Teledyne RDI binary output files from both master and slave as well as a CTD data file processed specifically for LADCP processing, and determines the u and v components of velocity and their depth. The software adjusts for heading, pitch, roll, vertical velocity, and position of the rosette, as well as the sound speed of the water surrounding it. One input to the software is CTD data from the same cast processed with SBE SeaBird Processing Software. The steps are given in Table 5.2.3. The final

output from this processing is a 1 second averaged time series with variables listed in Table 5.2.4. The majority of stations used the processing software without any changes. It was necessary, however, to adjust the software to accommodate unique cast types.

Table 5.2.3. CTD processing steps from .cnv header

```
# datcnv_date = Aug 15 2018 08:50:07, 7.22.4 [datcnv_vars = 11]
# datcnv_in = C:\CTD\CTD_processing\msm76_043_01.hex
C:\CTD\CTD_processing\msm76_043_01.XMLCON
# datcnv_skipover = 0
# datcnv_ox_hysteresis_correction = yes
# datcnv_ox_tau_correction = yes
# wilddedit_date = Aug 15 2018 08:50:08, 7.22.4
# wilddedit_in = C:\CTD\CTD_processing\msm76_043_01.cnv
# wilddedit_pass1_nstd = 2.0
# wilddedit_pass2_nstd = 5.0
# wilddedit_pass2_mindelta = 0.000e+000
# wilddedit_npoint = 100
# wilddedit_vars = prDM t090C c0S/m sbeox0ML/L t190C c1S/m sbeox0Mm/Kg
# wilddedit_excl_bad_scans = yes
# filter_date = Aug 15 2018 08:50:09, 7.22.4
# filter_in = C:\CTD\CTD_processing\msm76_043_01s1.cnv
# filter_low_pass_tc_A = 0.030
# filter_low_pass_tc_B = 0.150
# filter_low_pass_A_vars =
# filter_low_pass_B_vars = latitude longitude prDM
# celltm_date = Aug 15 2018 08:50:10, 7.22.4
# celltm_in = C:\CTD\CTD_processing\msm76_043_01s1s2.cnv
# celltm_alpha = 0.0300, 0.0300
# celltm_tau = 7.0000, 7.0000
# celltm_temp_sensor_use_for_cond = primary, secondary
# loopedit_date = Aug 15 2018 08:50:11, 7.22.4
# loopedit_in = C:\CTD\CTD_processing\msm76_043_01s1s2s3.cnv
# loopedit_minVelocity = 0.250
# loopedit_surfaceSoak: minDepth = 8.0, maxDepth = 20, useDeckPress = 1
# loopedit_excl_bad_scans = yes
# Derive_date = Aug 15 2018 08:50:12, 7.22.4 [derive_vars = 2]
# Derive_in = C:\CTD\CTD_processing\msm76_043_01s1s2s3s4.cnv
C:\CTD\CTD_processing\MSM76_043_01.XMLCON
# binavg_date = Aug 15 2018 08:50:13, 7.22.4
# binavg_in = C:\CTD\CTD_processing\msm76_043_01s1s2s3s4s5.cnv
# binavg_bintype = seconds
# binavg_binsize = 1
# binavg_excl_bad_scans = yes
# binavg_skipover = 0
# binavg_surface_bin = no, min = 0.000, max = 0.000, value = 0.000
# file_type = ascii
```

Table 5.2.4. CTD variables from .cnv header

```
# name 0 = scan: Scan Count
# name 1 = timeJ: Julian Days
# name 2 = latitude: Latitude [deg]
# name 3 = longitude: Longitude [deg]
# name 4 = prDM: Pressure, Digiquartz [db]
# name 5 = t090C: Temperature [ITS-90, deg C]
# name 6 = c0S/m: Conductivity [S/m]
# name 7 = sbeox0ML/L: Oxygen, SBE 43 [ml/l]
# name 8 = t190C: Temperature, 2 [ITS-90, deg C]
```

```
# name 9 = c1S/m: Conductivity, 2 [S/m]
# name 10 = sbeox0Mm/Kg: Oxygen, SBE 43 [umol/Kg]
# name 11 = sal00: Salinity, Practical [PSU]
# name 12 = sal11: Salinity, Practical, 2 [PSU]
# name 13 = flag: flag
```

[5.2.2.1 Deep surface soak](#)

A few stations exhibited a surface soak greater than 20 m depth. The SeaBird processing on those stations subsequently removed all data shallower than 20 m. We processed these stations with a surface soak extending to 30 m to retain data reaching to the surface.

[5.2.2.2 Yo-yo](#)

Station 103 was a so-called yoyo station (see Fig. 5.1.11), where the rosette descends and ascends one position without exiting the water. A new cast began each time the rosette returned to the shallowest depth, which is reflected in the CTD files. However, the LADCP recorded one file for the duration of the yoyo cast since it is a self-recording device. The processing software, by default, considers data from when the LADCP leaves and then nears the surface. Processing the yoyo casts therefore required modifications to the software. We adjusted each LADCP cast start and end time within the processing software to be determined by the start and end time of the corresponding CTD cast file (Table 5.2.5). In this way, each LADCP cast of the yoyo station could be treated separately in the subsequent processing.

Table 5.2.5. Edit start and end time in `set_cast_params.m`

```
%read the CTD file to get start and end time
C=textscan(fopen(f.ctd),...
    '%f %*[^\\n]',...
    'CommentStyle',{ '* Sea-Bird', '*END*' });
JDays=C{1};

%start and end time
p.time_start=datevec(JDays(1)+datenum(2018,00,00,00,00,00));
p.time_end=datevec(JDays(end)+datenum(2018,00,00,00,00,00));
```

[5.2.2.3 Tow-yo](#)

Another style of CTD casts during MSM76 were tow-yo stations. These stations (154, 158, and 159) contain many casts starting and ending roughly 300m above the seafloor with slight variations in position as the vessel moved slowly over a seamount. However, fatal errors occur in the software when the start and end pressures are much greater than the expected zero. Since the casts truly did start with pressures greater than zero, we commented out these error-producing checks to allow processing to continue (Table 5.2.6). Since the software extrapolates all data to the ocean surface, we also edited the output mat file to only include data from the depths that were truly measured according to the CTD (Table 5.2.7).

Table 5.2.6: Edit error when cast doesn't start at surface

```
%{
  if abs(data(1,1)-p.cut)<10
    p.ctdtime=1;
  else
    disp([' WARNING first CTD depth is: ',int2str(data(1,1)), ' [dB]'])
    disp([' WARNING ignore pressure time series '])
    p.ctddepth=0;
    p.ctdtime=0;
    return
  end
%}
```

Table 5.2.7. Edit final data output

```
%only keep the values below start depth
load(sprintf('C:\\LADCP\\processed\\All%03d_%02d.mat',stn,cst),'dr'
)
mindepth=abs(dr.zctd(1));
idx=find(dr.z>mindepth,1);
dr.z=dr.z(idx:end);
dr.u=dr.u(idx:end);
dr.v=dr.v(idx:end);
save(sprintf('C:\\LADCP\\processed\\All%03d_%02d.mat',stn,cst),...
      '-append','dr')
```

5.2.2.4 File Names

Before station 103, the file names included the station number but not the cast number. Station 103, the yoyo, included the cast number in the file name. After station 103, the file name for each cast at a regular station also included the cast number, assumed to be 01. We added an input capability to the software to allow for cast number as well as station number (Table 5.2.8).

Table 5.2.8: Edit to process_cast.m to allow a cast number, cst, following the station number, stn

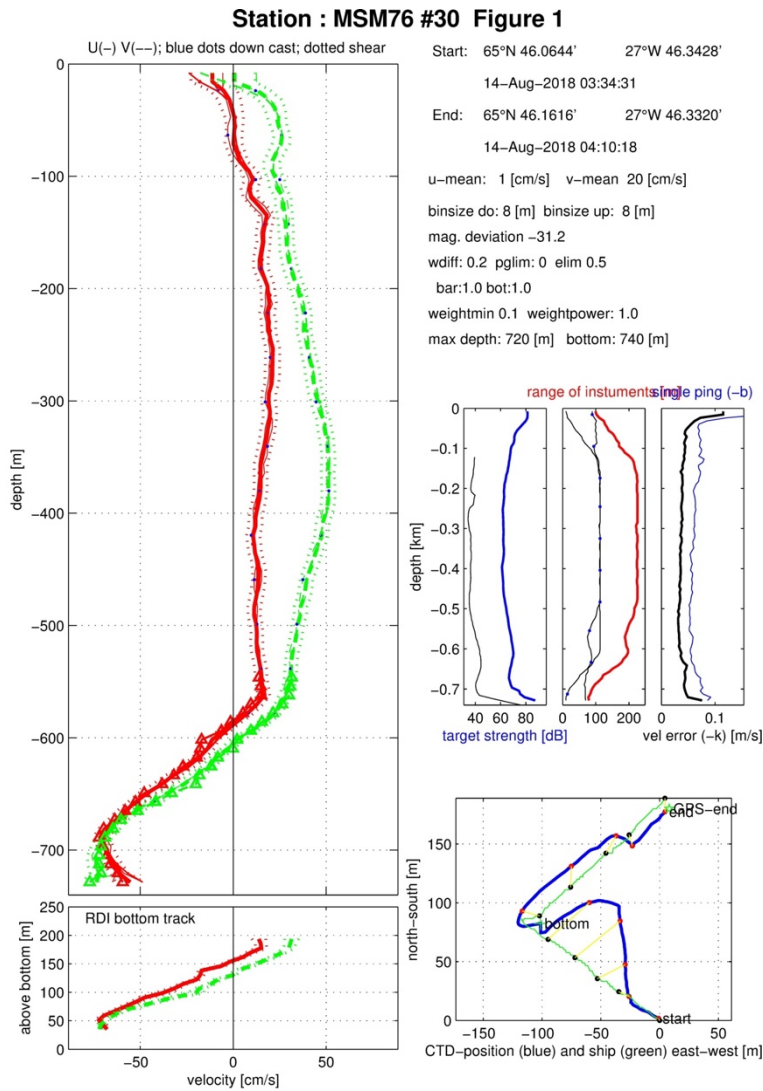
```
function [] = process_cast(stn,cst,begin_step,stop,eval_expr)
.....
%edit to allow for cst
if nargin < 5, eval_expr = ''; end % by default, no variable
overrides
if nargin < 4, stop = 0; end % by default, no debug stops
if nargin < 3, begin_step = 1; end % by default, start from
scratch
```

5.2.2.5 Errors and notes

At station 109, the binary master file was double the size of the binary slave file. The reason is unknown. There does not appear to be an adverse effect on the processed file. Starting at station 172, there were large compass deviations. This is unsurprising since these stations sampled waters around 80°N latitude, close to magnetic north. As the stations move further and further south, the compass deviation decreases, further implying the deviation is due to latitude. At station 208, the operator reported that the binary master file was half the size of the binary slave

file and noted incorrectly set baud rates. The processing software reported similar errors that the mean ping rate and duration differ. However, the rest of the processing does not reveal any issues; it appears similar to other stations in the area. Stations after 228 went only to 800m below the surface. This means the LADCP did not often capture a reliable bottom track. There could be potential inaccuracies in the data.

After processing, there are 14 output figures to help diagnose the quality of the data. The primary figure shows the output u and v components and general information (Figure 5.2.1).

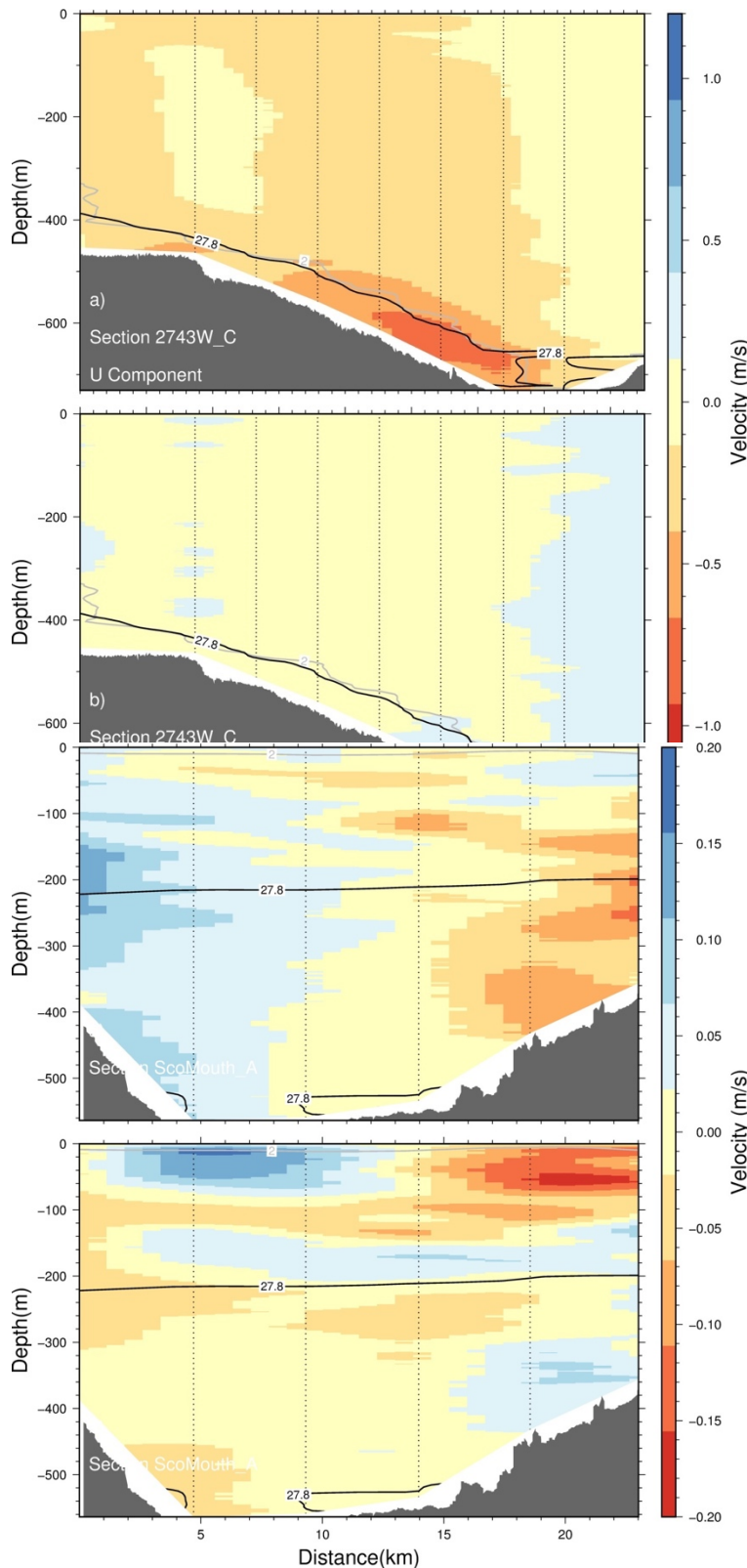


5.2.2.6 [Quality Control](#)

Figure 5.2.1. Sample output from LADCP processing. Left: u and v component; bottom track. Right: basic information; ping information; position.

5.2.3 Preliminary Results

5.2.3.1 Sections



Denmark Strait

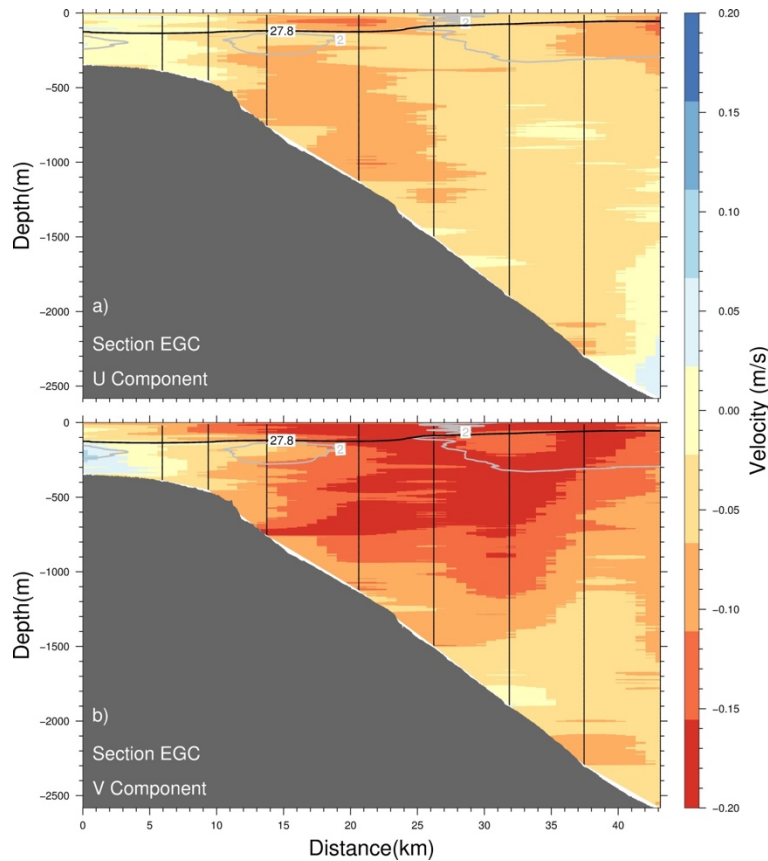
Figure 5.2.3: Velocity section (starting point 27°43'W; see Fig. 5.1.10) in Denmark Strait. In a) positive velocities represent a flow to the east and in b) positive velocities represent a flow to the north. Overlaid in black is the 27.8 kg/m³ density contour and in gray the 2°C temperature contour.

The purpose of the sections in the Denmark Strait is to capture the Denmark Strait Overflow plume. The upper boundary of the plume is marked by 27.8 kg/m³ density and 2°C temperature at depth. As seen in the sample section (Figure 5.2.3), within this defined area is strongly increased westward flow (i.e. along the continental slope of Greenland) exceeding 70 cm/s.

Scoresby Sund

Figure 5.2.4: As in 5.2.3 but for the mouth of Scoresby Sund. The section is displayed from south (distance = 0km) to north (distance = 23 km).

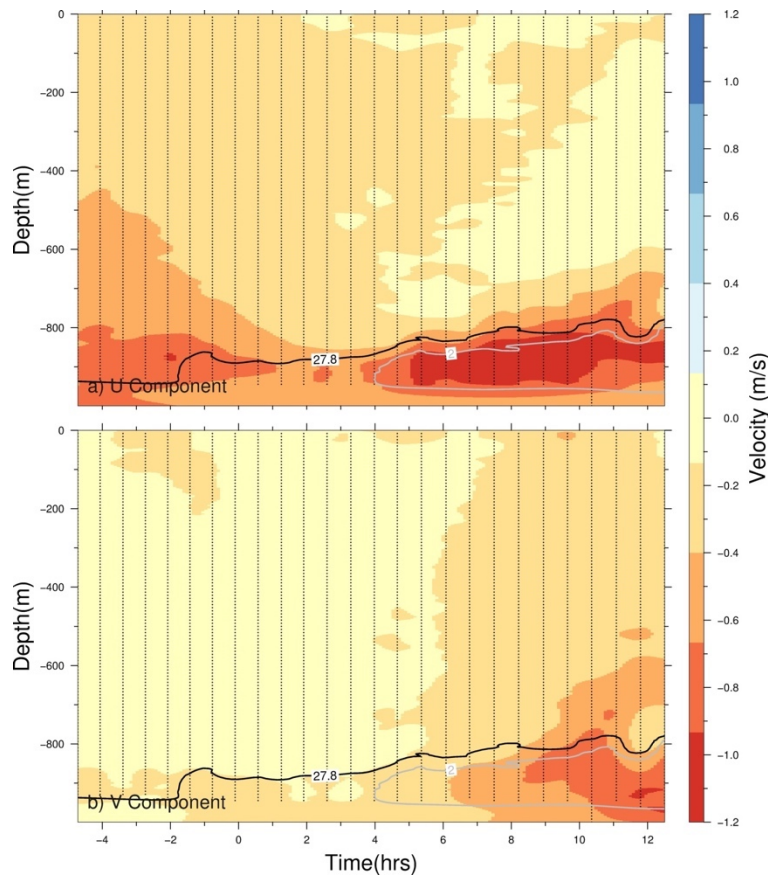
At the mouth of Scoresby Sund, we find westward flow at the northern end of the mouth and southward return flow at the southern end (Figure 5.2.4). Overall, this section implies flow of Atlantic Water into the Sund on the northern edge (with densities exceeding 27.8 kg m⁻³) and a return flow (possibly modified by interaction with the glaciers in Scoresby Sund) at a slightly shallower depth level.



East Greenland Current

Figure 5.2.5: As in 5.2.3 but on the Greenland Shelfbreak.

The purpose of this section across the Greenland Shelf was to capture the East Greenland Current. Here it is well represented with strong northward flow centered over the sloping bathymetry (Figure 5.2.5).



5.2.3.2 Time Series

Figure 5.2.6 Time series of U (East) and V (North) component of the current during the Yoyo cast, station 103. The 2 °C isotherm is given in grey and the 27.8 isopycnal is marked with black. The x axis is labelled with hours before and after midnight.

A YoYo station was conducted between the 18th and the 19th of August 2018 at the center of the main mooring site ~140km downstream of Denmark Strait (see Figs. 5.7.1). The station was comprised from 26 repeated CTD casts (~40min. per cast) at the same location for a total duration of ~17 hours. The goal was to capture the passage of the overflow at high vertical and temporal resolution and combine these data with simultaneous temperature microstructure measurements as well data from

the surrounding moorings. Figure 5.2.6 illustrates the onset of the overflow plume ($T < 2\text{ }^{\circ}\text{C}$ and of $\sigma_{\theta} > 28\text{ kg m}^{-3}$) around 03.30 UTC on August 19, 2018 with core velocities in the westward direction reaching up to 1.2 m/s. The onset of the bottom-intensified plume flow is consistent with the appearance of cold, dense waters at the same point of time (see Fig. 5.1.11). Core

velocities of up to 0.8 m/s are also detected for the southward component of the flow after around 08.30 UTC. This flow components adds up to a maximum absolute current velocity of 1.5 m/s pointing to the downstream, along-bathymetry direction.

5.3 Vessel-mounted acoustic Doppler current profiler (VmADCP) Measurements

Andreas Münchow

We operated two Teledyne RDI sonar system to measure ocean current profiles from about 24 m below the hull of the ship. Both 75 kHz and 38 kHz acoustic Doppler current profilers (ADCP) were operated continuously the entire time without any apparent problems. The 75 kHz (38 kHz) ADCP tracked the bottom to about 1200 m (2500 m) water depth which enabled accurate estimation of ship's speed and direction over ground with "bottom-tracking" pulses. Hence we use the same sonars and their respective geometries to measure both ocean currents with a "water-tracking" pulses relative to the moving ship measured by a "bottom-tracking" pulse. The difference between these two measurements give the absolute, earth-referenced velocity vector provided accurate heading, pitch, and roll data are available to properly remove ship motions and rotations from the measurements.

Data were collected opportunistically during stationary station work, ship maneuvering, and transits when the ship moved at speeds up to 13 knots (about 7.5 m/s). Our work on continental shelves and slopes off Greenland, Iceland, and Greenland was generally within about 1000 m depths and the higher vertical resolution 75 kHz VmADCP (16-m bins to about 650-m depth) was used more frequently than the 38 kHz VADCP (32-m bins to about 1000-m depth). Measurements made within about 15% of the bottom must be discarded on account of sidelobe interference of a 30 degree beam angle from the vertical, that is, in 1000-m deep water, the maximal profiling range is limited to 850-m or less.

5.3.1 Instrument setup and configuration

Each system contains a small array of transducers that project 4 acoustic beams into the water column at nominal 30 degree angles from the vertical. Some of the acoustic energy is scattered back to the transducers and is received in a range-gated form at a frequency that is proportional to the speed at which the scattering particle moves in the direction of the beam. The range gate is determined by the NN (number of bins or range gates considered), NS (length of each of NN bins), NF (length to first bin). All data are collected as single-ping data in beam co-ordinates, that is, no processing is done during the data collection controlled by VmDas Version 1.49 of Teledyne RD Instruments.

Table 5.3.1: Configurations; both BX and NN commands were changed frequently to optimize data collection, storage, and subsequent processing.

Configuration	Command	75 kHz	38 kHz
Bottom-Tracking (1-on, 0-off)	BP	BP1 or BP0	BP1 or BP0
Max. Bottom-tracking depth	BX	variable	variable
Narrow-Band Pings	NP	NP001	NP001
Number of Narrow-Band Bins	NN	variable	variable
Depth of Narrow-Band Bins	NS	NS1600	NS3200
Narrow-Band blanking interval	NF	NF1600	NF3200
Output variables	ND	ND111100000	ND111100000
Ping rate	TP	TP000000	TP000000
Output format (binary beam co-ordinates)	EX	EX00000	EX00000

5.3.2 Navigation Data

All navigational data aboard R/V Maria S. Merian originates from a Seapath 320 unit of Kongsberg. It consists of an inertial navigation system (INS) along with two Global Position System (GPS) antennas mounted on a pole perpendicular to the ship in a top mast. The VmADCP processing uses both altitude, (heading, pitch, and roll) and traditional GPS position data in NMEA-like format. The positional GPS information is written to a file with .N1R that contains UTC time (ZDA), location (GGA and GGL), and vessel speed and heading (VTG) information. The example below originates from 09-Aug.-2018 11:43:52.67 UTC when the ship was at 79:09.90746 N latitude and 062:20.187272 E longitude:

*Table 5.3.2: Navigational data in *.N1R ASCII files in NMEA Format (ZDA, GGA, GLL, and VTG)*

```
$INZDA,114352.67,08,09,2018,,*7D
$INGGA,114352.67,7909.903746,N,00620.187272,E,1,12,0.6,5.14,M,34.66,M,,*7A
$INGLL,7909.903746,N,00620.187272,E,114352.67,A,A*7D
$INVTG,51.36,T,48.85,M,0.7,N,1.3,K,A*36
```

N1R data are collected twice every second.

The attitude information from the INS is written in similar format (\$PRDID), however, the file also contains a time stamp from VmDas (\$PADCP) that also includes the ADCP ensemble number for reference. The example below originates from ensemble 12096 collected on 14-Aug.-2018 at 11:32:21.87 UTC:

*Table 5.3.3: Navigational data in *.N2R ASCII files (Pitch, Roll, Heading).*

```
$PADCP,12096,20180814,113221.87,0.33
$PRDID,+000.18,-000.58,067.37
$PRDID,+000.02,-000.49,067.30
$PRDID,-000.12,-000.39,067.24
$PRDID,-000.22,-000.28,067.19
$PRDID,-000.29,-000.17,067.16
$PRDID,-000.32,-000.05,067.16
$PRDID,-000.32,+000.05,067.18
$PRDID,-000.30,+000.15,067.25
$PRDID,-000.26,+000.22,067.33
$PRDID,-000.20,+000.27,067.41
$PRDID,-000.15,+000.28,067.49
$PRDID,-000.08,+000.26,067.58
$PRDID,-000.00,+000.22,067.67
$PRDID,+000.08,+000.15,067.73
$PADCP,12097,20180814,113226.08,0.33
```

The comma separated columns are pitch, roll, and heading. These are defined as shown in the attached figure that I extracted from the "Alignment Survey Report" by Overath & Sand Surveyors of Rendsburg, Germany (<http://www.overath-sand.de>) dated Oct.-2017.

3.4 Common coordinate reference system on board

Positive X-axis is forward and along the vessel's centreline (Centerline vessel is defined as the line from centre on underside keel at stern to centre on underside keel at bow.)
Positive Y-axis is starboard of centreline
Positive Z-axis is upwards of basis

Theoretical position of COG is the origin of the measurement, at the end the surveyed data are transformed into the system on top of MRU bracket/chassis.

Sign: positive pitch = bow upwards, positive roll = starboard downwards

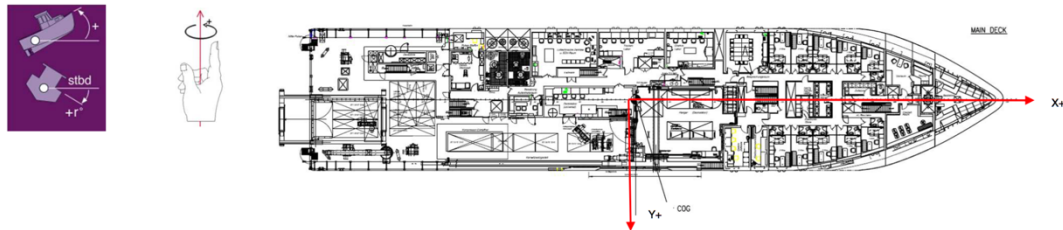


Figure 1 - Common coordinate reference system

1	Description 17.632.01	Lara Gutiérrez	Thore Overath	Thore Overath	02 November 2017
Rev	Survey Documentation	Prepared	Checked	Approved	Date

2017-11-02_Documentation__Rev1_add_survey_overath.xlsx

Page 11

Figure 5.3.1: Definition of the ship's co-ordinate system with pitch and roll sign conventions from official FS Maria S. Merian Alignment Survey Report.

5.3.3 Processing

Processing of raw, single-ping VmADCP (.ENS) and navigational (.N1R and .N2R) data is done via a linear sequence of Unix shell commands for file management and fortran codes for numerical transformations of raw binary to averaged and screened ASCII data. The single-ping data in beam co-ordinates are transformed into averaged earth co-ordinates using (a) standard geometric transformations that use pitch, roll, and heading data from navigational devices and (b) non-standard averaging of many individual pings into larger temporal sampling intervals.

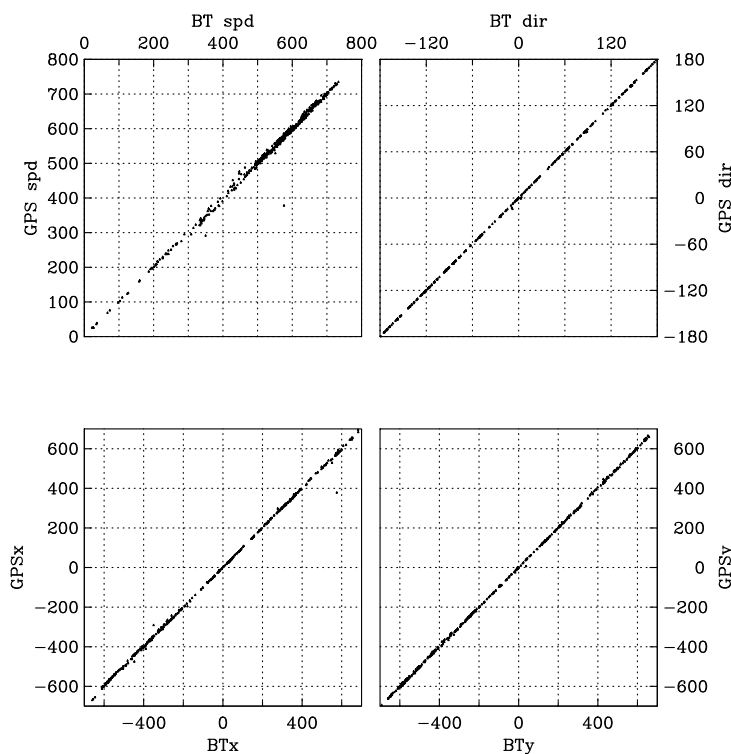
For each fixed sampling interval of, say, 2 minutes all pings that fall into this interval are sorted from largest to smallest velocity. All data from those pings that result in the largest and smallest 20% of the sorted velocities are removed from the averaging procedure. The remaining 60% of the pings within the sampling period are then averaged arithmetically for all variables of interest such as velocity, echo intensity, and correlation. This procedure removes, we surmise, undetected outliers from the averaging procedure and moves the probability density distribution of the single ping data towards a Gaussian distribution. Directional and tilt data are averaged using directional statistics, that is, for example, the average heading HeadAvg is

$$\text{HeadAvg} = \text{atan2} \{ \text{sum}[\sin(\text{head})], \text{sum}[\cos(\text{head})] \}$$

where "sum" is the arithmetic sum over all sensor readings head(i) within the averaging interval where i=1,N. For ocean current monitoring at sea I used a 2 minute averaging interval with east and north velocity components for "sorting" and "indexing" while for data calibration at sea I used a 30 minute average with east and north bottom-tracking velocity components for "sorting" and "indexing." The indexing and sorting is done by Numerical Recipe routines "hpsort" and "indexx", respectively, as described in Press et al. (1992). More details and an application to the 75 kHz ADCP aboard USCGC Healy can be found in the Appendix of Muenchow et al. (2007) while Fortran codes can be provided on request via muenchow@udel.edu

5.3.4 Calibration

ADCP calibration includes finding the physical misalignment of the transducer as well as a scaling constant that relates to beam forming characteristics, speed of sound uncertainties, etc. Finding these coefficients, we use two independent measurements to accurately estimate the ship's absolute velocity vector. The first uses a specific bottom tracking ping of the ADCP while the second uses the ship's navigation system, e.g., GPS. Comparing these two methods when the ship operates in water shallow enough for the sonar to detect the bottom (<1200 m for the 75 kHz and ~2400 m for the 38 kHz systems), we can accurately calibrate the instrument for misalignment and scaling of the transducers, e.g., Joyce (1989).



More specifically, we here use all available bottom-track data between 11.-August and 9.-September 2018 at latitudes from 63 N to 80 N between Iceland, Greenland, and Svalbard. We require that each 30 minute average satisfies ALL the following criteria for each ping: 1. Bottom-tracking Error Velocity < 2 cm/s (4-beam solutions only); 2. Bottom-tracking correlations > 245 counts;

Figure 5.3.2: Comparison of the vessel's velocity vector determined from 75 kHz ADCP bottom tracking (BTx, BTy) and GPS longitude (GPSx) and latitude (GPSy) after calibration. Bottom panel shows cartesian co-ordinates while top panel shows speed and direction.

Fig. 5.3.2 shows the resulting 512 ensembles each of 30-minute duration after a uniform misalignment angle $\alpha = -47.259$ degrees and a scaling constant $\beta = 1.0053024$ is used to rotate the ADCP bottom-tracking (BT) velocity components into the geographic (GPS) reference. The angle β describes the deviation (positive counter-clockwise) of the ADCP-reference relative to the GPS system, that is, the ADCP co-ordinate system must be rotated by $-\alpha$ to coincide with the GPS system. While the large velocity range of ± 700 cm/s gives the impression of an almost perfect fit, a more meaningful and quantitative intercomparison is shown in Fig.-5.3.3 that shows a histogram of the deviations from the "perfect fit" for both east (BTx-GPSx) and north (BTy-GPSy) components that are interpreted as errors in either BT or GPS measurements. About 90% of the 514 values are contained within the error interval of $[-8, +4]$ and $[-6, +6]$ cm/s for east and north components, respectively. It thus appears that the north component appears symmetric about zero with a Gaussian-like distribution, however, the east component contains an uncertainty bias of 2 cm/s due to a secondary negative peak in the histogram near 5 cm/s, that is, the bottom track in east-west components reads low on many occasion by 5 cm/s relative to GPSx estimates. I note that a 1 m/s GPS position error translates into a 2-3 cm/s random error in GPS-derived ship velocity for a 30-minute average that contains about 180 independent samples or pings.

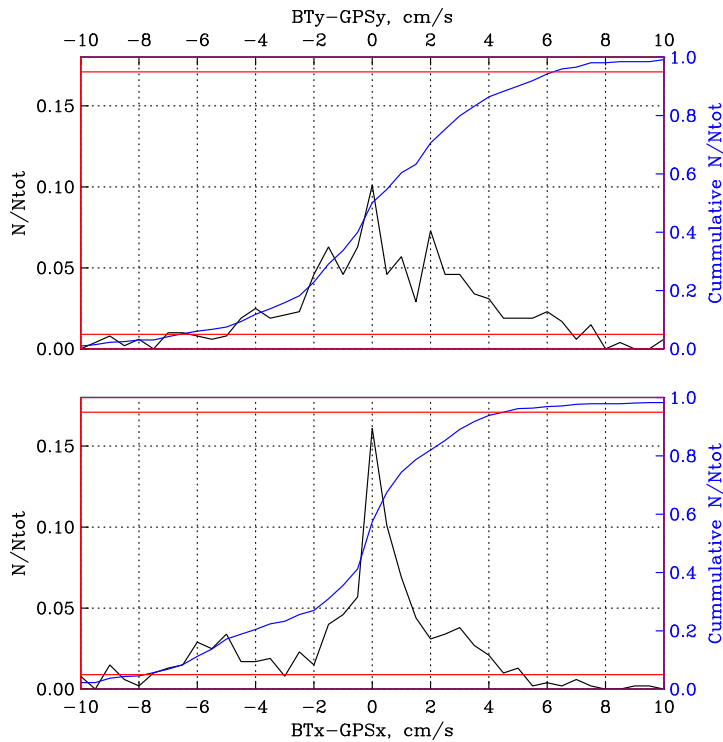


Figure 5.3.3: Histogram of uncertainty estimate of 30-minute averaged ADCP bottom-track velocity components (BTx, BTy) relative to GPS-derived velocities after uniform data calibration. Red lines refer to 5% and 95% of the cumulative (integrated) histogram shown in blue.

The large number of calibration data allows evaluation of the calibration coefficients (alpha, beta) as a function of time throughout the expedition. Fig.5.3.4 shows daily values for the 75 kHz that I overlay with daily averaged temperatures T measured at the transducer head for each ping. The visual correlation is stunning and the linear regressions:

$$\begin{aligned} \text{beta}(T) &= 1.02726 - 2.4036 \times 10^{-3} * T && \text{for 75 kHz} \\ \text{beta}(T) &= 1.02786 - 2.6817 \times 10^{-3} * T && \text{for 38 kHz} \end{aligned}$$

explains 87% and 94% of the variance of 24 and 27 daily samples for 75 and 38 kHz systems, respectively. The misalignment angle alpha does not show this temperature dependence, as the linear regression explains little of the variance. The outlier on Day-27 (27 Aug.) can be ignored, because the ship moved through a storm when winds and waves exceeded 50 m/s and 4 m, respectively, south of Iceland.

I could not confirm the initial suspicion that an incorrectly estimated speed of sound causes this variability as I experimented with a number of different implementations. Hence I speculate that the beam forming of the phased-array ADCP depends on temperature. More specifically, I hypothesize that the angle from the vertical of the 4 beams deviates from their nominal 30 degree angle.

Calibrated and processed data were distributed to the science party as 2-minute and 30-minute averages in ASCII format for use in other projects. The format is explained with a read.me file reproduced as Table 5.3.4 to allow further processing, screening, and plotting in a variety of forms shown in the next section.

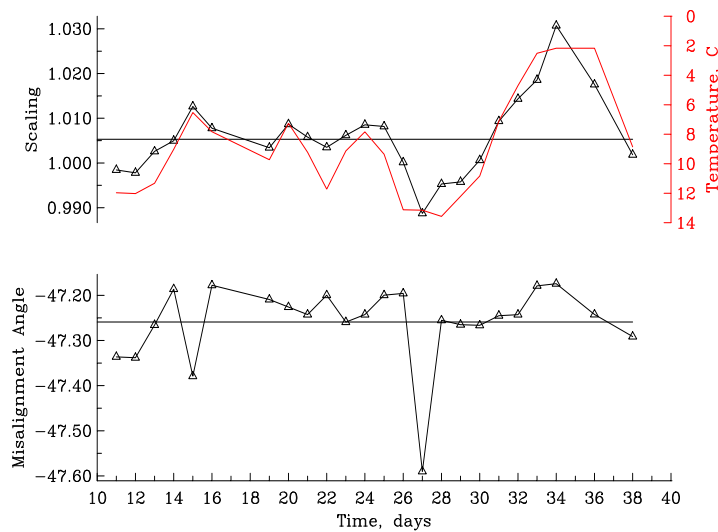


Figure 5.3.4: Time series of calibration coefficients from 10 August through 8 Sept. 2018 (black lines) and temperature. The spike at -47.6 misalignment originates from data collected during winds exceeding 50 m/s when wave heights exceeded 4 m.

5.3.5 Preliminary Results

VmADCP data were collected opportunistically as other science operations took place concurrently. I here show three examples from Denmark Strait near 66° N.

Denmark Strait

Figs. 5.3.5 and 5.3.6 show the velocity vectors across the sill of the Denmark Strait as profiled by the 75 kHz VmADCP during 22 hours of hydrographic station work on 14./15. Aug. 2018. Currents are strongly sheared in the horizontal by more than 1.2 m/s in 5 km as currents over the slope off Iceland exceed 0.8 m/s to the north and those over the slope off Greenland exceed 0.5 m/s to the south. The 10°C warm northward flow represents the North Icelandic Irminger Current (Pickart et al., 2017) which appears largely barotropic with little vertical shear (Fig. 5.3.6). In contrast, the 5°C cooler southward flow represents the East Greenland Current and, perhaps, North Icelandic Current merging into it (Håvik et al, 2017). This southward flow has some vertical shear ($5 \times 10^{-4} \text{ s}^{-1}$) as maximal speeds occur within about 100-m off the bottom near km-50. The large upslope velocity near the bottom at km-60 to the west warrants special scrutiny. While this may be a signal related to the spilling of dense water over the sill, I cannot exclude some sidelobe interference. Note that the 30 degree beam angle of the ADCPs prevents penetration within about 75-m off the bottom at 600-m water depth. Complementary lowered ADCP measurements do not have this short-coming.

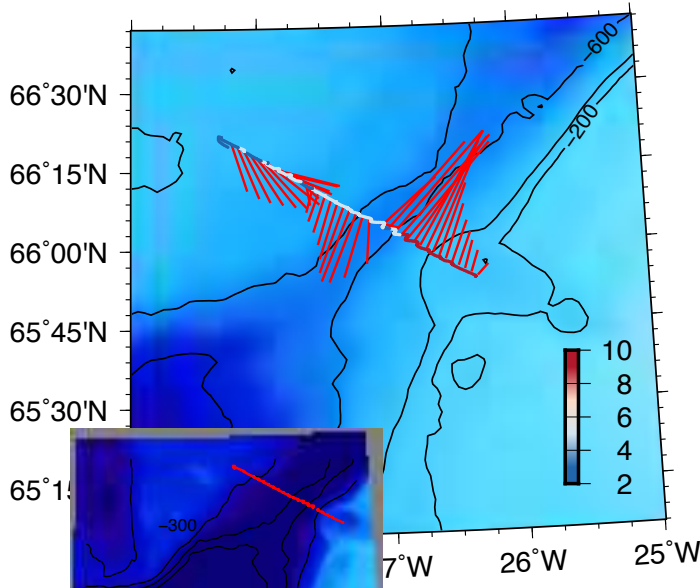


Figure 5.3.5: Velocity vectors near the sill location of the Denmark Strait at about 85-m below the surface (red). Black contours indicate 200, 400, and 600 m bottom contours while the color scale indicates surface temperatures measured along the ship track by thermosalinograph. See Figure 5.3.6 for the full transect data.

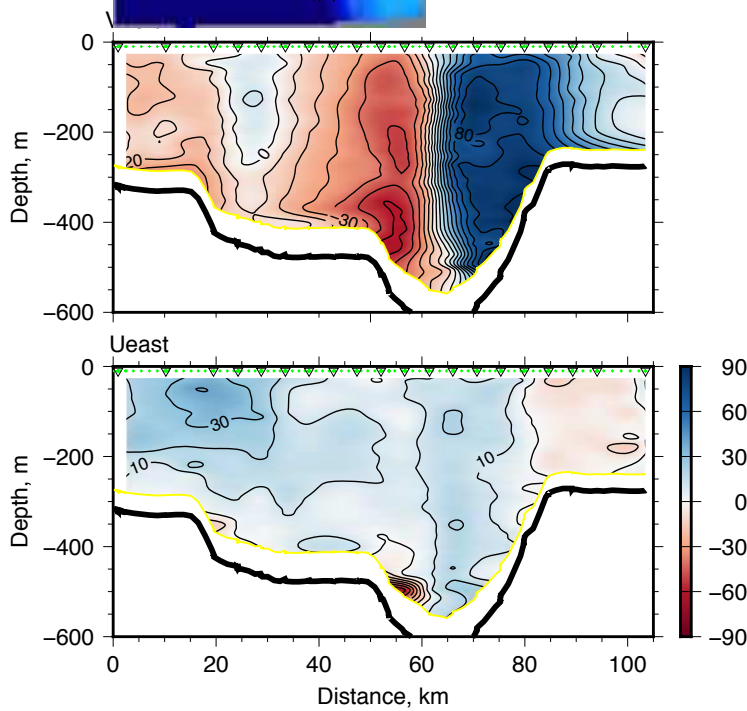


Figure 5.3.6: Section across Denmark Strait in along-shore (top, positive northward) and across-shore (bottom, positive eastward) shore directions. Color bar indicates velocity in cm/s; view is towards the north. Small green dots indicate ADCP profile locations as 5 minute averages. Triangles near the surface indicate concurrent CTD station locations for cast #031 (14. Aug. 2018, 07:33 UTC) near km-100 to cast #050 (15. Aug. 2018, 05:09 UTC). See Fig-5.3.5 for map.

Nevertheless, the lateral shear $\partial_y U \approx 2.4 \times 10^{-4} \text{ s}^{-1}$ is a robust feature. It estimates relative vorticity that exceeds the planetary vorticity $f \sim 10^{-4} \text{ s}^{-1}$. Hence the flow is strongly nonlinear.

We tracked the cold and dense overflow to the south of Denmark Strait with a number of sections at different angles, locations, and times that are described elsewhere in this document. I here only show an early non-synoptic summary of VmADCP current vectors from data collected between 12.-20. August 2018 at 300-m depth in Fig. 5.3.7

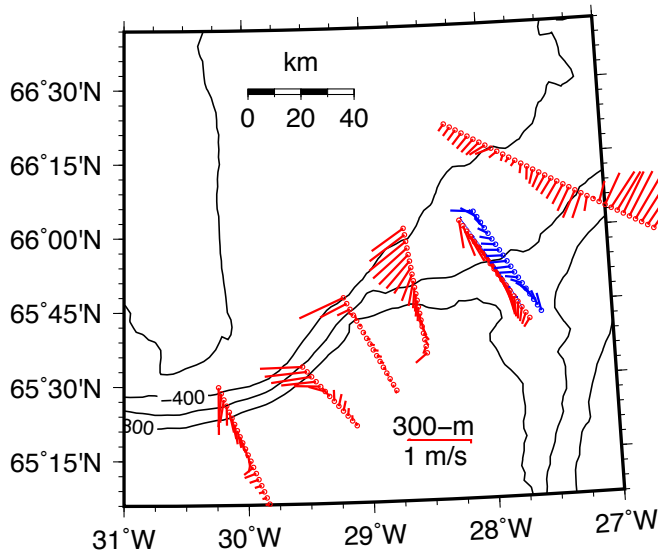


Figure 5.3.7: Current vectors at 300-m depth over the continental slope off Greenland to the south of Denmark Strait between 12-20 August 2018. The blue section is a repeat of the section to the south and is offset for visibility. Data are neither fully calibrated nor processed. Nevertheless, flows to the south are intensified over the slope, but vary in both speed and direction at daily time scales that are not always fully resolved.

5.4 Profiling Microstructure (Chipod)

Stylios Kritsotalakis

5.4.1 System and operation

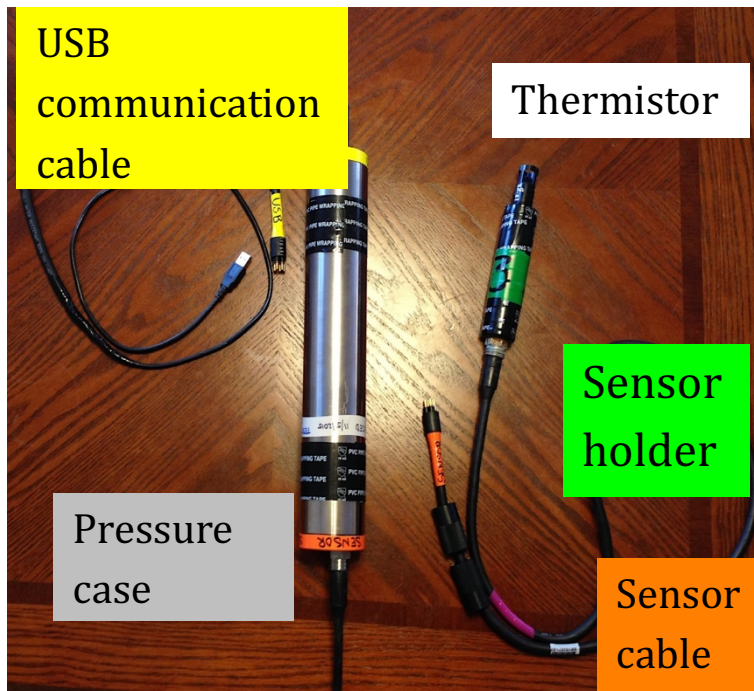


Figure 5.4.1: Picture showing a complete Chipod set (courtesy of Jonathan Nash, OSU). Each Chipod consists of a pressure case that has 4-pin female wet connect bulkhead connector on each end, and a 2-pin male to 4-pin male connector cable, a sensor holder, and a thermistor. The 4-pin male USB connector is used to download data from the Chipod.

Chipods are self-contained devices that measure temperature at a rate of approximately 100Hz using fast-response FP07 Thermistors. For this cruise the Chipods were provided from Jonathan Nash (nash@coas.oregonstate.edu) of the Ocean Mixing group from Oregon State University (OSU).

A chipod consists of a pressure case with electronics powered by 2 Lithium D-cell batteries and the thermistor that is attached to the pressure case with a cable. The unit has no on/off switch, but is “ON” whenever the sensor is connected to the pressure case, and “OFF” whenever the cable is removed. The pressure case needs to be oriented vertically, as it measures accelerations of the CTD in addition to the temperature.

The sensors themselves need to sense an undisturbed stream of fluid passing over the thermistor tip. Therefore, it is important that the upward-looking sensors are positioned above all other instruments and Niskin bottles, ideally near the outer rim of the rosette. Sensors should be mounted as far from the frame of the rosette and any other instruments approximately 1 inch above the bottom of the rosette to avoid damaging the thermistor on recovery (Fig. 5.4.2).

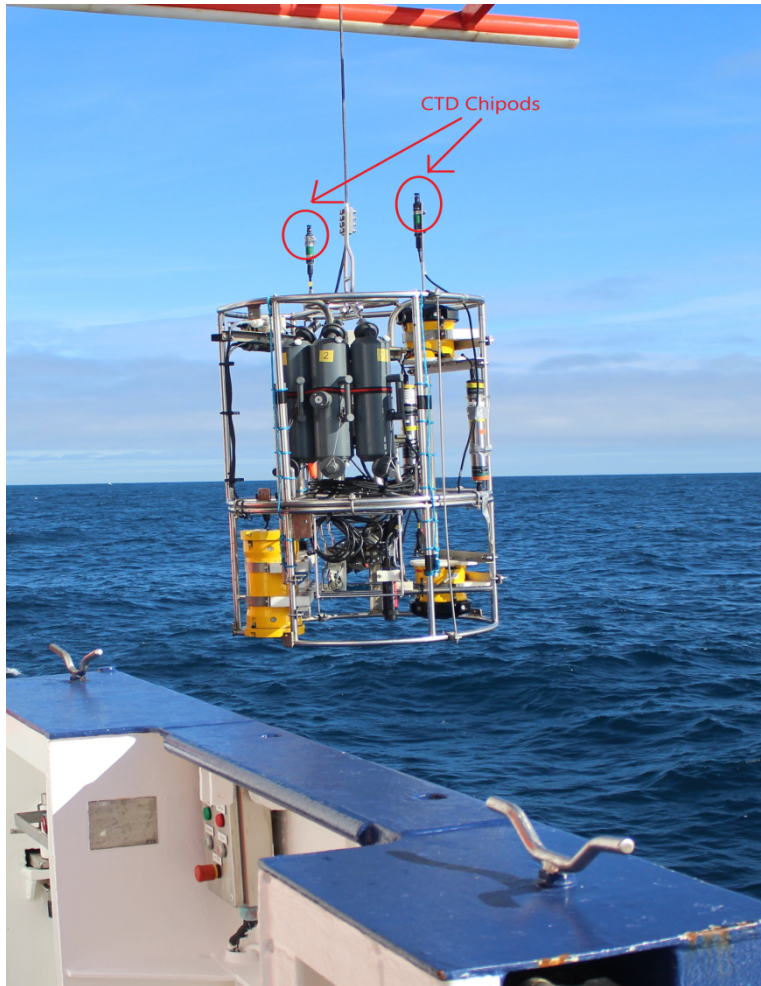


Figure 5.4.2: The CTD χ -pod being deployed during the MSM76 cruise downstream of the Denmark Strait Sill. In this configuration, there were 2 sensors at the top of the rosette.

5.4.2 Raw data

The chipods were attached to the CTD rosette and used during hydrographic sections at the working area of Denmark Strait, recording temperature, dT/dt and acceleration (horizontal and vertical). The raw data from the YoYo station that was conducted at the center of the main mooring area approximately 120km downstream of the Denmark Strait Sill are clean and of good quality. They are in good agreement with the processed CTD data and show the arrival of low temperatures of the overflow water starting approximately at 03.00.

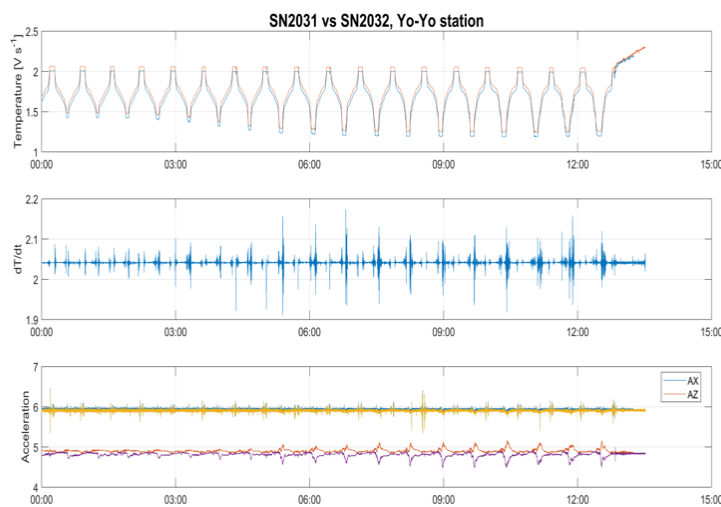


Figure 5.4.3: Example of Chipod raw data from the two sensors (SN2031 and SN2032) during the YoYo station that took place at the center of the main mooring area 120 km downstream of the Denmark Strait Sill. Temperature (V/s), dT/dt and acceleration (horizontal and vertical) are plotted from top to bottom for a 13h period of the station.

5.5: Surface Current Measurements using the Wave Monitoring System

Sunke Macarena Trace-Kleeberg

5.5.1 System Operations

A **Wave Monitoring System II (WaMoS® II)** Version 3.15.1 (156) is installed on R/V Maria S. Merian. This system remotely observes the sea surface by analyzing the spatial and temporal evolution of *sea clutter* in X-Band radar images. The WaMoS provides live information on the actual sea state with wave parameters such as significant wave height, peak wave period, peak wave length and wave direction. The measurements can also be used to derive of the surface current speed and direction.

In this regard, it is a unique system, as conventional current measurement techniques such as satellite altimetry provide only the geostrophic component of surface currents at much coarser resolution while ADCP based measurements are typically limited to subsurface currents only. The intention during the MSM76 cruise was to analyze the surface current data provided by the WaMoS System to determine if this system provides valid underway measurements of surface current.

The WaMoS system consists of hardware and software components. The hardware components are comprised of a standard marine X-Band radar, a FURUNO NAVnet C-MAP NT radar mounted onto the foremast was used during MSM76; the WaMoS II A/D converter and a standard PC. “WinWaMoS”, the specially developed control program, captures and stores the sequence of radar images of the sea surface. This also includes radar test routines, configuration facilities, wave analysis and the display, storage and data handling routines. The wave and current data are displayed graphically on the PC as well as being made available as a text output, in data files and/or remotely.

Throughout the expedition the system was running on automatic recording, taking 33 images with an approximate update rate of 2 minutes (1 minute interval and 1 minute duration). Table 5.5.1 below shows nominal the accuracy of current parameters from the WaMoS system as stated by the manufacturer.

Table 5.5.1: Accuracy of surface current parameters (Source: OceanWaveS)

Surface Current Parameter	Accuracy
Speed	±0.2 m/s
Direction	±2°

One limitation is that wind speeds greater than 3 m/s are needed in order for the backscatter from the sea surface to produce good quality data (Hessner et al., 2017, Hessner et al., 2018 and OceanWaveS). Water depth also needs to be supplied as input to the system so that it can determine wave characteristics in the correct regime (shallow or deep water waves).

During mooring recovery operations (see section 5.7), the echo sounders were switched off so as not to interfere with the hydrophone communication to the acoustic releaser. Therefore during these time periods there is a gap in the WaMoS data.

5.5.2 Preliminary Findings

The aim was to assess how well the WaMoS can determine surface currents. In the following, the VMADCP (see section 5.3) will be used as a reference in this regard. The VMADCP has its shallowest bin at 32m, so there is a gap of data in the top layer. This certainly makes comparisons to the WaMoS-derived velocities at the sea surface challenging, especially when strong vertical stratification near the sea surface or shallow mixed layers should be accompanied by strong decoupling of surface and subsurface currents. In the following, various data sets are compared to the WaMoS, such as wind speed, VMADCP-derived velocities, and vessel speed to validate the surface current measurements.

5.5.2.1 WaMoS-derived surface current and wind speed

Assuming that the surface flow can be described by Ekman dynamics (steady state), the surface current would be expected to be rotated by 45° to the right of the wind direction. Following this simple assumption, in this section the relationship between WaMoS-derived surface currents and wind speeds – observed by R/V Merian's meteorological station (chapter 6) is analyzed.

Contrary to the usual meteorological convention, for comparison with the surface currents the wind vectors in Fig. 5.5.1 are rotated by 180° to indicate the direction the wind blows to. Both WaMoS and wind data arrows correspond to 10-minute averages and every tenth vector is plotted (Figs. 5.5.1 and 5.5.2).

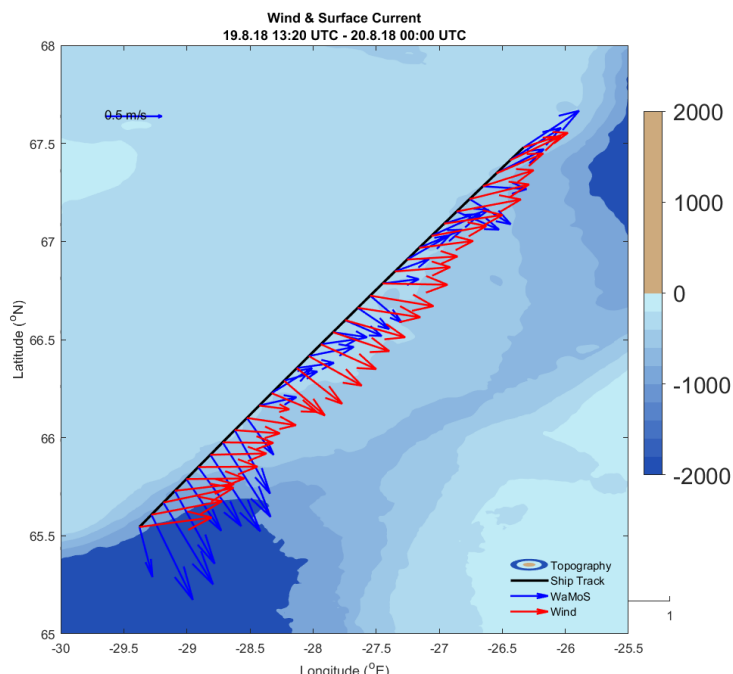


Figure 5.5.1: Comparison of wind (red) and surface current (blue) vector for transit on the 19.8.18 till 20.8.18. Ship track from south to north (black line). Seafloor topography contoured underneath.

At the beginning of the track in Denmark Strait (Fig. 5.5.1) the wind (red arrows) blow at an angle relative to the surface currents (blue arrows) that is broadly consistent with Ekman dynamics. As the ship crosses the shelf break to shallower water the wind direction changes slightly and the surface current direction also alters. The blue current vectors begin to describe

clockwise rotating circles ($66.2^\circ\text{N} - 66.7^\circ\text{N}$ and $66.8^\circ\text{N} - 67.2^\circ\text{N}$). This change could be due to the wind no longer being the dominant forcing and another process is defining the surface flow such as an eddy.

The data for the return transit shows a very different pattern (Fig. 5.5.2), this casts doubt on the previous conclusions. Here there is a time period where the wind and surface current are offset by almost 180°. The magnitude of some of the WaMoS determined surface currents are also rather large (1.4 m/s from 10:08 to 10:44 around 67N and -26E).

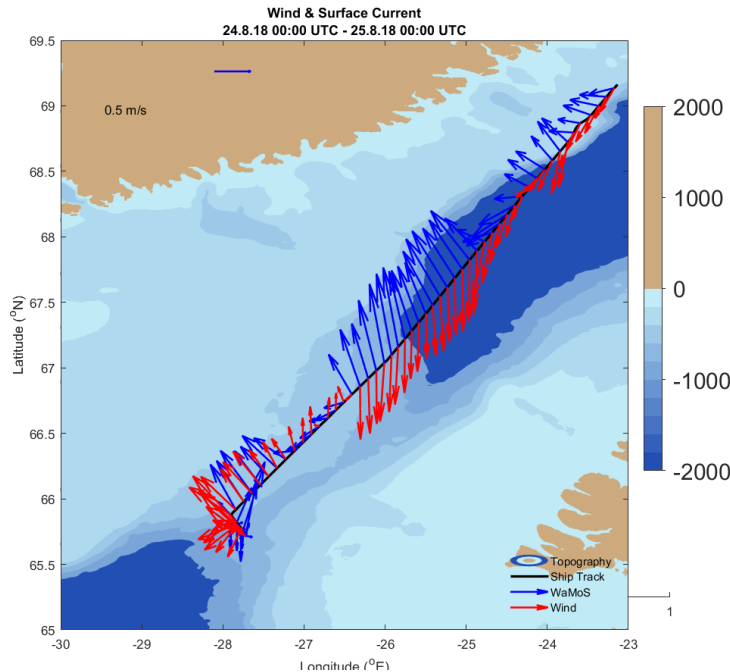


Figure 5.5.2: Comparison of wind (red) and surface current (blue) vectors on the 24.8.18 to the 25.8.18. Ship trip (black line) from the north to south. Topography contoured underneath.

Further time periods need to be analyzed to determine more definitely how the wind and WaMoS surface current are related.

5.5.2.1 WaMoS data compared to VMADCP-derived velocities

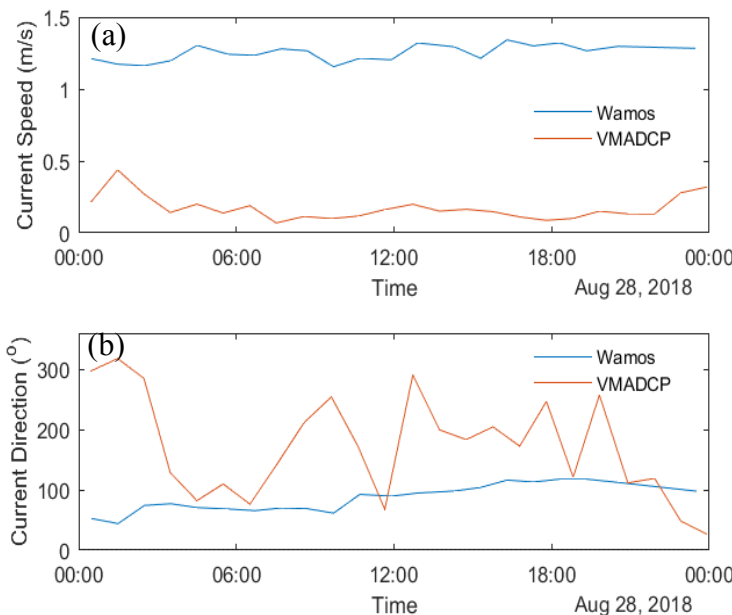
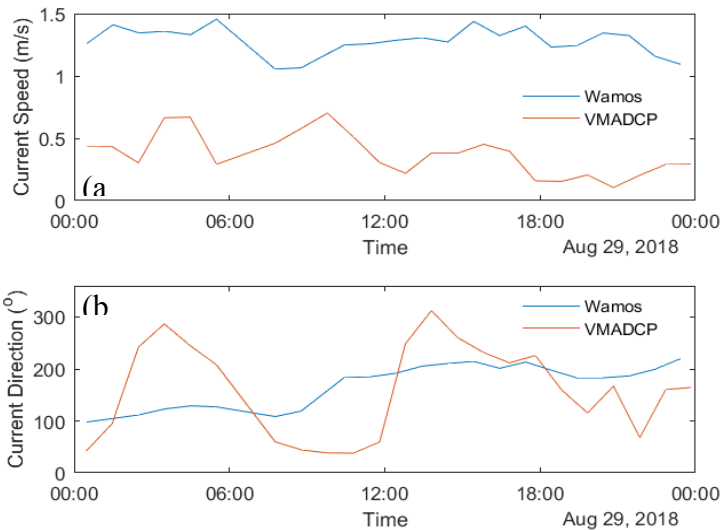


Figure 5.5.3: Comparison between WaMoS (blue) and VMADCP (red), (a) current speed and (b) current direction for the 28.08.18.

The VMADCP measures subsurface current, with its shallowest bin being at 32m. This has been used to compare with the WaMoS surface current measurements. Figs. 5.5.3 and 5.5.4 show this comparison for selected data sets, which were acquired whilst on transit around the south coast of Iceland on the 28 and 29.08.18 (see ship track in Fig 1.1).

Both figures clearly show huge discrepancies between the two data sets. Whereas WAMOS-inferred currents exceeds 1 m s^{-1} consistently throughout the data set, with rather stable directions, the VMADCP ones are much smaller (most smaller than 0.4 m s^{-1}), with current directions changing over time strongly. It is unlikely, that the discrepancies can be explained in



terms of ocean dynamics, e.g. caused by large vertical velocity shear which would be resulting in a complete decoupling of the surface and subsurface flows.

Figure 5.5.4: Comparison between WaMoS (blue) and VMADCP (red), (a) current speed and (b) current direction for the 29.08.18

5.5.2.1 WaMoS-derived velocities compared to the vessel movement

Noticing the large discrepancies between the WaMoS and VMADCP-derived velocities, and realizing the high degree of consistency between the VMADCP and LADCP throughout the cruise (not shown), we subsequently test, whether the vessel movement may have contaminated the WAMOS-derived velocities. For this, the correlation between vessel motion and the inferred current speed was tested. First a histogram of the vessel speed was computed (Fig. 5.5.5) to define which measurements were taken during stations (speeds < 0.3 knots) and which were taken during transits (speeds > 0.4 knots). For this, a 0.3 kn limit was chosen as a definition for being on station, rather than 0.0 kn, to account for the fact that the vessel drifted multiple times during CTD casts with speeds of up to 0.3 kn. Additionally, the WaMoS data set was cleared of measurements that were taken both when the wind speed was too low (< 3 m/s; which is when the radar backscatter signal becomes too low), and when there was no depth measurement being fed to the system (often due to mooring work, when the echosounder was switched off).

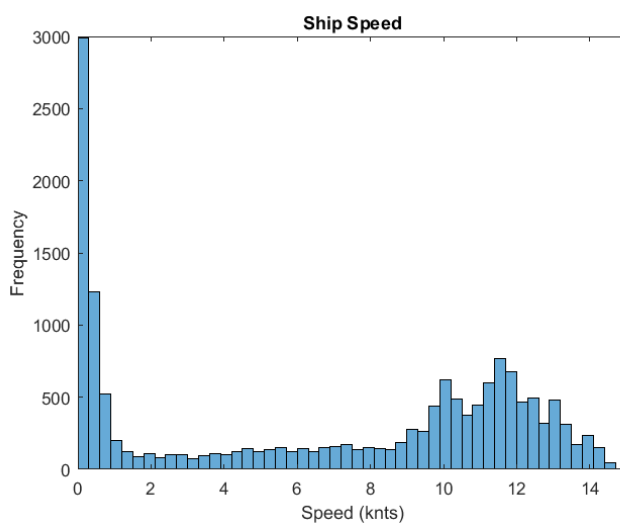


Figure 5.5.5: Histogram of the vessel speed during the MSM76 cruise (Bin width: 0.3 knots).

Hourly averaged underway data-derived current velocities were then plotted as a time series together with the vessel speed (Fig. 5.5.6).

There is substantial visual agreement between both time series. This impression is confirmed by means of statistics, as linear correlation coefficients are found to amount to 0.57 for raw data and 0.67 for hourly averaged data.

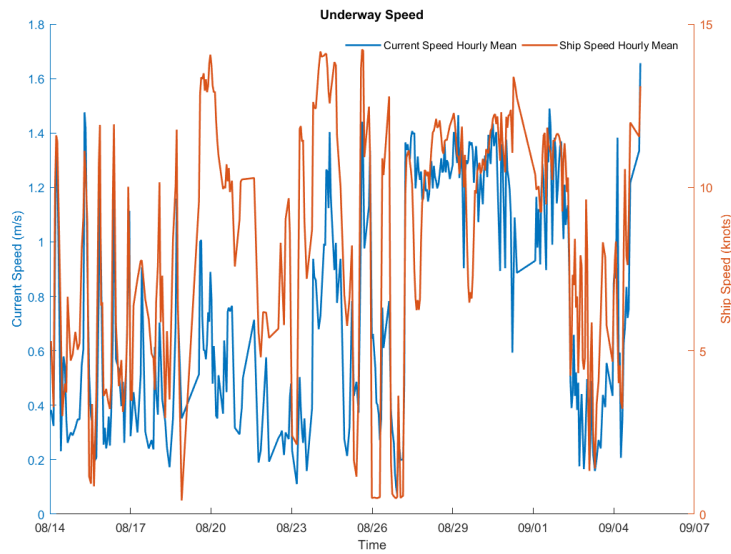


Figure 5.5.6: Comparison of hourly mean underway ship speed (red) and WaMoS-derived current speed (blue). Mind the different velocity scales.

Both visual inspection of Fig. 5.5.6 and statistics suggest there to be a linear relationship between the two data sets. This suggests that there is a direct contamination of the WaMoS determined surface currents by the vessel motion, possibly caused by some kind of misalignment in the WaMoS system. While we were unable to

clarify the exact origin of the high correlation between the two data sets, at least it is plausible to assume, that the WaMoS-derived currents can't be used in the present form for scientific investigations of ocean surface currents.

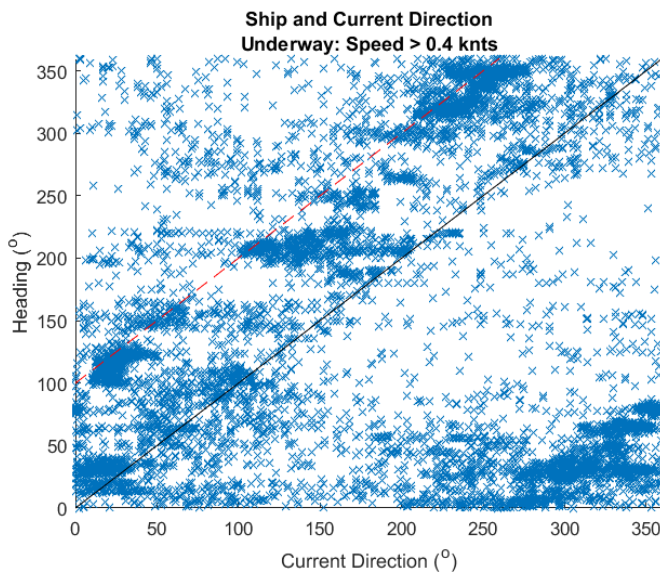


Figure 5.5.7: Comparison between underway ship heading (direction) and WaMoS current direction (blue crosses). The black line indicates a slope of one and passes through the coordinate origin ($x=y=0$).

As well as plotting ship speed, ship heading was also compared to the WaMoS data (Fig. 5.5.7). The scatter plot seems to show a high density of points at the bottom left corner where ship heading is close to 0° and the surface current is between 250 and 360° . A straight line (black)

has been superimposed with a slope of 1. By eye, the plot is suggestive of there being an accumulation of points along a line (red line) parallel to the black line (red dashed). This could again be an indication that the contamination by the vessel movement is seen in the WaMoS determined surface current. Further investigations are required to establish whether corrections can be made such that this data set can be corrected for the vessel motion to become useful for oceanographic studies on ocean currents.

5.5.2.2 WaMoS and Ice

In Scoresby Sund (research area 2) and in the region around the 79N glacier (research area 3) we encountered icebergs and sea ice. Due to the high reflectivity of the radar signal from the ice the determined wave parameters and likely also the current measurements were impeded.



Table 5.5.2: Surface current, wave parameters and metadata

Date	2018/09/03
Time	21:26:00
Latitude	79.612186 N
Longitude	-16.397985 E
Absolute Wind Speed	3.3 m/s
Significant Wave Height	1.5 m
Surface Current Speed	0.3 m/s
Surface Current Direction	132.00°

Figure 5.5.8: Picture taken from on board on the 03.09.18 at 21:26

The picture shown in Fig. 5.5.8 was taken on the 3 September aboard R/V Merian. The Table 5.5.2 shows the meta data, significant wave height and current parameters for the time when picture was taken. It can be seen that the sea surface is very flat with the few ripples being created by the movement of the vessel. This disagrees with the significant wave height of 1.5 ms⁻¹ that is shown by the WaMoS system (1.5 m). As the system is obviously unable to measure the wave parameters in the presence of sea ice, we assume that the surface current velocities can't be reliably inferred either.

5.5.3 Data Management

Data began to be saved in DSHIP on 2018/08/13 at 13:14:00. It is available every 2 minutes until the 2018/09/10 at 17:56 and has been saved as a *.dat file and a *.mat structure. Table 5.5.3 below shows the wave and current parameters recorded, their units and their formats.

Table 5.5.3: WaMoS data variable and meta data saved from cruise MSM76

Column	Name	Units	Format
1	Date		yyyy/mm/dd
2	Time		HH:mm:ss
3	Latitude	Degrees [°]	xx.xxxxxx
4	Longitude	Degrees [°]	xx.xxxxxx
5	Depth	Meters [m]	xxx.x
6	Absolute Wind Speed	Meters per second [m/s]	xx.x
7	Absolute Wind Direction	Degrees [°]	xxx.xxx
8	Ship Heading	Degrees [°]	xxx.x
9	Ship Speed	Knots [kn]	x.xx
10	Current Direction	Degrees [°]	xxx.xxx
11	Current Speed	Meters per second [m/s]	x.x

5.5.4 References

- Hessner, K., El Naggar, S., Strass, V., Krägefsky, S., & Witte, H. (2017). Evaluation of X-band MR surface and ADCP subsurface currents obtained onboard the German research vessel Polarstern during ANT-XXXI expedition 2015/16. *Oceans*.
- Hessner, K., El Naggar, S., von Appen, W., & Strass, V. (2018). WaMoS II: Radar-based measurements of surface waves and currents.
- OceanWaveS, *Wave Monitoring System: Operating Manual and Installation Guide*. Lüneburg: OceanWaveS.

5.6 Hydrographic underway measurements

Sayed Mubashshir Ali

5.6.1 System operation and preliminary results

R/V Maria S. Merian is equipped with Reinseewasserversorgungssystem (RSWS) which takes in water from the sea surface continuously to be available for measurements of water temperature, and conductivity at a 1 second interval during the duration of the expedition. Specifically, the sea surface conductivity and sea surface temperature (SST) were measured by a thermosalinograph (TSG), from which from which sea surface salinity (SSS) was inferred. There are two separate, identical measurement systems (MC1, MC2) which alternatively carry out the measurements during 12 hour-long intervals. The systems are alternatively used, with the one system being in use, while the other is being cleaned and flushed. The depth of the sensors ranges between 6-7 m depending vessel's draft (depending ultimately on the weight of the fuel on board). Both of the TSG sensors packages are SBE 45 Micro TSG and have serial numbers 333 (MC1) and 690 (MC2) respectively.

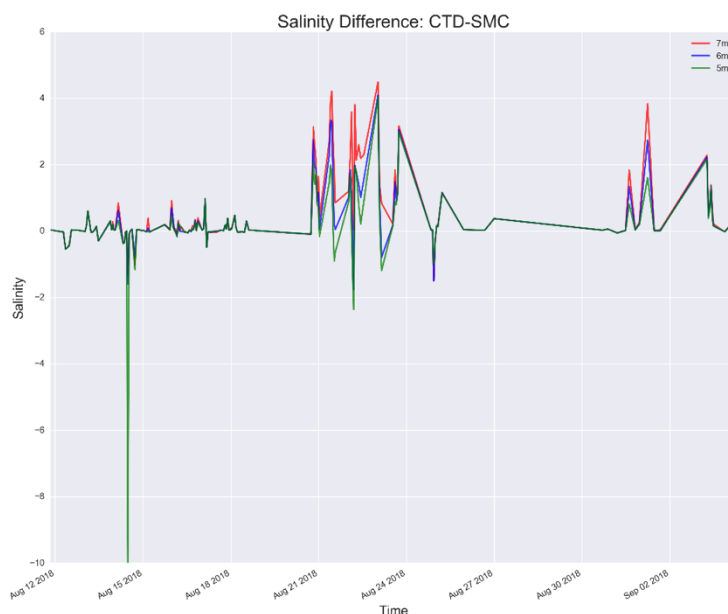


Figure 5.6.1.1: Differences between lowered CTD and thermosalinograph measurements for SSS

In order to study the accuracy of the data, a comparison of the salinity and temperature differences between the lowered CTD system and the TSG was made. We found, that the highest correlation was obtained when using lowered CTD measurements obtained at 6 m depth, for which the results are shown in Figs. 5.6.1 and 5.6.2. The mean SSS difference (CTD-TSG) was +0.318 PSU and SST difference were -0.074 °C. The

standard deviation in the SSS and SST differences were 0.790 PSU and 0.576°C, respectively.

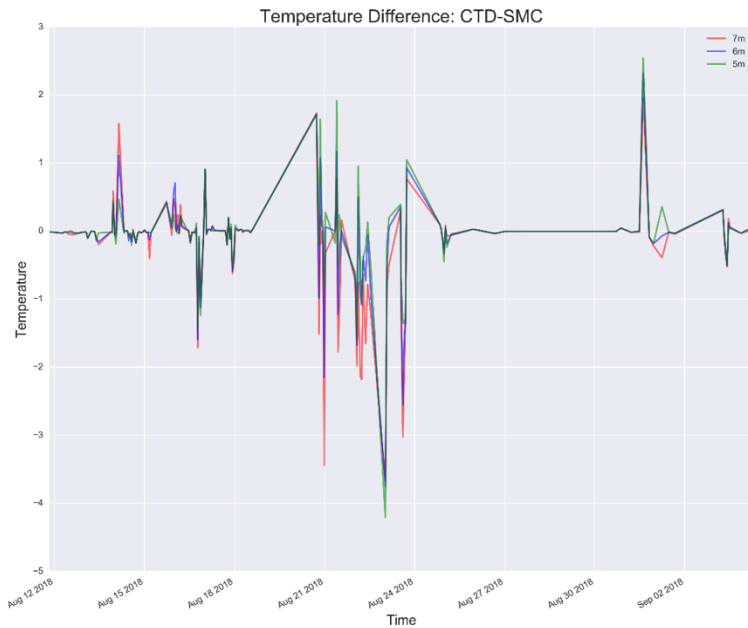


Figure 5.6.1.2: Difference between lowered CTD and thermosalinograph measurements for SST

The SSS measured for the whole duration of cruise by the TSG of the ship ranged between 29.79 and 35.41 psu. Particularly low values of salinity were observed in Scoresby Sund. Fig. 5.6.3 shows the difference in SSS between the lowered CTD and the TSG as a function of geographical position, with the largest difference observed in Scoresby Sund. Further analyses indicated the pronounced SSS difference were mostly seen in the regions having a high vertical

gradient in salinity (not shown), such that a slight difference in observation depth between the CTD and TSG can result in a significant difference in salinity. We assume coastal glacial freshwater runoff and submarine glacial melt to have resulted in sharp, shallow salinity gradients in Scoresby Sund, which made comparisons between the two systems highly uncertain in this fjord. The SST measured for the whole duration of cruise ranged between -1.43 and 10.05 °C.

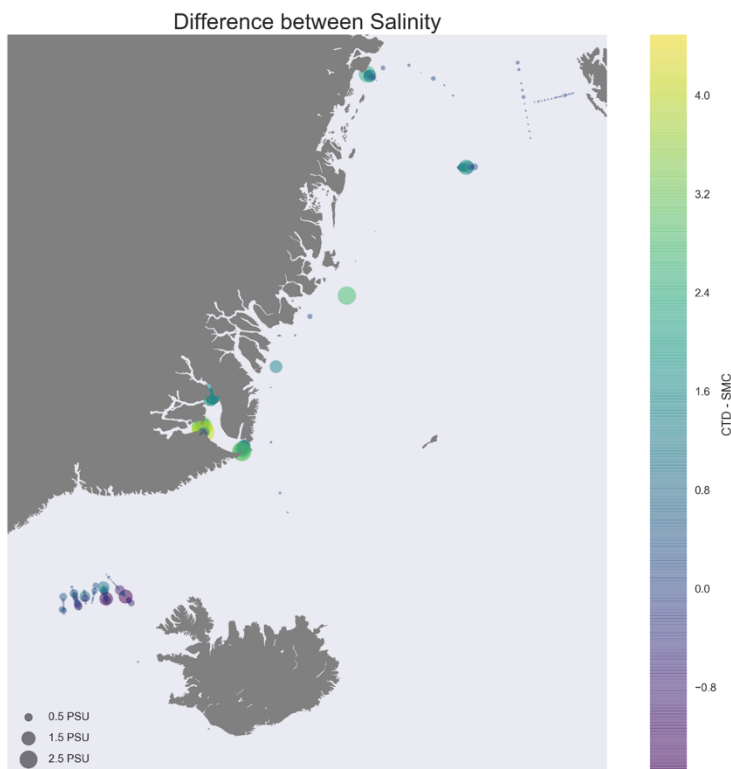


Figure 5.6.3: Geographical distribution of the differences between salinities measured by the lowered CTD and vessel's thermosalinograph (TSG). The differences are particularly large in the regions with low SSS near the coast due to fresh water runoff & glacial melt, causing a pronounced, shallow vertical salinity gradient in the surface waters.

5.7. Moorings

Stylianos Kritsotalakis and Frederike Benz

During the MSM76 cruise a total number of 14 moorings were successfully recovered and a total number of 16 moorings were successfully deployed. The following chapter includes all information about recoveries and deployments in the research areas Denmark Strait (Tables 5.7.1 and 5.7.4), Iceland-Faroe Ridge (Table 5.7.2), Fram Strait (Tables 5.7.3 and 5.7.7), Scoresby Sund (Table 5.7.5) and 79-North-Glacier (Table 5.7.6), as well as preliminary results from the Denmark Strait recoveries.

5.7.1 Recoveries

Denmark Strait

Table 5.7.1: Recovered moorings in Denmark Strait (sill and south of the sill).

Mooring No.	Recovery date	Time UTC	Latitude	Longitude	Depth m
DS-2-17	15.08.2018	8:59	66°07.276' N	27°16.852' W	565
DS-28-17	24.08.2018	18:25	65°50.850' N	27°50.346' W	700
DS-27-17	24.08.2018	18:53	65°52.790' N	27°54.320' W	600
DS-B-18	25.08.2018	18:08	65°32.236' N	29°33.142' W	697
DS-F-18	25.08.2018	18:47	65°33.760' N	29°30.376' W	692
DS-D-18	25.08.2018	20:25	65°32.473' N	29°18.558' W	971
DS-E-18	26.08.2018	11:19	65°28.843' N	29°36.570' W	929
DS-A-18	26.08.2018	12:00	65°28.367' N	29°36.023' W	1145
DS-C-18	26.08.2018	13:50	65°27.642' N	29°21.191' W	1145

A total number of six moorings were deployed southern of the sill of Denmark Strait between the 12th and 13rd of August 2018 (DS-A-18, DS-B-18, DS-C-18, DS-D-18, DS-E-18 and DS-F-18). The same moorings were recovered during this cruise between the 25th and 26th of August 2018. These short-term moorings are part of the TRR181 project and were deployed to detect the energy transfers across scales on the Denmark Strait Overflow plume.

To monitor the Denmark Strait overflow at the Denmark Strait sill, two mooring positions have been occupied since 1996 (RACEII). The DS-2-17 was deployed in 2017 during the cruise 64PE426 aboard R/V Pelagia. During the current cruise the mooring DS2-2017 was recovered and redeployed on the 15th of August 2018.

The moorings DS-27-17 and DS-28-17 were deployed during the cruise 64PE426 aboard R/V Pelagia, approximately 45 km downstream of the sill of Denmark Strait. During the current cruise, these moorings were recovered on the 24th of August 2018. They are part of the project RACEII and were deployed to detect the temporal variability of the already accelerated plume.

Iceland-Faroe Ridge*Table 5.7.2: Recovered Pressure Inverted Echo Sounders (PIES) at the Iceland-Faroe Ridge (Western Valley).*

Mooring No.	Recovery date	Time UTC	Latitude	Longitude	Depth m
WICE-P2-16	29.08.2018	07:32	64°17.191' N	12°26.698' W	459
WICE-P1-16	29.08.2018	09:32	64°27.078' N	12°03.342' W	400

To monitor the overflow east of Iceland the PIES WICE-P2-16 and WICE-P1-16 were deployed in the Western Valley (channel of the Iceland-Faroe Ridge) in 2016 during the cruise POS503 with R/V Poseidon. During the current cruise these PIES were recovered on the 29th August of 2018.

Fram Strait*Table 5.7.3: Recovered moorings in Fram Strait.*

Mooring No.	Recovery date	Time UTC	Latitude	Longitude	Depth m
F5-17	06.09.2018	15:52	79°1.261' N	5°40.395' E	1931.5
F3-17	07.09.2018	6:17	78°59.815' N	7°59.044' E	1073.3
F2-18	07.09.2018	7:53	78°59.954' N	8°18.907' E	800.4

To monitor the inflow of the Atlantic Water towards the Arctic Ocean, a total number of five long-term moorings were deployed in the West Spitsbergen Current. During the current cruise, three of those were recovered between the 6th and the 7th of September 2018.

5.7.2 DeploymentsDenmark Strait*Table 5.7.4: Deployed moorings in Denmark Strait (sill and downstream of the sill).*

Mooring No.	Deployment date	Time UTC	Latitude	Longitude	Depth m
DS-C-18	12.08.2018	19:53	65°27.600' N	29°19.170' W	1145.5
DS-A-18	12.08.2018	20:40	65°28.339' N	29°34.712' W	1145
DS-E-18	12.08.2018	22:44	65°28.537' N	29°34.205' W	929.5
DS-B-18	13.08.2018	12:34	65°33.772' N	29°31.665' W	697.4
DS-F-18	13.08.2018	12:58	65°34.274' N	29°30.412' W	692.5
DS-D-18	13.08.2018	15:05	65°32.602' N	29°17.803' W	971.5
DS-2-18	15.08.2018	19:40	66°07.294' N	27°16.729' W	565.6

Scoresby Sund

Table 5.7.5: Deployed moorings in Scoresby Sund.

Mooring No.	Deployment date	Time UTC	Latitude	Longitude	Depth m
SCO1-1	22.08.2018	16:13	71°16.970' N	25°9.879' W	638.1
SCO2-1	22.08.2018	17:45	71°13.855' N	25°17.986' W	36.9
SCO3-1	23.08.2018	12:25	70°21.252' N	21°59.736' W	416.2

A total number of three moorings were deployed in the fjord Scoresby Sund to detect the interaction between ocean circulation and marine terminating glaciers between the 22nd and 23rd August 2018 (SCO1-1, SCO1-2 and SCO1-3).

79N Glacier

Table 5.7.6: Deployed mooring next to the 79N Glacier.

Mooring No.	Deployment date	Time UTC	Latitude	Longitude	Depth m
79NG-2	03.09.2018	18:04	79°40.159' N	16°53.876' W	262.3 m

As a part of the project GRACE the mooring 79NG-2 was deployed on the 3rd of September 2018 to detect the interaction between ocean and marine terminating glaciers.

Fram Strait

Table 5.7.7: Deployed moorings in Fram Strait.

Mooring No.	Deployment date	Time UTC	Latitude	Longitude	Depth m	Comments
F1-19	07.09.2018	13:10	79°00,00' N	8°32.557' E	238	
F2-19	07.09.2018	14:50	78°59.994' N	8°19.728' E	783	
F5-18	08.09.2018	8:16	78°59.985' N	5°40.079' E	2091	
F4-OZA	08.09.2018	14:51	79°9.988' N	6°19.962' E	1418	deployed twice
F3-18	09.09.2018	6:16	78°59.988' N	7°59.718' E	10723	

5.7.3 Mooring Casualties

There was an unsuccessful attempt to recover the moorings **DS-23-17** on the 15th of August 2018 and the DS-26-17 on the 25th of August 2018. Both moorings were equipped with one conventional RCM. The moorings did not include a releaser (on purpose), therefore we tried to recover them with a wire equipped with grapnels Both attempts to recover the moorings failed.

The **DS-23-17** was deployed on the 19th September 2017 during the cruise 64PE426 with R/V Pelagia at 66°02.87'N and 26°59.67' W and at a depth of 631 m. The **DS-26-17** was also deployed in 2017 during the cruise 64PE426 with R/V Pelagia at 65°57.38'N and 28°01.73'W in 543 m depth on the 19th of September 2017.

In addition, we tried to recover the mooring **79N2-2** next to the 79-North-Glacier. We could not reach it because it the bay blocked by sea ice. The mooring 79N2-2 was deployed on the 23 September, 2017, during the cruise PS109 with R/V Polarstern at 79° 34.01'N 19° 27.83'W at 476 m.

Furthermore, we tried to recover the mooring **F1-16** on 07 September, 2018, in the West Spitsbergen Current, but it was lost, probably due to fishery. The mooring F1-16 was deployed on the 24 July, 2016, during the cruise PS100 aboard R/V Polarstern at 79° 0.01'N and 008° 32.51'E at a depth of 346 m.

Moreover, the mooring **F4-OZA** was first deployed on 8th of September 2018. It was then detected that the mooring was too long, so that it needed to be recovered again. It was then deployed correctly for a second time during the same day.

[5.7.4 Preliminary results from Denmark Strait recoveries](#)

[5.7.4.1: Hydrographic measurements](#)

The measurements at the sill of Denmark Strait obtained by mooring DS2-17 (Fig. 5.7.1) are expected to show water mass characteristics associated with the Denmark Strait Overflow. Indeed, temperatures at a depth of 543 m primarily fluctuate around 0°C with rare excursions to values above 1°C, while salinity exhibits values around 34.9 psu (Fig. 5.7.2).

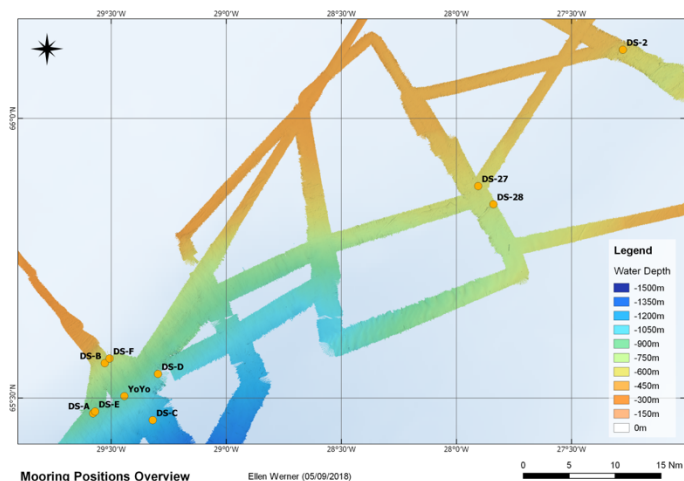


Figure 5.7.1: Overview Map of the moorings positions where the contour lines indicate the bathymetry. DS-2 is located at the Denmark Strait Sill whereas the mooring pair DS-27 and DS-28 and the mooring array consisting of DS-A, DS-B, DS-C, DS-D, DS-E and DS-F are located approximately 45 and 140 km downstream, respectively.

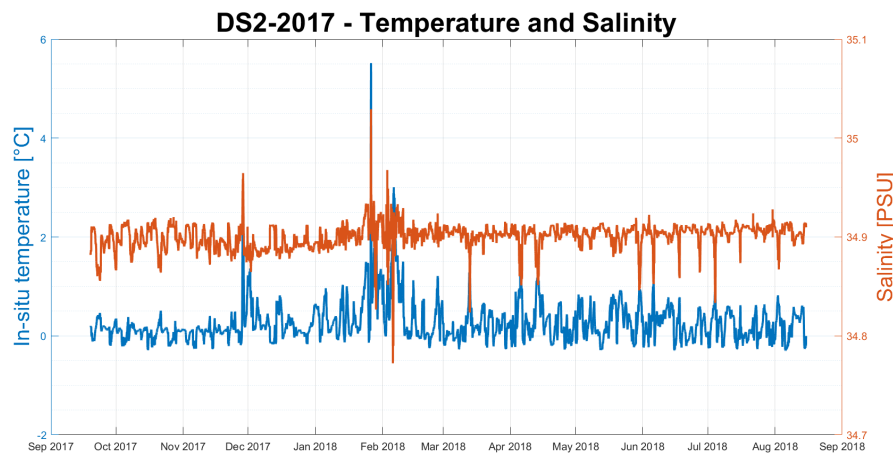


Figure 5.7.2: In-situ temperature [°C] and salinity [PSU] measured at a depth of 565m by the MicroCAT of site DS2-17 on the sill of Denmark Strait between September 2017 and September 2018. The temporal resolution is 30 minutes.

The mooring that was located approximately 45 km downstream of the sill (DS28-17) and at a depth of 630m exhibited clearly higher variability in the hydrographic properties than at DS2-17 at the sill of Denmark Strait (compare Figs. 5.7.2 and 5.7.3). The frequent occurrence of warm waters at DS28-17, with temperatures that exceed 3°C, and pronounced fluctuations in salinity around 34.9 psu indicate a different situation than the one shown by DS2-17 at the sill. The alternation between overflow waters and ambient warm waters is clearly evident at mooring site DS28-17.

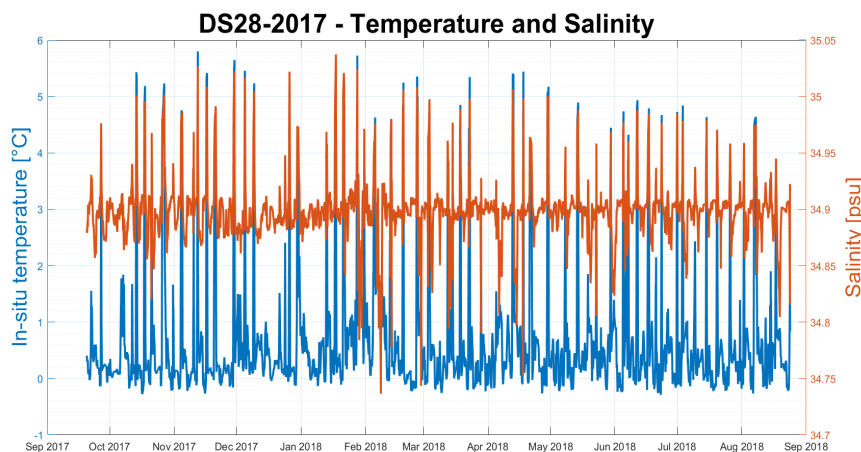


Figure 5.7.3: In-situ temperature [°C] and Salinity [PSU] measured at a depth of 700m by the MicroCAT of DS28-2017 located 45km downstream of Denmark Strait between September 2017 and September 2018. The temporal resolution is 10 minutes.

Further downstream (~140km from the sill) a mooring array, consisting of 4 four moorings DS-B-18, DS-D-18, DS-E-18 and DS-C-18 (see Figs. 5.7.1 and 5.7.4), recorded temperature simultaneously for approximately 11 days between the sea floor and 300 m above it (Fig. 5.7.5). The vertical coverage of the moorings was such that successfully captured the height of the plume, defined by the 2°C isotherm, during most of the cold events. Core-plume temperatures (0°C) are consistently seen first at the upstream mooring location (DS-D-18) and a few hours later at the rest of the array. While the first three moorings exhibit similar plume heights and temperatures, the offshore one (DS-C-18) shows weaker plume temperatures and sometimes shallower plume heights.

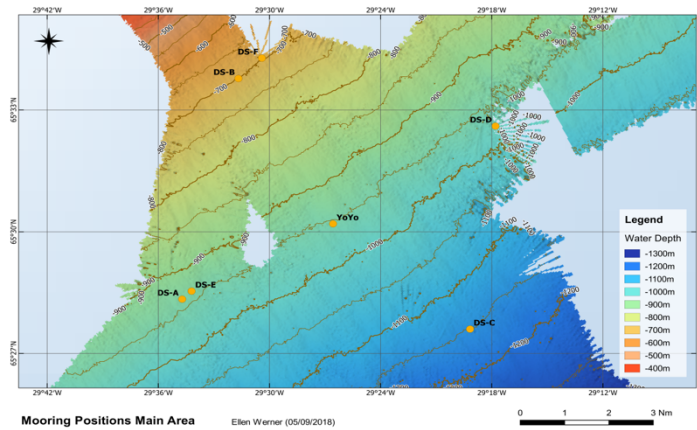


Figure 5.7.4: Map of the main working area (~140km downstream of the Denmark Strait Sill) showing the position of the moorings and of the YoYo CTD station, where the contour lines indicate the bathymetry. The mooring array was extending approximately 14km both in the along and the across bathymetry direction.

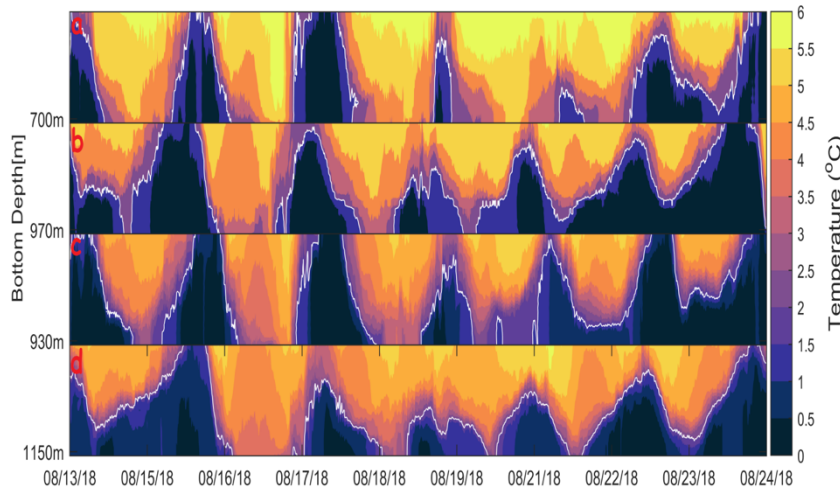


Figure 5.7.5: Contour plot of temperature [°C] measured by temperature recorders 140km downstream of Denmark Strait. The measurements cover a period of 11 days between the 13 and the 24 August, 2018 and have a vertical extent of 300m above the bottom. Moorings DS-B-18 (panel a), DS-D-18 (panel b), DS-E-18 (panel c) and DS-C-18 (panel d) were anchored at 700m, 970m, 930m and 1150m respectively. The 2°C isotherm contour is shown as white line.

5.7.3.2: Velocity Measurements

Velocity measurements from five upward-looking ADCPs at DS2-17, DS27-17, DS28-17, DS-A-18 and DSF-18 (fig. 5.7.1) were used to construct time-mean velocity profiles up to 300m above the bottom for each of these locations (Fig. 5.7.6). At the sill, the velocity profile exhibits a maximum of 0.5 m/s around 50m off the bottom but the extent of the plume is not clearly visible as the velocity gradient towards the top is comparatively small (<0.2m/s over 200m). Additionally, the profile exhibits an inversion close to the bottom.

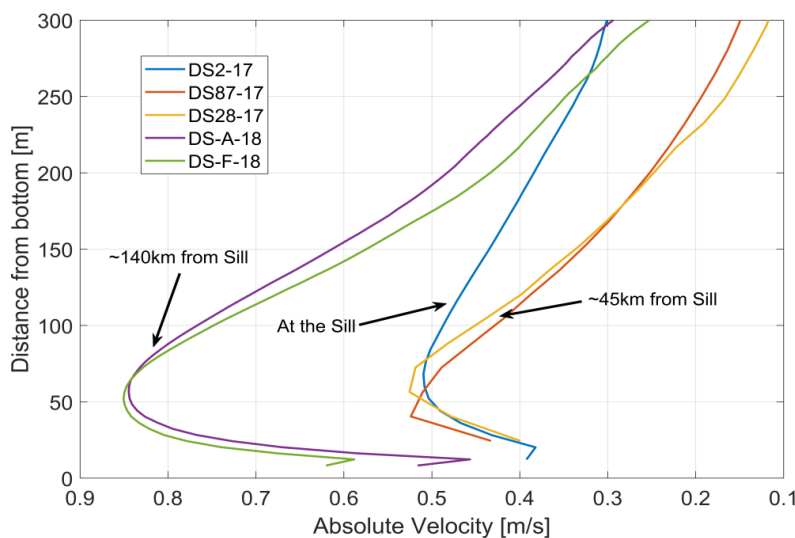


Figure 5.7.6: Time-mean vertical profile of absolute horizontal velocity (m/s), up to 300m above the bottom, at five mooring locations along the path of the Denmark Strait Overflow Water.

At the next mooring site downstream (~45km from the sill) the profiles show a velocity maximum that slightly exceeds

0.5 m/s at around the same altitude (distance from the sea floor) as observed at the sill. The plume shape is now apparent as the velocity gradient towards the top is sharper here (around 0.35 m/s). Further downstream at the main mooring site (~140km from the sill) the situation is quite different. As expected, the plume accelerates as it cascades deeper down the slope and increases its height as it entrains ambient water. Strong core velocities around 0.85 m/s are apparent here at the same altitude above the bottom as seen the previous locations. The profile, as at the sill, also exhibits an inversion close to the bottom.

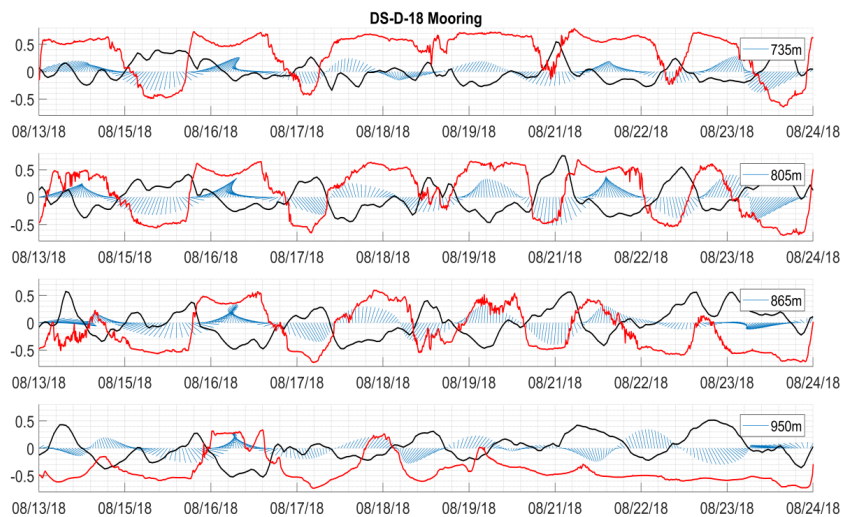


Figure 5.7.7: Stick plot of bandpassed (1-3 days), rotated currents (m/s) from Aquadopps at 735m, 805m, 865m and 950m at site DS-D-18. Downward looking arrows point downstream and arrows looking to the left (right) point upslope (downslope). Hourly averaged absolute velocity and temperature anomalies are shown as black and red lines, respectively. The scale on the y-axis indicates velocity (m/s) and temperature ($^{\circ}\text{C}$) normalized by a factor of 4.

To illustrate changes during the deployment period at the main mooring site, time-averaged currents at 4 different depths are shown from one of the moorings (DS-D-18, Fig. 5.7.7). Rotational flow is apparent throughout the time-series at all depths. Convergent and divergent vector patterns correspond to cyclonic and anti-cyclonic eddies propagating past the mooring, respectively (Foldvik et al., 1998). Anti-cyclonic rotation is correlated with positive velocity and negative temperature anomalies whereas the less frequent cyclonic rotation is correlated with negative velocity and positive temperature anomalies and seems to be increasing with depth. The situation is a bit different during the last two days of the deployment at the two deepest points. Negative temperature anomalies are persistent while velocity anomalies and current directions change in this period.

Finally, to take a first look at the energy contained in different frequencies the power spectra of raw (1 min) absolute velocities were computed for the same mooring and depths as above (Fig. 5.7.8). A peak at 1.6 days is evident at 735m. This signal gets stronger at 805m but then fades in the deeper parts of the water column where a peak around the frequency of the semi-diurnal tide is clear. Additionally, a coherent pattern of increasing energy content at frequencies higher than the Coriolis frequency (f) with increasing depth is also evident.

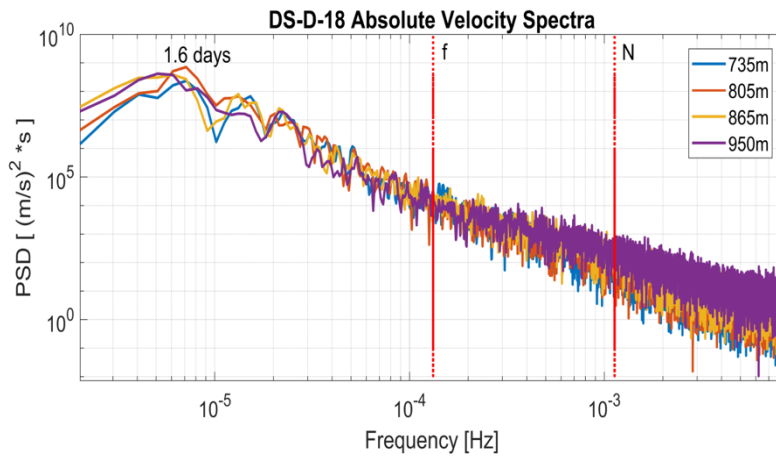


Figure 5.7.8: Power spectral density of absolute currents (m/s) at four depths (735m, 805m, 865m and 950m) from Aquadopps at mooring DS-D-18. Coriolis (f) and buoyancy (N) frequencies are indicated by red lines.

5.7.5 MicroCAT sensor calibration

Setups, operation, and preliminary results

In order to be able to assess the accuracy of the MicroCAT CTD sensors used during mooring deployments, we attached them to the CTD frame and lowered them during CTD casts to obtain comparisons to measurements of the lowered CTD. For this, we set the MicroCAT CTD sensors to sample every 10 seconds. On each of the CTD upcasts, when MicroCATs were attached, the rosette was then stopped at two different water depths for 7 minutes each, to allow the MicroCAT CTD sensors to equilibrate to the surrounding temperature and salinity (Kanzow et al., 2006). Table 5.7.8 gives an overview over the MicroCAT calibration dips. Fig. 5.7.9 shows exemplarily the measurements of salinity (top) and temperature (bottom) obtained from the lowered CTD and selected MicroCATs during one calibration cast. Table 5.7.9 then gives the values of the inferred average differences in temperature, salinity, conductivity and pressure between the CTD and the MicroCATs obtained at one equilibration depth level.

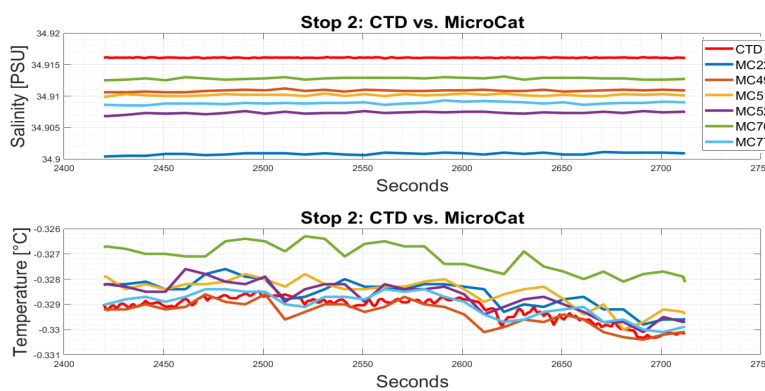


Figure 5.7.9: Salinity (top) and temperature (bottom) measured by the lowered CTD (red line) and by individual MicroCATs during cast 16 at one equilibration stop. Note the MC 22, 49, 51, 52, 70, 77 refer to MicroCAT serial numbers 11422, 10949, 10951, 10952, 12470, 12477, respectively.

Table 5.7.8: overview over the MicroCAT dips including e.g. CTD cast number, serial number of MicroCATs (sn), equilibration stop depths and duration ("about the cast") and origin of MicroCATs ("comment").

date	CTD-Station	Latitude	Longitude	SN	about the cast	comments
30.08.18	162	68°56.926' N	19°5.4896' W	7515	2 Stopps	HH
30.08.18	162	68°56.926' N	19°5.4896' W	7516	7 min	HH
30.08.18	162	68°56.926' N	19°5.4896' W	14626	Depth1 = 1.603.7 m	HH
30.08.18	162	68°56.926' N	19°5.4896' W	15176	Depth2 = 1005.1 m	HH
30.08.18	162	68°56.926' N	19°5.4896' W	1603		deployment Fram Strait
30.08.18	162	68°56.926' N	19°5.4896' W	2383		deployment Fram Strait
30.08.18	162	68°56.926' N	19°5.4896' W	10949		deployment Fram Strait
30.08.18	162	68°56.926' N	19°5.4896' W	10951		deployment Fram Strait
30.08.18	162	68°56.926' N	19°5.4896' W	10952		deployment Fram Strait
30.08.18	162	68°56.926' N	19°5.4896' W	11422		deployment Fram Strait
30.08.18	162	68°56.926' N	19°5.4896' W	12470		deployment Fram Strait
30.08.18	162	68°56.926' N	19°5.4896' W	12477		deployment Fram Strait
30.08.18	163	69°22.973' N	18°50.983' W	7517	2 Stopps, 7 min	HH
30.08.18	163	69°22.973' N	18°50.983' W	7518	Depth1 = 1566m	HH
30.08.18	163	69°22.973' N	18°50.983' W	15176	Depth2 = 1104 m	HH
30.08.18	163	69°22.973' N	18°50.983' W	15202		HH
30.08.18	163	69°22.973' N	18°50.983' W	1235		deployment Fram Strait
30.08.18	163	69°22.973' N	18°50.983' W	1605		deployment Fram Strait
30.08.18	163	69°22.973' N	18°50.983' W	2097		deployment Fram Strait
05.09.18	192	77°37.962' N	5°13.606' W	6380	3 Stopps a 7 min	DS-B
05.09.18	192	77°37.962' N	5°13.606' W	6381	Depth1 = 748.4 m	DS-B
05.09.18	192	77°37.962' N	5°13.606' W	8477	Depth2 = 502.1 m	DS-B
05.09.18	192	77°37.962' N	5°13.606' W	8478	Depth3 = 191.7 m	DS-B
05.09.18	192	77°37.962' N	5°13.606' W	8479		DS-B
05.09.18	192	77°37.962' N	5°13.606' W	8480		DS-B
05.09.18	192	77°37.962' N	5°13.606' W	8481		DS-B
05.09.18	192	77°37.962' N	5°13.606' W	8483		DS-B
05.09.18	192	77°37.962' N	5°13.606' W	8484		DS-B
05.09.18	192	77°37.962' N	5°13.606' W	8485		DS-B
05.09.18	192	77°37.962' N	5°13.606' W	8486		DS-B
05.09.18	192	77°37.962' N	5°13.606' W	630		DS-B and SBE16
05.09.18	193	77°37.583' N	4°65.374' W	6222	3 Stopps a 7 min	DS-D
05.09.18	193	77°37.583' N	4°65.374' W	6335	Depth1 = 1118.7m	DS-D
05.09.18	193	77°37.583' N	4°65.374' W	6358	Depth2 = 799.6 m	DS-D
05.09.18	193	77°37.583' N	4°65.374' W	6362	Depth3 = 300.9m	DS-D
05.09.18	193	77°37.583' N	4°65.374' W	6373		DS-D
05.09.18	193	77°37.583' N	4°65.374' W	6374		DS-D
05.09.18	193	77°37.583' N	4°65.374' W	6377		DS-D
05.09.18	193	77°37.583' N	4°65.374' W	6378		DS-D
05.09.18	193	77°37.583' N	4°65.374' W	6379		DS-D
05.09.18	193	77°37.583' N	4°65.374' W	6384		DS-D
05.09.18	193	77°37.583' N	4°65.374' W	6385		DS-D
05.09.18	193	77°37.583' N	4°65.374' W	6386		DS-D
05.09.18	193	77°37.583' N	4°65.374' W	6387		DS-D
05.09.18	193	77°37.583' N	4°65.374' W	2420		DS-D and SBE16
09.09.18	227	80°0.042' N	2°44.994' E	13900		recoveries Fram Strait
09.09.18	227	80°0.042' N	2°44.994' E	13902	2 Stopps a 7 min	recoveries Fram Strait
09.09.18	227	80°0.042' N	2°44.994' E	13903	Depth1 = 1497m	recoveries Fram Strait
09.09.18	227	80°0.042' N	2°44.994' E	13905	Depth2 = 799.6m	recoveries Fram Strait
09.09.18	227	80°0.042' N	2°44.994' E	13920		recoveries Fram Strait
09.09.18	227	80°0.042' N	2°44.994' E	13697		recoveries Fram Strait

Table 5.7.9: Average temperature, salinity, pressure and conductivity measured by the lowered CTD and by individual MicroCAT and the respective differences CTD-Mircocat (Diff) during cast 16 computed for one equilibration stop. Note the MC 22, 49, 51, 52,70, 77 refer to MicroCAT serial numbers 11422, 10949, 10951, 10952,12470, 12477, respectively.

	Temperature [°C]		Salinity [PSU]		Pressure [dbar]		Conductivity [S/m]	
	MW	Diff	MW	Diff	MW	Diff	MW	Diff
CTD	-0.564		34.919		1627		2.921	
MC49	-0.564	-3e-04	34.913	-0.006	1631	4.0	2.921	-3e-04
MC51	-0.564	5e-04	34.912	-0.007	1631	3.9	2.921	-3e-04
MC52	-0.564	3e-04	34.909	-0.009	1631	4.1	2.921	-5e-04
MC22	-0.564	5e-04	34.903	-0.016	1624	-2.5	2.920	-12e-04
MC70	-0.562	18e-04	34.915	-0.004	1629	2.6	2.921	-2e-04
MC77	-0.564	6e-04	34.910	-0.009	1630	2.8	2.9205	-5e-04

[5.8 Bathymetry](#)

Ellen Werner

Most areas of the Polar Seas have not yet been surveyed by swath bathymetry systems. Therefore, seabed topography data is unreliable and depth information is insufficient for navigation, especially at the northern East Greenland Shelf, where this expedition was heading to. So, one part of the MSM76 research program was a detailed bathymetric mapping in the research area of Scoresby Sund as well as on the Greenland Shelf to extend our knowledge of the seafloor topography in the Arctic. Additionally, other parts of the research program required detailed bathymetric maps, e.g. for station planning purposes. Furthermore, historic bathymetry data from former research cruises could not necessarily give detailed depth information and the coverage needed for the MSM76 cruise track. Due to ice coverage and a lack of up to date optical satellite images, the track over the East Greenland Shelf had to be changed several times and used bathymetric data acquisition for navigational purpose.

Therefore, the main task for the bathymetry was to operate the multibeam echosounders (MBES) Kongsberg EM122, including calibration and correction of the data for environmental circumstances (sound velocity, systematic errors in bottom detection, etc.), the post processing and cleaning of the data, as well as data management for on-site map creation. The MBES was run constantly throughout the cruise for underway surveying and systematic surveys were conducted at sites of special interest. Due to the simultaneous underway surveying of the Vessel Mounted ADCP on board, the second MBES Kongsberg EM712 could not be used because of frequency interference.

[5.8.1 System and Operations](#)

[5.8.1.1 Technical Description](#)

During the MSM76 cruise, the bathymetric surveys were conducted with the hull-mounted MBES Kongsberg EM122. The EM122 is a deep water system for continuous mapping with full swath potential (~12 kHz). Unfortunately, the acoustic bandwidth of the EM712 (40-100 kHz) and the harmonics of the Vessel Mounted ADCP (38 and 75 kHz) create strong interferences, so the EM712 was basically not used at all.

The EM122 operates on a frequency of 12 kHz ranging from 10.5 to 13 kHz within the four different transmission sectors. On R/V Maria S. Merian, the EM122 transducer arrays are arranged in a hull-mounted Mills cross configuration of 8 m (transmission unit) by 8 m (receiver unit) to achieve an angular beam accuracy of 1° by 1°. The combined motion, position, and time data comes from a Kongsberg Seapath 320 system and the signal goes directly into the Processing Unit (PU) of the MBES to allow real-time motion compensation in Pitch, Roll and Yaw in the range of +/-10°. With a combination of phase and amplitude detection algorithms the PU computes the water depth from the returning backscatter signal. The system can cover a sector of up to 150° with each 75° per side. The EM122 distributes its 288 beams per swath (432 soundings per swath) with 1°x1° beam width either in equidistant or equiangular mode on the swath angle. During the cruise the system was always set to equidistant mode.

[5.8.1.2 Data acquisition and processing](#)

Data acquisition was carried out throughout the entire cruise, starting the 11th of August 2018 at 17:16 UTC in the fjord mouth of Reykjavik and ended the 11th of August at 03:00 UTC in the arrival to Spitsbergen. Where possible, cruise tracks were planned parallel to existing bathymetric data and the surveys were performed to extend already mapped regions. Furthermore, in some areas surveys without predefined waypoints were conducted to fill gaps that occurred while mapping regions with very variable topography. The multibeam surveys were generally run at around 8 kts and less during fog or difficult ice conditions. The long transits between the main research areas were conducted at around 13 kts or less, also depending on the weather.

Most of the time a swath angle of about 140° was used. In shallow water, the swath angle was partially set to a maximum of 150° to cover wider areas. In times of a lack of up to date Sound Velocity Profiles the swath angle was sometimes reduced down to 120° to get a cleaner data acquisition. For data acquisition, the Kongsberg SIS (Seafloor Information System) software was used. It processes and logs the collected data, applies all corrections and defined filters, and finally displays the resulting depths on a geographical display. The recorded data was stored in 60 min blocks in the Kongsberg *.all format. Subsequent data processing was performed using Caris HIPS and SIPS. The data editing revealed a good data quality of the EM122 with rejected beams. For generating maps, data was exported to Quantum GIS in the GeoTIFF raster format.

From time to time, the SIS grid engine broke down because it stored too many cells. In these cases, the system was restarted during the next CTD station, the produced grids were saved as background images and then deleted and a new survey was initialised. This happened once during a transit time and ended up in a full SIS breakdown. However, due to a quick restart not much data was lost. Besides that, the software was working pretty reliably.

5.8.1.3 Sound velocity profiles

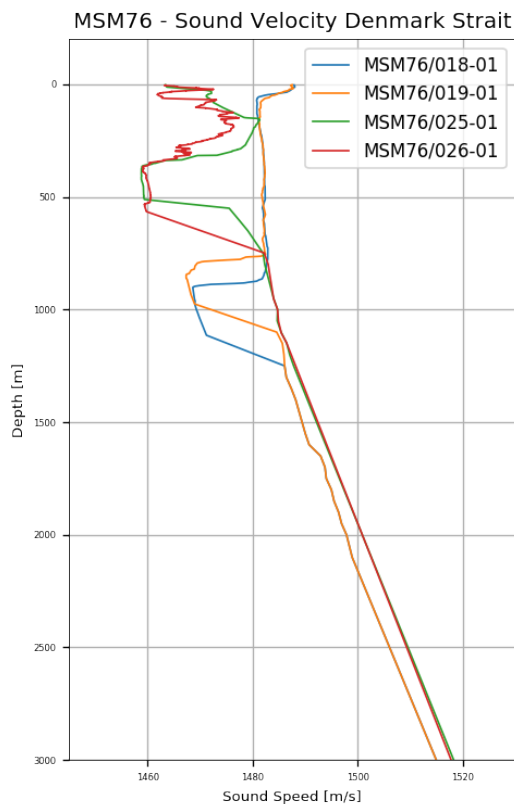


Figure 5.8.1: Examples of sound velocity profiles that captured the Denmark Strait overflow in the deep water layers

For best survey results with correct depths, CTD (Conductivity, Temperature, Depth; see Chapter 5.1) casts were regularly performed to determine the sound velocity through water at different depths. This is essential, as the acoustic signal travels through the water column from the transducer to the seafloor and back to the surface through several different layers of water masses with each a different sound velocity. The sound velocity is influenced by density and compressibility, both depending on pressure, temperature and salinity. Wrong or outdated sound velocity profiles lead to refraction errors and reduced data quality.

The CTD measures conductivity, temperature and depth in the water column while it is lowered to the seafloor. From these parameters in the downcast, the sound velocity is calculated. The sound velocity profiles obtained by the CTD were immediately processed with the Sound Speed Manager Software (all profiles are virtually extended to 12000m water depth for Kongsberg SIS to accept them and the descent was smoothed) and directly applied within Kongsberg SIS for correct beamforming during the survey. 192 CTD stations were used for sound velocity correction during the expedition. Besides the sound velocity profiles of the entire water column, the system permanently measures the current sound velocity information from the c-keel-probe, directly mounted at the transducer under the keel for correct beam forming.

Unfortunately, in some regions of the cruise we were researching over rapidly varying water columns. Due to the overflow in the deep water layers in Denmark Strait, unmixed surface freshwater produced by ice melting in Scoresby Sund and on the northern Greenland Shelf we were affected by permanent changes in sound velocity. This resulted in distorted outer beam depth information and caused some systematic errors which need to be corrected in the postprocessing. Examples for the Sound Velocity Profiles in Denmark Strait are shown in Fig. 5.8.1. Due to the large number of CTD casts at least in research areas a good local coverage of the water column was given.

5.8.2 Preliminary results

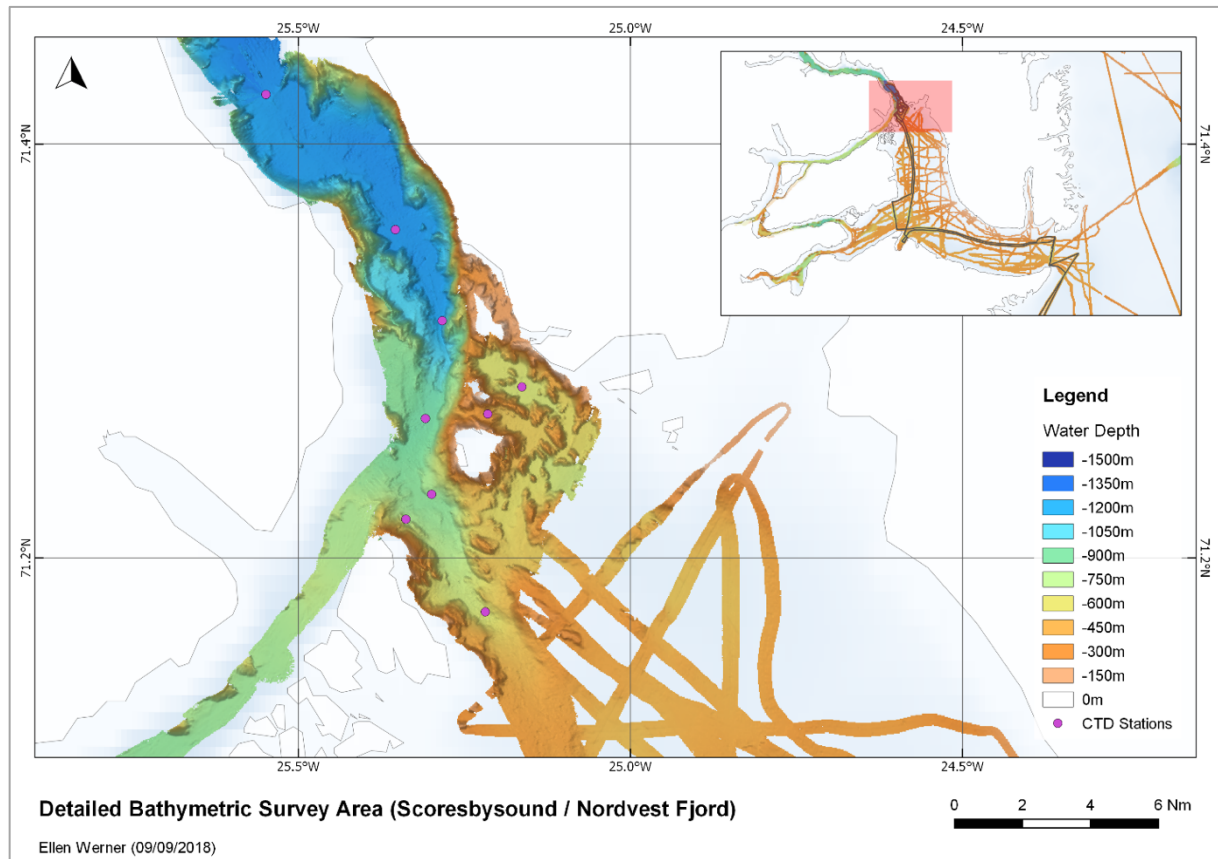


Figure 5.8.2: Bathymetric map of the transition of Scoresby Sund to Nordvest Fjord (work area 2 of the expedition).

Throughout the cruise a continuous recording of data was achieved, except for small data gaps due to unexpected system/software errors and shutdowns. By the end of the cruise, some of the EM122 raw data in the research areas was already processed. During 32 days of survey, a track length of 4,755 nm (8,805 km) was surveyed. The raw data volume of the EM712 is 35.8 GB within 639 separate files. The water depths ranged between a minimum of 66 m in Scoresby Sund to a maximum of 5563 m in Fram Strait close to Spitsbergen.

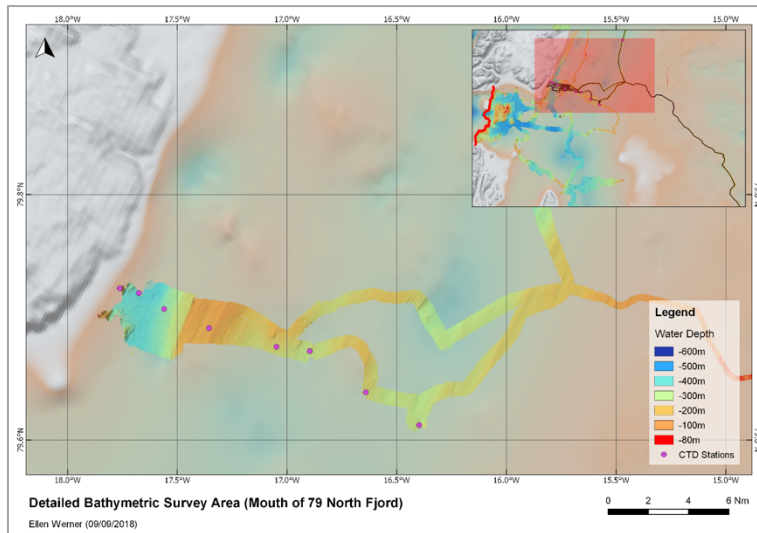


Figure 5.8.4: Map of Bathymetric Research Area 2

During MSM76 two extended bathymetric surveys were performed, one in the mouth of Nordvest Fjord to Scoresby Sund (see Fig. 5.8.2) and another one close to the 79 North Glacier (see Fig. 5.8.3). Besides that, important underway datasets were collected and especially helpful for the ships navigation. Additionally, bathymetric profiles were extracted for specific CTD Sections to be used

as a data background (see section plots in chapter 5.1.5).

5.8.3 Data management

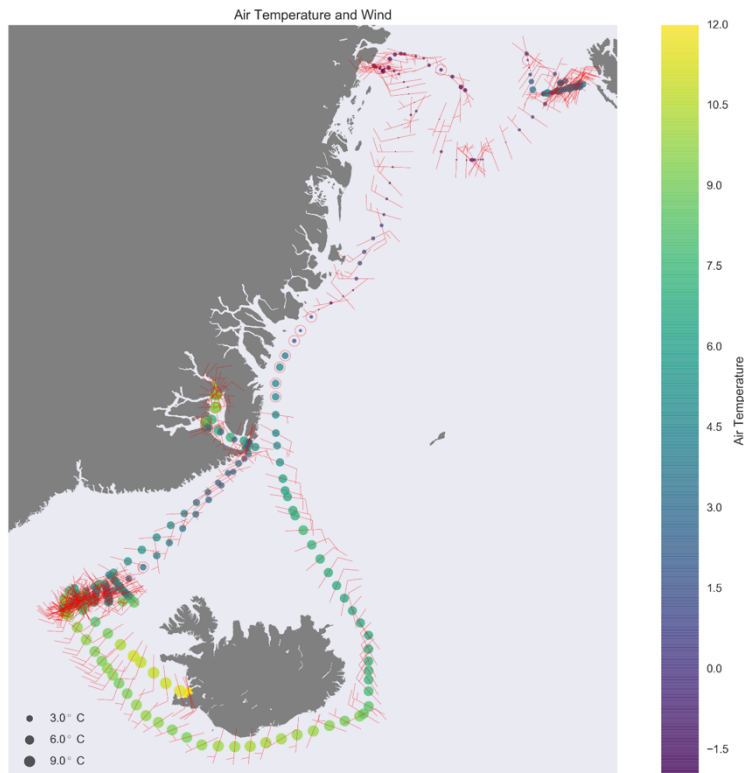
The collection of underway data during MSM76 will contribute to the bathymetry data archive at the AWI and additionally contribute to bathymetric world datasets like GEBCO (General Bathymetric Chart of the Oceans). The raw datasets will be ingested to the long-term scientific data warehouse PANGAEA.

6. Ship's meteorological station

Saeyd Ali Mubashshir

6.1 System Operation

R/V Maria S. Merian has meteorological sensors provided by DWD which measured air temperature, air pressure, wind velocity, humidity and surface water temperature for the whole

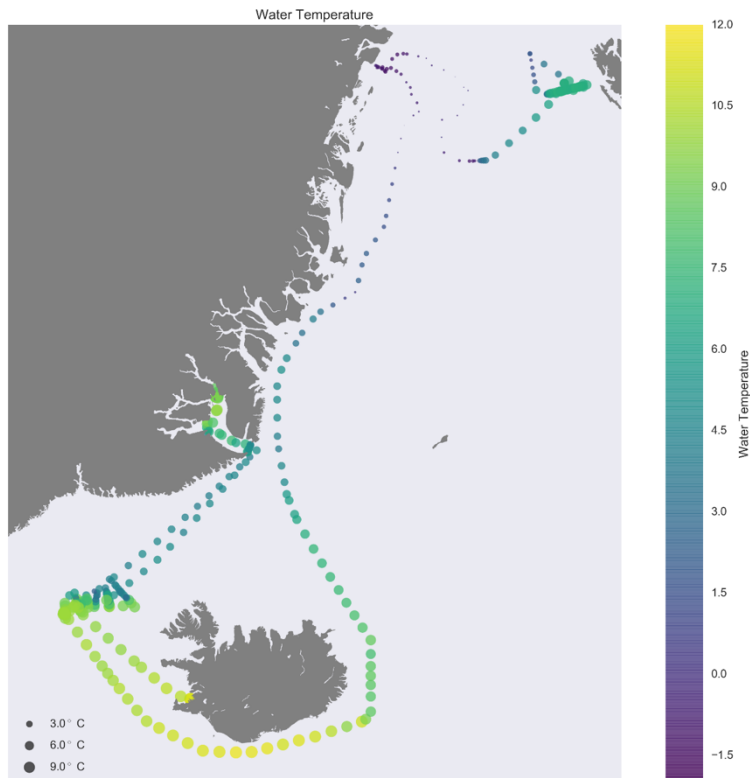


period of cruise. The temperature and humidity sensors are located on the elevated pile deck. The air temperature sensor comes from the company Thies. It uses a temperature dependent thermistor PT-100, relying on a four-wire principle. Accuracy is indicated as 1/3 DIN B or EN60751. The humidity sensor manufactured by Rotronic which features a measurement range of 0-100%, corresponding to 0-100mV.

Figure 6.1.1: Air temperature and wind speed measured during the cruise. The data is averaged and plotted in a 2-h interval.

6.2 Preliminary Results

The surface water temperature sensor has also been made by Friedrichs. It measures the temperature at 2 meters below the sea surface. The air pressure sensor is located in the converter room and is made by the company AIR. In order to avoid the air to equilibrate within in the ship, the air pressure sensor has a separate air inlet located outside of the ship. The resolution of the pressure sensor is 0.1 HPa. The accuracy is 0.5 HPa.



The wind direction and speed sensor has also been made by Thies. The sensor was mounted at the highest point of the radar mast. The location of the sensor is relatively free of wind turbulence created by the vessel superstructure, such that this setting results in most accurate wind direction measurements. The wind speed is obtained from a frequency dependent measurement of the wind force exerted onto the sensor. The frequency range is 0-800 Hz which is used to obtain wind speeds in the range of 0-40 m/s. The wind data is stored both as absolute wind speed & direction and as wind speed & direction relative to the moving ship.

Figure 6.1.2: Water temperature measured during the cruise. The data is averaged and plotted in a 2-h interval.

During the cruise we observed air temperatures in the range of -1.69 to +12.24 °C (Fig 6.1.1). The winds were mild during most of the part of the cruise and we mostly managed to avoid the stormy weather in the North Atlantic Ocean as can be seen in Fig 6.1.1. The water temperature measured during the cruise ranged from -1.33 to 3.58 °C. Fig 6.1.2 shows that the water temperature measured in the Denmark Strait was relatively warm. The surface water became colder as the ship moved northwards. The transition of cold waters west of 79°N of Greenland to the warmer West Spitsbergen current is depicted in the both Fig 6.1.2 and Fig 6.1.3.

7. Station List

Table 7.1: Station list of MSM76 expedition

Cruise_Station Nr_CastNr	Device	Date(dd.mm.yyy y) Time (HH:mm, UTC)	Action	Latitude	Longitude	Depth [m]	max. depth CTD [m]	Depth above bottom [m]	Comments
MSM76_1-1	RO/CTD/ADC P	11.08.18 20:08	in the water	64° 34.978' N	024° 58.157' W	241,7			
MSM76_1-1	RO/CTD/ADC P	11.08.18 20:20	max. depth	64° 34.977' N	024° 58.155' W	239,2		14,8	
MSM76_1-1	RO/CTD/ADC P	11.08.18 20:33	on deck	64° 34.978' N	024° 58.156' W	241			salt and oxygen sampled
MSM76_2-1	RO/CTD/ADC P	12.08.18 06:34	in the water	65° 21.080' N	029° 06.353' W	1404,2			
MSM76_2-1	RO/CTD/ADC P	12.08.18 07:05	max. depth	65° 21.082' N	029° 06.348' W	1405,6		13,7	
MSM76_2-1	RO/CTD/ADC P	12.08.18 07:39	on deck	65° 21.084' N	029° 06.346' W	1403,9			salt and oxygen sampled
MSM76_3-1	RO/CTD/ADC P	12.08.18 08:17	in the water	65° 24.177' N	029° 12.438' W	1331,5			
MSM76_3-1	RO/CTD/ADC P	12.08.18 08:47	max. depth	65° 24.179' N	029° 12.436' W	1331,5	1310	15	
MSM76_3-1	RO/CTD/ADC P	12.08.18 09:16	on deck	65° 24.344' N	029° 12.254' W	1329,1			salt and oxygen sampled
MSM76_4-1	RO/CTD/ADC P	12.08.18 09:50	in the water	65° 26.079' N	029° 16.321' W	1245,1			
MSM76_4-1	RO/CTD/ADC P	12.08.18 10:18	max. depth	65° 26.085' N	029° 16.312' W	1245,3	1231	14,9	
MSM76_4-1	RO/CTD/ADC P	12.08.18 10:46	on deck	65° 26.083' N	029° 16.306' W	1244,1			salt and oxygen sampled
MSM76_5-1	RO/CTD/ADC P	12.08.18 11:26	in the water	65° 28.007' N	029° 20.158' W	1122,3			
MSM76_5-1	RO/CTD/ADC P	12.08.18 11:53	max. depth	65° 28.004' N	029° 20.138' W	1119,8	1104	19	
MSM76_5-1	RO/CTD/ADC P	12.08.18 12:20	on deck	65° 28.005' N	029° 20.137' W	1121			salt and oxygen sampled

MSM76_14-1	RO/CTD/ADC P	13.08.18 01:30	in the water	65° 37.621' N	029° 39.400' W	362,4				χ-pods attached
MSM76_14-1	RO/CTD/ADC P	13.08.18 01:41	max. depth	65° 37.620' N	029° 39.403' W	360,4	353	12,6		
MSM76_14-1	RO/CTD/ADC P	13.08.18 01:55	on deck	65° 37.620' N	029° 39.399' W	362,2				salt sampled
MSM76_15-1	RO/CTD/ADC P	13.08.18 02:36	in the water	65° 39.554' N	029° 43.256' W	338,4				χ-pods attached
MSM76_15-1	RO/CTD/ADC P	13.08.18 02:46	max. depth	65° 39.555' N	029° 43.258' W	339,5	320	15,7		
MSM76_15-1	RO/CTD/ADC P	13.08.18 02:59	on deck	65° 39.554' N	029° 43.259' W	338,7				salt and oxygen sampled
MSM76_16-1	RO/CTD/ADC P	13.08.18 05:11	in the water	65° 24.164' N	029° 12.471' W	1325				χ-pods attached
MSM76_16-1	RO/CTD/ADC P	13.08.18 05:40	max. depth	65° 24.162' N	029° 12.465' W	1324,2	1309,8	20,2		
MSM76_16-1	RO/CTD/ADC P	13.08.18 06:11	on deck	65° 24.164' N	029° 12.470' W	1324,6				salt sampled
MSM76_17-1	RO/CTD/ADC P	13.08.18 06:39	in the water	65° 26.083' N	029° 16.311' W	1244,4				χ-pods attached
MSM76_17-1	RO/CTD/ADC P	13.08.18 07:06	max. depth	65° 26.084' N	029° 16.308' W	1246,5	1231,5	13,5		
MSM76_17-1	RO/CTD/ADC P	13.08.18 07:38	on deck	65° 26.082' N	029° 16.308' W	1244,3				salt and oxygen sampled
MSM76_18-1	RO/CTD/ADC P	13.08.18 08:08	in the water	65° 28.893' N	029° 17.439' W	1130,4				χ-pods attached
MSM76_18-1	RO/CTD/ADC P	13.08.18 08:35	max. depth	65° 28.892' N	029° 17.437' W	1128		15		
MSM76_18-1	RO/CTD/ADC P	13.08.18 08:57	on deck	65° 28.890' N	029° 17.436' W	1129,5				
MSM76_19-1	RO/CTD/ADC P	13.08.18 09:35	in the water	65° 29.925' N	029° 23.973' W	988,1				χ-pods attached
MSM76_19-1	RO/CTD/ADC P	13.08.18 09:59	max. depth	65° 29.936' N	029° 23.976' W	987,9	974	18,2		

MSM76_19-1	RO/CTD/ADC P	13.08.18 10:26	on deck	65° 29.935' N	029° 23.976' W	988,3				salt and oxygen sampled
MSM76_20-1	RO/CTD/ADC P	13.08.18 11:16	in the water	65° 33.776' N	029° 31.666' W	697				χ-pods attached
MSM76_20-1	RO/CTD/ADC P	13.08.18 11:36	max. depth	65° 33.773' N	029° 31.664' W	696,4		15		
MSM76_20-1	RO/CTD/ADC P	13.08.18 11:51	on deck	65° 33.773' N	029° 31.664' W	696,7				
MSM76_20-2	MOOR	13.08.18 12:10	start	65° 33.770' N	029° 32.415' W	682,8				
MSM76_20-2	MOOR	13.08.18 12:34	deployed	65° 33.772' N	029° 31.676' W	697,4				DS-B-18
MSM76_21-1	MOOR	13.08.18 12:58	deployed	65° 34.274' N	029° 30.411' W	692,5				DS-F-18, ADCP mooring
MSM76_22-1	MOOR	13.08.18 14:40	start	65° 32.601' N	029° 18.630' W	971				
MSM76_22-1	MOOR	13.08.18 15:05	deployed	65° 32.602' N	029° 17.798' W	971,5				DS-D-18
MSM76_23-1	VmADCP	13.08.18 17:03	profile start	65° 42.458' N	028° 33.660' W	958				true course= 352°
MSM76_24-1	RO/CTD/ADC P	13.08.18 21:03	in the water	65° 58.754' N	028° 06.266' W	474				χ-pods attached
MSM76_24-1	RO/CTD/ADC P	13.08.18 21:17	max. depth	65° 58.762' N	028° 06.242' W	473	460	18,4		
MSM76_24-1	RO/CTD/ADC P	13.08.18 21:34	on deck	65° 58.640' N	028° 06.344' W	475				salt and oxygen sampled
MSM76_25-1	RO/CTD/ADC P	13.08.18 22:08	in the water	65° 56.621' N	028° 02.981' W	526				χ-pods attached
MSM76_25-1	RO/CTD/ADC P	13.08.18 22:24	max. depth	65° 56.574' N	028° 02.983' W	527		16,1		
MSM76_25-1	RO/CTD/ADC P	13.08.18 22:36	on deck	65° 56.493' N	028° 02.982' W	533				
MSM76_26-1	RO/CTD/ADC P	13.08.18 23:00	in the water	65° 54.589' N	027° 59.725' W	573				χ-pods attached
MSM76_26-1	RO/CTD/ADC P	13.08.18 23:17	max. depth	65° 54.512' N	027° 59.663' W	571	570	15,8		
MSM76_26-1	RO/CTD/ADC P	13.08.18 23:35	max. depth	65° 54.430' N	027° 59.692' W	577				salt and oxygen sampled
MSM76_27-1	RO/CTD/ADC P	14.08.18 00:02	in the water	65° 52.500' N	027° 56.365' W	623				χ-pods attached

MSM76_27-1	RO/CTD/ADC P	14.08.18 00:19	max. depth	65° 52.436' N	027° 56.358' W	629	615	13	
MSM76_27-1	RO/CTD/ADC P	14.08.18 00:37	on deck	65° 52.398' N	027° 56.352' W	631			salt sampled
MSM76_28-1	RO/CTD/ADC P	14.08.18 01:10	in the water	65° 50.343' N	027° 53.080' W	692			χ-pods attached
MSM76_28-1	RO/CTD/ADC P	14.08.18 01:30	max. depth	65° 50.329' N	027° 53.108' W	691	669	17,5	
MSM76_28-1	RO/CTD/ADC P	14.08.18 01:49	on deck	65° 50.270' N	027° 53.251' W	691			salt and oxygen sampled
MSM76_29-1	RO/CTD/ADC P	14.08.18 02:19	in the water	65° 48.260' N	027° 49.721' W	739			χ-pods attached
MSM76_29-1	RO/CTD/ADC P	14.08.18 02:37	max. depth	65° 48.267' N	027° 49.696' W	740	714	22,3	
MSM76_29-1	RO/CTD/ADC P	14.08.18 02:58	on deck	65° 48.217' N	027° 49.830' W	738			salt sampled
MSM76_30-1	RO/CTD/ADC P	14.08.18 03:33	in the water	65° 46.060' N	027° 46.322' W	733			χ-pods attached
MSM76_30-1	RO/CTD/ADC P	14.08.18 03:51	max. depth	65° 46.108' N	027° 46.490' W	733	718	20	
MSM76_30-1	RO/CTD/ADC P	14.08.18 04:11	on deck	65° 46.165' N	027° 46.327' W	737			salt and oxygen sampled
MSM76_31-1	RO/CTD/ADC P	14.08.18 07:33	in the water	65° 53.987' N	026° 20.021' W	281			χ-pods attached
MSM76_31-1	RO/CTD/ADC P	14.08.18 07:44	max. depth	65° 53.994' N	026° 20.026' W	281	271,3	14,8	
MSM76_31-1	RO/CTD/ADC P	14.08.18 07:56	on deck	65° 53.992' N	026° 20.022' W	281			salt sampled
MSM76_32-1	RO/CTD/ADC P	14.08.18 08:39	in the water	65° 56.516' N	026° 30.622' W	282			χ-pods attached
MSM76_32-1	RO/CTD/ADC P	14.08.18 08:52	max. depth	65° 56.516' N	026° 30.624' W	282	273	15,1	
MSM76_32-1	RO/CTD/ADC P	14.08.18 09:05	on deck	65° 56.517' N	026° 30.620' W	283			salt and oxygen sampled

MSM76_33-1	RO/CTD/ADC P	14.08.18 09:36	in the water	65° 57.773' N	026° 36.016' W	281					χ-pods attached
MSM76_33-1	RO/CTD/ADC P	14.08.18 09:47	max. depth	65° 57.800' N	026° 36.060' W	281	296,7	14,8			
MSM76_33-1	RO/CTD/ADC P	14.08.18 09:59	on deck	65° 57.855' N	026° 36.140' W	274					salt sampled
MSM76_34-1	RO/CTD/ADC P	14.08.18 10:29	in the water	65° 59.034' N	026° 41.355' W	288					χ-pods attached
MSM76_34-1	RO/CTD/ADC P	14.08.18 10:40	max. depth	65° 59.087' N	026° 41.361' W	291	277	14,1			
MSM76_34-1	RO/CTD/ADC P	14.08.18 10:54	on deck	65° 59.221' N	026° 41.301' W	289					salt and oxygen sampled
MSM76_35-1	RO/CTD/ADC P	14.08.18 11:23	in the water	66° 00.308' N	026° 46.629' W	385					χ-pods attached
MSM76_35-1	RO/CTD/ADC P	14.08.18 11:36	max. depth	66° 00.426' N	026° 46.570' W	388	383	15,3			
MSM76_35-1	RO/CTD/ADC P	14.08.18 11:53	on deck	66° 00.665' N	026° 46.428' W	400					salt and oxygen sampled
MSM76_36-1	RO/CTD/ADC P	14.08.18 12:30	in the water	66° 01.573' N	026° 51.794' W	515					χ-pods attached
MSM76_36-1	RO/CTD/ADC P	14.08.18 12:44	max. depth	66° 01.753' N	026° 51.696' W	518	501	21			
MSM76_36-1	RO/CTD/ADC P	14.08.18 13:01	on deck	66° 02.054' N	026° 51.241' W	526					salt and oxygen sampled
MSM76_37-1	RO/CTD/ADC P	14.08.18 13:42	in the water	66° 02.761' N	026° 57.184' W	590					χ-pods attached
MSM76_37-1	RO/CTD/ADC P	14.08.18 13:59	max. depth	66° 02.945' N	026° 56.896' W	593	576	17,9			
MSM76_37-1	RO/CTD/ADC P	14.08.18 14:18	on deck	66° 03.198' N	026° 56.501' W	592					salt sampled
MSM76_38-1	RO/CTD/ADC P	14.08.18 14:49	in the water	66° 04.020' N	027° 02.510' W	641					χ-pods attached
MSM76_38-1	RO/CTD/ADC P	14.08.18 15:05	max. depth	66° 04.174' N	027° 02.269' W	642	621,6	18,6			

MSM76_38-1	RO/CTD/ADC P	14.08.18 15:25	on deck	66° 04.395' N	027° 01.927' W	642			salt and oxygen sampled
MSM76_39-1	RO/CTD/ADC P	14.08.18 16:02	in the water	66° 05.279' N	027° 07.656' W	641			χ-pods attached
MSM76_39-1	RO/CTD/ADC P	14.08.18 16:20	max. depth	66° 05.278' N	027° 07.656' W	641	624,6	14,6	
MSM76_39-1	RO/CTD/ADC P	14.08.18 16:37	on deck	66° 05.280' N	027° 07.652' W	642			salt sampled
MSM76_40-1	RO/CTD/ADC P	14.08.18 17:11	in the water	66° 06.541' N	027° 13.190' W	610			χ-pods attached
MSM76_40-1	RO/CTD/ADC P	14.08.18 17:27	max. depth	66° 06.538' N	027° 13.184' W	603	581,1	29,1	
MSM76_40-1	RO/CTD/ADC P	14.08.18 17:46	on deck	66° 06.480' N	027° 13.279' W	606			salt and oxygen sampled
MSM76_41-1	RO/CTD/ADC P	14.08.18 18:37	in the water	66° 07.785' N	027° 18.454' W	520			χ-pods attached
MSM76_41-1	RO/CTD/ADC P	14.08.18 18:52	max. depth	66° 07.782' N	027° 18.473' W	520	502,7	23,5	
MSM76_41-1	RO/CTD/ADC P	14.08.18 19:09	on deck	66° 07.739' N	027° 18.597' W	522			salt and oxygen sampled
MSM76_42-1	RO/CTD/ADC P	14.08.18 19:44	in the water	66° 09.034' N	027° 23.845' W	484			χ-pods attached
MSM76_42-1	RO/CTD/ADC P	14.08.18 19:58	max. depth	66° 09.034' N	027° 23.851' W	483	471,3		
MSM76_42-1	RO/CTD/ADC P	14.08.18 20:16	on deck	66° 08.953' N	027° 24.037' W	484			salt and oxygen sampled
MSM76_43-1	RO/CTD/ADC P	14.08.18 20:44	in the water	66° 10.241' N	027° 29.049' W	481			χ-pods attached
MSM76_43-1	RO/CTD/ADC P	14.08.18 20:59	max. depth	66° 10.242' N	027° 29.048' W	481	467	15,9	
MSM76_43-1	RO/CTD/ADC P	14.08.18 21:14	on deck	66° 10.243' N	027° 29.052' W	482			salt sampled
MSM76_44-1	RO/CTD/ADC P	14.08.18 21:45	in the water	66° 11.551' N	027° 34.527' W	484			χ-pods attached

MSM76_44-1	RO/CTD/ADC P	14.08.18 22:00	max. depth	66° 11.552' N	027° 34.525' W	484	469,8	14,7	
MSM76_44-1	RO/CTD/ADC P	14.08.18 22:18	on deck	66° 11.550' N	027° 34.525' W	483			salt and oxygen sampled
MSM76_45-1	RO/CTD/ADC P	14.08.18 22:57	in the water	66° 12.793' N	027° 39.820' W	484			χ-pods attached
MSM76_45-1	RO/CTD/ADC P	14.08.18 23:12	max. depth	66° 12.810' N	027° 39.813' W	484	471,3	14,9	
MSM76_45-1	RO/CTD/ADC P	14.08.18 23:27	on deck	66° 12.811' N	027° 39.813' W	484			salt sampled
MSM76_46-1	RO/CTD/ADC P	14.08.18 23:58	in the water	66° 14.068' N	027° 45.240' W	474			χ-pods attached
MSM76_46-1	RO/CTD/ADC P	15.08.18 00:12	max. depth	66° 14.067' N	027° 45.243' W	475	462	15,2	
MSM76_46-1	RO/CTD/ADC P	15.08.18 00:29	on deck	66° 14.069' N	027° 45.242' W	473			salt and oxygen sampled
MSM76_47-1	RO/CTD/ADC P	15.08.18 01:42	in the water	66° 15.297' N	027° 50.421' W	458			χ-pods attached
MSM76_47-1	RO/CTD/ADC P	15.08.18 01:55	max. depth	66° 15.300' N	027° 50.422' W	458	452	5,9	
MSM76_47-1	RO/CTD/ADC P	15.08.18 02:11	on deck	66° 15.299' N	027° 50.427' W	458			salt sampled
MSM76_48-1	RO/CTD/ADC P	15.08.18 02:45	in the water	66° 16.570' N	027° 55.965' W	430			χ-pods attached
MSM76_48-1	RO/CTD/ADC P	15.08.18 02:59	max. depth	66° 16.570' N	027° 55.955' W	429	418	15,9	
MSM76_48-1	RO/CTD/ADC P	15.08.18 03:13	on deck	66° 16.572' N	027° 55.957' W	429			salt and oxygen sampled
MSM76_49-1	RO/CTD/ADC P	15.08.18 04:03	in the water	66° 19.064' N	028° 06.702' W	337			χ-pods attached
MSM76_49-1	RO/CTD/ADC P	15.08.18 04:14	max. depth	66° 19.068' N	028° 06.698' W	338	325,3	13,6	
MSM76_49-1	RO/CTD/ADC P	15.08.18 04:28	on deck	66° 19.066' N	028° 06.697' W	338			salt sampled

MSM76_50-1	RO/CTD/ADC P	15.08.18 05:09	in the water	66° 21.588' N	028° 17.478' W	329			χ-pods attached
MSM76_50-1	RO/CTD/ADC P	15.08.18 05:19	max. depth	66° 21.590' N	028° 17.472' W	329	320,5	12,4	
MSM76_50-1	RO/CTD/ADC P	15.08.18 05:34	on deck	66° 21.589' N	028° 17.471' W	328			salt and oxygen sampled
MSM76_51-1	MOOR	15.08.18 08:42	released	66° 07.018' N	027° 17.431' W	565			
MSM76_51-1	MOOR	15.08.18 08:45	at surface	66° 07.005' N	027° 17.468' W	565			
MSM76_51-1	MOOR	15.08.18 08:59	recovered	66° 07.276' N	027° 16.852' W	565			DS-2-17
MSM76_52-1	MOOR	15.08.18 11:24	begin dredging	66° 03.358' N	026° 59.327' W	623			
MSM76_52-1	MOOR	15.08.18 14:38	course 050°, begin dredging	66° 02.962' N	027° 00.334' W	614			
MSM76_52-1	MOOR	15.08.18 15:23	begin dredging, course 206°	66° 03.132' N	026° 59.743' W	614			
MSM76_52-1	MOOR	15.08.18 16:19	begin dredging, course 055°	66° 02.802' N	027° 00.093' W	613			
MSM76_52-1	MOOR	15.08.18 17:32	all on deck	66° 03.048' N	026° 59.206' W	606			dredging of DS 23-17 unsuccessful
MSM76_53-1	RO/CTD/ADC P	15.08.18 17:37	in the water	66° 03.049' N	026° 59.204' W	604			χ-pods attached, MicroCATs attached
MSM76_53-1	RO/CTD/ADC P	15.08.18 18:07	max. depth	66° 03.050' N	026° 59.240' W	604	557,1	16,2	
MSM76_53-1	RO/CTD/ADC P	15.08.18 18:38	on deck	66° 03.061' N	026° 59.507' W	607			salt and oxygen sampled
MSM76_54-1	MOOR	15.08.18 19:40	deployed	66° 07.294' N	027° 16.729' W	565			DS2-18, ADCP mooring
MSM76_55-1	RO/CTD/ADC P	15.08.18 21:53	in the water	66° 02.696' N	028° 12.144' W	464			χ-pods attached
MSM76_55-1	RO/CTD/ADC P	15.08.18 22:09	max. depth	66° 02.599' N	028° 12.166' W	466	451	15	
MSM76_55-1	RO/CTD/ADC P	15.08.18 22:23	on deck	66° 02.457' N	028° 12.199' W	465			salt sampled
MSM76_56-1	RO/CTD/ADC P	15.08.18 23:19	in the water	65° 58.743' N	028° 06.223' W	470			χ-pods attached
MSM76_56-1	RO/CTD/ADC P	15.08.18 23:34	max. depth	65° 58.693' N	028° 06.152' W	474	463,3	15,7	

MSM76_56-1	RO/CTD/ADC P	15.08.18 23:52	on deck	65° 58.560' N	028° 05.856' W	480			salt and oxygen sampled
MSM76_57-1	RO/CTD/ADC P	16.08.18 00:28	in the water	65° 56.635' N	028° 02.916' W	522			χ-pods attached
MSM76_57-1	RO/CTD/ADC P	16.08.18 00:41	max. depth	65° 56.570' N	028° 02.770' W	523	510	15,7	
MSM76_57-1	RO/CTD/ADC P	16.08.18 00:57	on deck	65° 56.432' N	028° 02.485' W	525			
MSM76_58-1	RO/CTD/ADC P	16.08.18 01:30	in the water	65° 54.548' N	027° 59.627' W	571			χ-pods attached
MSM76_58-1	RO/CTD/ADC P	16.08.18 01:44	max. depth	65° 54.455' N	027° 59.402' W	576	563	14,6	
MSM76_58-1	RO/CTD/ADC P	16.08.18 02:02	on deck	65° 54.301' N	027° 59.082' W	581			salt and oxygen sampled
MSM76_59-1	RO/CTD/ADC P	16.08.18 02:41	in the water	65° 52.442' N	027° 56.359' W	619			χ-pods attached
MSM76_59-1	RO/CTD/ADC P	16.08.18 02:56	max. depth	65° 52.351' N	027° 56.170' W	630		17,1	
MSM76_59-1	RO/CTD/ADC P	16.08.18 03:13	on deck	65° 52.154' N	027° 55.760' W	634			
MSM76_60-1	RO/CTD/ADC P	16.08.18 03:44	in the water	65° 50.341' N	027° 53.100' W	682			χ-pods attached
MSM76_60-1	RO/CTD/ADC P	16.08.18 04:00	max. depth	65° 50.241' N	027° 52.876' W	685	674	17,9	
MSM76_60-1	RO/CTD/ADC P	16.08.18 04:19	on deck	65° 50.094' N	027° 52.878' W	689			salt and oxygen sampled
MSM76_61-1	RO/CTD/ADC P	16.08.18 04:46	in the water	65° 48.215' N	027° 49.785' W	732			χ-pods attached
MSM76_61-1	RO/CTD/ADC P	16.08.18 05:05	max. depth	65° 48.099' N	027° 49.855' W	734	723,9	15,6	
MSM76_61-1	RO/CTD/ADC P	16.08.18 05:26	on deck	65° 47.963' N	027° 49.944' W	734			salt sampled
MSM76_62-1	RO/CTD/ADC P	16.08.18 05:55	in the water	65° 46.095' N	027° 46.506' W	734			χ-pods attached

MSM76_62-1	RO/CTD/ADC	16.08.18 06:12	max. depth	65° 45.984' N	027° 46.550' W	735	726,6	
	P							
MSM76_62-1	RO/CTD/ADC	16.08.18 06:31	on deck	65° 45.851' N	027° 46.602' W	737		salt and oxygen sampled
	P							
MSM76_63-1	RO/CTD/ADC	16.08.18 07:10	in the water	65° 43.113' N	027° 43.325' W	670		χ-pods attached
	P							
MSM76_63-1	RO/CTD/ADC	16.08.18 07:26	max. depth	65° 43.114' N	027° 43.323' W	670	662,5	15
	P							
MSM76_63-1	RO/CTD/ADC	16.08.18 07:45	on deck	65° 43.114' N	027° 43.323' W	669		salt sampled
	P							
MSM76_64-1	RO/CTD/ADC	16.08.18 09:56	in the water	65° 35.842' N	028° 32.501' W	1027		χ-pods attached
	P							
MSM76_64-1	RO/CTD/ADC	16.08.18 10:21	max. depth	65° 35.843' N	028° 32.499' W	1029	1017	13
	P							
MSM76_64-1	RO/CTD/ADC	16.08.18 10:49	on deck	65° 35.843' N	028° 32.501' W	1028		salt and oxygen sampled
	P							
MSM76_65-1	RO/CTD/ADC	16.08.18 11:17	in the water	65° 38.676' N	028° 33.024' W	1055		χ-pods attached
	P							
MSM76_65-1	RO/CTD/ADC	16.08.18 11:42	max. depth	65° 38.676' N	028° 33.023' W	1054	1041	15,3
	P							
MSM76_65-1	RO/CTD/ADC	16.08.18 12:08	on deck	65° 38.677' N	028° 33.026' W	1055		salt sampled
	P							
MSM76_66-1	RO/CTD/ADC	16.08.18 12:42	in the water	65° 41.109' N	028° 33.803' W	997		χ-pods attached
	P							
MSM76_66-1	RO/CTD/ADC	16.08.18 13:04	max. depth	65° 41.110' N	028° 33.802' W	999	981	19
	P							
MSM76_66-1	RO/CTD/ADC	16.08.18 13:27	on deck	65° 41.110' N	028° 33.802' W	997		salt and oxygen sampled
	P							
MSM76_67-1	RO/CTD/ADC	16.08.18 13:59	in the water	65° 43.628' N	028° 34.771' W	919		χ-pods attached
	P							
MSM76_67-1	RO/CTD/ADC	16.08.18 14:18	max. depth	65° 43.629' N	028° 34.769' W	918	903	16,8
	P							
MSM76_67-1	RO/CTD/ADC	16.08.18 14:42	on deck	65° 43.628' N	028° 34.770' W	917		
	P							

MSM76_68-1	RO/CTD/ADC P	16.08.18 15:11	in the water	65° 46.095' N	028° 35.621' W	812				χ-pods attached
MSM76_68-1	RO/CTD/ADC P	16.08.18 15:30	max. depth	65° 46.099' N	028° 35.620' W	811	800	18,1		
MSM76_68-1	RO/CTD/ADC P	16.08.18 15:49	on deck	65° 45.987' N	028° 35.741' W	820				salt and oxygen sampled
MSM76_69-1	RO/CTD/ADC P	16.08.18 16:26	in the water	65° 48.558' N	028° 36.516' W	661				χ-pods attached
MSM76_69-1	RO/CTD/ADC P	16.08.18 16:43	max. depth	65° 48.496' N	028° 36.608' W	664	653,7	16,3		
MSM76_69-1	RO/CTD/ADC P	16.08.18 17:01	on deck	65° 48.391' N	028° 36.757' W	669				
MSM76_70-1	RO/CTD/ADC P	16.08.18 17:32	in the water	65° 51.035' N	028° 37.340' W	568				χ-pods attached
MSM76_70-1	RO/CTD/ADC P	16.08.18 17:46	max. depth	65° 50.994' N	028° 37.414' W	570	558,7	15,8		
MSM76_70-1	RO/CTD/ADC P	16.08.18 18:04	max. depth	65° 50.852' N	028° 37.653' W	571				salt and oxygen sampled
MSM76_71-1	RO/CTD/ADC P	16.08.18 18:36	in the water	65° 53.518' N	028° 38.197' W	506				χ-pods attached
MSM76_71-1	RO/CTD/ADC P	16.08.18 18:48	max. depth	65° 53.480' N	028° 38.272' W	506	490,1	15,6		
MSM76_71-1	RO/CTD/ADC P	16.08.18 19:04	on deck	65° 53.338' N	028° 38.545' W	510				
MSM76_72-1	RO/CTD/ADC P	16.08.18 19:37	in the water	65° 55.987' N	028° 39.066' W	451				χ-pods attached
MSM76_72-1	RO/CTD/ADC P	16.08.18 19:51	max. depth	65° 55.938' N	028° 39.166' W	451	439	16,6		
MSM76_72-1	RO/CTD/ADC P	16.08.18 20:05	on deck	65° 55.884' N	028° 39.507' W	457				salt and oxygen sampled
MSM76_73-1	RO/CTD/ADC P	16.08.18 20:51	in the water	66° 01.178' N	028° 40.803' W	382				χ-pods attached
MSM76_73-1	RO/CTD/ADC P	16.08.18 21:04	max. depth	66° 01.144' N	028° 40.929' W	383	367	14,5		

MSM76_73-1	RO/CTD/ADC P	16.08.18 21:18	on deck	66° 01.058' N	028° 41.257' W	384			
MSM76_74-1	RO/CTD/ADC P	16.08.18 23:23	in the water	65° 47.455' N	029° 11.826' W	403			χ-pods attached
MSM76_74-1	RO/CTD/ADC P	16.08.18 23:37	max. depth	65° 47.375' N	029° 12.112' W	396	396	16,4	
MSM76_74-1	RO/CTD/ADC P	16.08.18 23:54	on deck	65° 47.252' N	029° 12.577' W	418			salt and oxygen sampled
MSM76_75-1	RO/CTD/ADC P	17.08.18 00:28	in the water	65° 45.354' N	029° 08.682' W	587			χ-pods attached
MSM76_75-1	RO/CTD/ADC P	17.08.18 00:44	max. depth	65° 45.294' N	029° 08.866' W	586	574	17,2	
MSM76_75-1	RO/CTD/ADC P	17.08.18 01:03	on deck	65° 45.204' N	029° 09.144' W	588			
MSM76_76-1	RO/CTD/ADC P	17.08.18 01:35	in the water	65° 43.213' N	029° 05.755' W	746			χ-pods attached
MSM76_76-1	RO/CTD/ADC P	17.08.18 01:53	max. depth	65° 43.161' N	029° 05.887' W	746	734	18,2	
MSM76_76-1	RO/CTD/ADC P	17.08.18 02:15	on deck	65° 43.069' N	029° 06.119' W	746			salt and oxygen sampled
MSM76_77-1	RO/CTD/ADC P	17.08.18 02:46	in the water	65° 40.809' N	029° 03.395' W	854			χ-pods attached
MSM76_77-1	RO/CTD/ADC P	17.08.18 03:05	max. depth	65° 40.810' N	029° 03.403' W	853	844	16,5	
MSM76_77-1	RO/CTD/ADC P	17.08.18 03:28	on deck	65° 40.810' N	029° 03.397' W	855			
MSM76_78-1	RO/CTD/ADC P	17.08.18 04:04	in the water	65° 38.568' N	029° 00.523' W	950			χ-pods attached
MSM76_78-1	RO/CTD/ADC P	17.08.18 04:24	max. depth	65° 38.569' N	029° 00.524' W	950	940	17,5	
MSM76_78-1	RO/CTD/ADC P	17.08.18 04:49	on deck	65° 38.567' N	029° 00.523' W	950			salt and oxygen sampled
MSM76_79-1	RO/CTD/ADC P	17.08.18 05:14	in the water	65° 36.387' N	028° 57.795' W	1039			χ-pods attached

MSM76_90-1	RO/CTD/ADC P	17.08.18 21:47	on deck	65° 37.482' N	029° 39.800' W	369			salt and oxygen sampled
MSM76_91-1	RO/CTD/ADC P	17.08.18 22:13	in the water	65° 39.529' N	029° 43.349' W	337			χ-pods attached
MSM76_91-1	RO/CTD/ADC P	17.08.18 22:26	max. depth	65° 39.516' N	029° 43.384' W	339	326,3	15	
MSM76_91-1	RO/CTD/ADC P	17.08.18 22:40	on deck	65° 39.442' N	029° 43.613' W	337			
MSM76_92-1	RO/CTD/ADC P	17.08.18 23:23	in the water	65° 43.217' N	029° 50.383' W	313			χ-pods attached
MSM76_92-1	RO/CTD/ADC P	17.08.18 23:32	max. depth	65° 43.218' N	029° 50.385' W	312	302,7	15,4	
MSM76_92-1	RO/CTD/ADC P	17.08.18 23:46	on deck	65° 43.218' N	029° 50.385' W	312			salt and oxygen sampled
MSM76_93-1	RO/CTD/ADC P	18.08.18 00:33	in the water	65° 46.990' N	029° 58.351' W	354			χ-pods attached
MSM76_93-1	RO/CTD/ADC P	18.08.18 00:44	max. depth	65° 46.990' N	029° 58.351' W	354	354	15	
MSM76_93-1	RO/CTD/ADC P	18.08.18 00:58	on deck	65° 46.989' N	029° 58.354' W	354			
MSM76_94-1	RO/CTD/ADC P	18.08.18 03:06	in the water	65° 29.362' N	030° 14.347' W	382			χ-pods attached
MSM76_94-1	RO/CTD/ADC P	18.08.18 03:18	max. depth	65° 29.341' N	030° 14.368' W	384	375	15,6	
MSM76_94-1	RO/CTD/ADC P	18.08.18 03:32	on deck	65° 29.199' N	030° 14.362' W	386			salt and oxygen sampled
MSM76_95-1	RO/CTD/ADC P	18.08.18 04:14	in the water	65° 24.755' N	030° 09.513' W	741			χ-pods attached
MSM76_95-1	RO/CTD/ADC P	18.08.18 04:33	max. depth	65° 24.713' N	030° 09.388' W	747	737,1	15,6	
MSM76_95-1	RO/CTD/ADC P	18.08.18 04:55	on deck	65° 24.694' N	030° 09.421' W	747			
MSM76_96-1	RO/CTD/ADC P	18.08.18 05:22	in the water	65° 22.473' N	030° 07.150' W	904			χ-pods attached

MSM76_103-1	RO/CTD/ADC	18.08.18 23:32	surface	65° 30.086' N	029° 26.730' W	952		yoyo
	P							
MSM76_103-1	RO/CTD/ADC	18.08.18 23:53	max. depth	65° 30.060' N	029° 26.785' W	951	14,8	yoyo
	P							
MSM76_103-1	RO/CTD/ADC	19.08.18 00:14	surface	65° 30.036' N	029° 26.830' W	951		yoyo
	P							
MSM76_103-1	RO/CTD/ADC	19.08.18 00:34	max. depth	65° 30.035' N	029° 26.835' W	952	14,6	yoyo
	P							
MSM76_103-1	RO/CTD/ADC	19.08.18 00:54	surface	65° 30.020' N	029° 26.859' W	951		yoyo
	P							
MSM76_103-1	RO/CTD/ADC	19.08.18 01:15	max. depth	65° 30.018' N	029° 26.861' W	951	13,3	yoyo
	P							
MSM76_103-1	RO/CTD/ADC	19.08.18 01:34	surface	65° 30.019' N	029° 26.865' W	953		yoyo
	P							
MSM76_103-1	RO/CTD/ADC	19.08.18 01:54	max. depth	65° 30.018' N	029° 26.867' W	952	12,8	yoyo
	P							
MSM76_103-1	RO/CTD/ADC	19.08.18 02:12	surface	65° 30.018' N	029° 26.866' W	952		yoyo
	P							
MSM76_103-1	RO/CTD/ADC	19.08.18 02:35	max. depth	65° 30.018' N	029° 26.865' W	951	13,2	yoyo
	P							
MSM76_103-1	RO/CTD/ADC	19.08.18 02:55	surface	65° 30.019' N	029° 26.867' W	952		yoyo
	P							
MSM76_103-1	RO/CTD/ADC	19.08.18 03:17	max. depth	65° 30.019' N	029° 26.868' W	951	13,9	yoyo
	P							
MSM76_103-1	RO/CTD/ADC	19.08.18 03:36	surface	65° 30.019' N	029° 26.868' W	952		yoyo
	P							
MSM76_103-1	RO/CTD/ADC	19.08.18 03:58	max. depth	65° 30.019' N	029° 26.868' W	951	15,3	yoyo
	P							
MSM76_103-1	RO/CTD/ADC	19.08.18 04:20	surface	65° 30.019' N	029° 26.868' W	951		yoyo
	P							
MSM76_103-1	RO/CTD/ADC	19.08.18 04:39	max. depth	65° 30.019' N	029° 26.869' W	951	13,9	yoyo
	P							
MSM76_103-1	RO/CTD/ADC	19.08.18 05:01	surface	65° 30.024' N	029° 26.861' W	951		yoyo
	P							

MSM76_103-1	RO/CTD/ADC	19.08.18 05:21	max. depth	65° 30.079' N	029° 26.762' W	951	16,4	yoyo
	P							
MSM76_103-1	RO/CTD/ADC	19.08.18 05:43	surface	65° 30.104' N	029° 26.718' W	950		yoyo
	P							
MSM76_103-1	RO/CTD/ADC	19.08.18 06:05	max. depth	65° 30.141' N	029° 26.650' W	949	16,4	yoyo
	P							
MSM76_103-1	RO/CTD/ADC	19.08.18 06:26	surface	65° 30.141' N	029° 26.649' W	950		yoyo
	P							
MSM76_103-1	RO/CTD/ADC	19.08.18 06:46	max. depth	65° 30.140' N	029° 26.651' W	950	14,4	yoyo
	P							
MSM76_103-1	RO/CTD/ADC	19.08.18 07:06	surface	65° 30.141' N	029° 26.650' W	950		yoyo
	P							
MSM76_103-1	RO/CTD/ADC	19.08.18 07:30	max. depth	65° 30.141' N	029° 26.650' W	953	14,2	yoyo
	P							
MSM76_103-1	RO/CTD/ADC	19.08.18 07:52	surface	65° 30.146' N	029° 26.642' W	951		yoyo
	P							
MSM76_103-1	RO/CTD/ADC	19.08.18 08:12	max. depth	65° 30.153' N	029° 26.635' W	950	18,4	yoyo
	P							
MSM76_103-1	RO/CTD/ADC	19.08.18 08:32	surface	65° 30.153' N	029° 26.637' W	956		yoyo
	P							
MSM76_103-1	RO/CTD/ADC	19.08.18 08:56	max. depth	65° 30.154' N	029° 26.639' W	950	18,4	yoyo
	P							
MSM76_103-1	RO/CTD/ADC	19.08.18 09:15	surface	65° 30.136' N	029° 26.653' W	952		yoyo
	P							
MSM76_103-1	RO/CTD/ADC	19.08.18 09:39	max. depth	65° 30.135' N	029° 26.656' W	951	20,7	yoyo
	P							
MSM76_103-1	RO/CTD/ADC	19.08.18 09:58	surface	65° 30.111' N	029° 26.665' W	952		yoyo
	P							
MSM76_103-1	RO/CTD/ADC	19.08.18 10:21	max. depth	65° 30.111' N	029° 26.665' W	952	22,2	yoyo
	P							
MSM76_103-1	RO/CTD/ADC	19.08.18 10:40	surface	65° 30.071' N	029° 26.681' W	953		yoyo
	P							
MSM76_103-1	RO/CTD/ADC	19.08.18 11:05	max. depth	65° 30.063' N	029° 26.683' W	954	22,7	yoyo
	P							

MSM76_133-1	RO/CTD/ADC	23.08.18 12:55	max. depth	70° 22.409' N	021° 59.396' W	366	354	15,2	
	P								
MSM76_133-1	RO/CTD/ADC	23.08.18 13:09	on deck	70° 22.408' N	021° 59.397' W	365			
	P								
MSM76_134-1	RO/CTD/ADC	23.08.18 13:09	in the water	70° 22.408' N	021° 59.397' W	365			χ-pods attached
	P								
MSM76_134-1	RO/CTD/ADC	23.08.18 13:50	max. depth	70° 20.067' N	022° 00.665' W	445	431,2	18,4	
	P								
MSM76_134-1	RO/CTD/ADC	23.08.18 14:05	on deck	70° 20.066' N	022° 00.665' W	445			salt and oxygen sampled
	P								
MSM76_135-1	RO/CTD/ADC	23.08.18 14:37	in the water	70° 17.603' N	022° 01.972' W	544			χ-pods attached
	P								
MSM76_135-1	RO/CTD/ADC	23.08.18 14:51	max. depth	70° 17.607' N	022° 01.999' W	546	529,3	19,5	
	P								
MSM76_135-1	RO/CTD/ADC	23.08.18 15:07	on deck	70° 17.607' N	022° 01.998' W	548			
	P								
MSM76_136-1	RO/CTD/ADC	23.08.18 15:39	in the water	70° 15.146' N	022° 03.315' W	569			
	P								
MSM76_136-1	RO/CTD/ADC	23.08.18 15:52	max. depth	70° 15.148' N	022° 03.314' W	568	556	15,4	
	P								
MSM76_136-1	RO/CTD/ADC	23.08.18 16:09	on deck	70° 15.148' N	022° 03.314' W	568			salt and oxygen sampled
	P								
MSM76_137-1	RO/CTD/ADC	23.08.18 16:42	in the water	70° 12.680' N	022° 04.637' W	574			
	P								
MSM76_137-1	RO/CTD/ADC	23.08.18 16:57	max. depth	70° 12.681' N	022° 04.636' W	573	573,1	6,7	
	P								
MSM76_137-1	RO/CTD/ADC	23.08.18 17:13	on deck	70° 12.681' N	022° 04.636' W	574			
	P								
MSM76_138-1	RO/CTD/ADC	23.08.18 17:42	in the water	70° 10.219' N	022° 05.939' W	388			
	P								
MSM76_138-1	RO/CTD/ADC	23.08.18 17:52	max. depth	70° 10.219' N	022° 05.940' W	388	374	14,8	
	P								
MSM76_138-1	RO/CTD/ADC	23.08.18 18:06	on deck	70° 10.219' N	022° 05.938' W	388			salt and oxygen sampled
	P								
MSM76_139-1	MOOR	24.08.18 18:32	released	65° 50.901' N	027° 50.406' W				no depth information

MSM76_146-1	RO/CTD/ADC	25.08.18 01:45	in the water	65° 54.543' N	027° 59.643' W	575			χ-pods attached
	P								
MSM76_146-1	RO/CTD/ADC	25.08.18 02:01	max. depth	65° 54.543' N	027° 59.645' W	576	561	15,6	
	P								
MSM76_146-1	RO/CTD/ADC	25.08.18 02:18	on deck	65° 54.546' N	027° 59.776' W	574			salt and oxygen sampled
	P								
MSM76_147-1	RO/CTD/ADC	25.08.18 02:53	in the water	65° 56.653' N	028° 02.944' W	523			χ-pods attached
	P								
MSM76_147-1	RO/CTD/ADC	25.08.18 03:07	max. depth	65° 56.654' N	028° 02.992' W	521	511	14	
	P								
MSM76_147-1	RO/CTD/ADC	25.08.18 03:23	on deck	65° 56.655' N	028° 03.045' W	521			
	P								
MSM76_148-1	RO/CTD/ADC	25.08.18 03:55	in the water	65° 58.754' N	028° 06.235' W	471			χ-pods attached
	P								
MSM76_148-1	RO/CTD/ADC	25.08.18 04:07	max. depth	65° 58.753' N	028° 06.235' W	471	461,8	13	
	P								
MSM76_148-1	RO/CTD/ADC	25.08.18 04:27	on deck	65° 58.753' N	028° 06.236' W	472			salt and oxygen sampled
	P								
MSM76_149-1	RO/CTD/ADC	25.08.18 05:09	in the water	66° 02.738' N	028° 12.189' W	465			χ-pods attached
	P								
MSM76_149-1	RO/CTD/ADC	25.08.18 05:22	max. depth	66° 02.742' N	028° 12.170' W	464	451,9	13,2	
	P								
MSM76_149-1	RO/CTD/ADC	25.08.18 05:38	on deck	66° 02.742' N	028° 12.172' W	466			
	P								
MSM76_150-1	MOOR	25.08.18 07:20	course 005°	65° 57.019' N	028° 01.992' W	534			
MSM76_150-1	MOOR	25.08.18 07:46	begin dredging	65° 57.831' N	028° 01.820' W	526			
MSM76_150-1	MOOR	25.08.18 09:52	all on deck	65° 57.330' N	028° 01.925' W	532			
MSM76_150-1	MOOR	25.08.18 10:53	course 005°	65° 57.155' N	028° 01.977' W	536			
MSM76_150-1	MOOR	25.08.18 11:16	begin dredging	65° 57.846' N	028° 01.806' W	523			
MSM76_150-1	MOOR	25.08.18 13:05	all on deck	65° 57.655' N	028° 01.539' W	531			dredging of DS 26-17 unsuccessful
MSM76_151-1	MOOR	25.08.18 17:23	released	65° 33.503' N	029° 31.753' W				no depth information
MSM76_151-1	MOOR	25.08.18 17:29	at surface	65° 33.504' N	029° 31.751' W				
MSM76_151-1	MOOR	25.08.18 18:08	recovered	65° 32.236' N	029° 33.142' W				DS-B-18
MSM76_152-1	MOOR	25.08.18 18:31	released	65° 33.531' N	029° 30.621' W				no depth information

MSM76_152-1	MOOR	25.08.18 18:35	at surface	65° 33.530' N	029° 30.640' W		
MSM76_152-1	MOOR	25.08.18 18:47	recovered	65° 33.760' N	029° 30.376' W		DS-F-18
MSM76_153-1	MOOR	25.08.18 19:27	released	65° 31.817' N	029° 18.085' W		no depth information
MSM76_153-1	MOOR	25.08.18 19:33	at surface	65° 31.833' N	029° 18.162' W		
MSM76_153-1	MOOR	25.08.18 20:25	recovered	65° 32.473' N	029° 18.558' W	970	DS-D-18
MSM76_154-1	RO/CTD/ADC	25.08.18 22:49	in the water	65° 13.305' N	029° 56.067' W	1454	χ-pods attached
	P						
MSM76_154-1	RO/CTD/ADC	25.08.18 23:19	max. depth	65° 13.275' N	029° 56.165' W	1456	Tow-Yo, course 244° v=0,5kn
	P						
MSM76_154-1	RO/CTD/ADC	26.08.18 01:16	information	65° 12.838' N	029° 58.241' W	1451	Tow-Yo, course 248° v=0,5kn
	P						
MSM76_154-1	RO/CTD/ADC	26.08.18 03:16	information	65° 12.457' N	030° 00.431' W	1347	Tow-Yo, course 272° v=0,5kn
	P						
MSM76_154-1	RO/CTD/ADC	26.08.18 05:01	information	65° 12.487' N	030° 02.497' W	1454	Tow-Yo, course 270° v=0,5kn
	P						
MSM76_154-1	RO/CTD/ADC	26.08.18 07:09	profile end	65° 12.488' N	030° 05.004' W	1445	
	P						
MSM76_154-1	RO/CTD/ADC	26.08.18 07:40	on deck	65° 12.532' N	030° 05.461' W	1450	
	P						
MSM76_155-1	MOOR	26.08.18 10:38	released	65° 28.053' N	029° 34.391' W		no depth information
MSM76_155-1	MOOR	26.08.18 10:42	at surface	65° 28.053' N	029° 34.492' W		
MSM76_155-1	MOOR	26.08.18 11:19	recovered	65° 28.843' N	029° 36.570' W		DS-E-18
MSM76_156-1	MOOR	26.08.18 11:38	released	65° 27.820' N	029° 34.800' W		no depth information
MSM76_156-1	MOOR	26.08.18 11:45	at surface	65° 27.814' N	029° 35.064' W		
MSM76_156-1	MOOR	26.08.18 12:00	recovered	65° 28.367' N	029° 36.023' W		DS-A-18
MSM76_157-1	MOOR	26.08.18 12:57	released	65° 26.963' N	029° 19.810' W		no depth information
MSM76_157-1	MOOR	26.08.18 13:12	at surface	65° 26.974' N	029° 19.842' W		
MSM76_157-1	MOOR	26.08.18 13:50	recovered	65° 27.642' N	029° 21.191' W		DS-C-18
MSM76_158-1	RO/CTD/ADC	26.08.18 16:07	in the water	65° 11.163' N	029° 59.185' W	1563	χ-pods attached
	P						
MSM76_158-1	RO/CTD/ADC	26.08.18 16:38	max. depth	65° 11.169' N	029° 59.192' W	1564	Tow-Yo, course 337° v=0,5kn
	P						
MSM76_158-1	RO/CTD/ADC	26.08.18 20:35	information	65° 12.989' N	030° 01.008' W	1421	Tow-Yo, course 335° v=0,5kn
	P						

MSM76_176-1	RO/CTD/ADC	03.09.18 10:55	in the water	79° 40.585' N	017° 02.905' W	241		
	P							
MSM76_176-1	RO/CTD/ADC	03.09.18 11:06	max. depth	79° 40.585' N	017° 02.901' W	241	228	14,6
	P							
MSM76_176-1	RO/CTD/ADC	03.09.18 11:19	on deck	79° 40.585' N	017° 02.901' W	241		
	P							
MSM76_177-1	RO/CTD/ADC	03.09.18 11:47	in the water	79° 40.375' N	016° 53.794' W	265		
	P							
MSM76_177-1	RO/CTD/ADC	03.09.18 11:57	max. depth	79° 40.375' N	016° 53.789' W	265	252	16,2
	P							
MSM76_177-1	RO/CTD/ADC	03.09.18 12:09	on deck	79° 40.375' N	016° 53.791' W	265		
	P							
MSM76_178-1	EM122	03.09.18 13:33	profile start	79° 41.029' N	017° 41.102' W	399		v= 10kn
MSM76_178-1	EM122	03.09.18 17:28	profile end	79° 40.378' N	016° 57.211' W	265		
MSM76_179-1	MOOR	03.09.18 17:41	start	79° 40.183' N	016° 53.848' W	263		
MSM76_179-1	MOOR	03.09.18 18:04	deployed	79° 40.159' N	016° 53.876' W	262		79N6-2
MSM76_180-1	RO/CTD/ADC	03.09.18 19:19	in the water	79° 38.352' N	016° 38.451' W	242		
	P							
MSM76_180-1	RO/CTD/ADC	03.09.18 19:31	max. depth	79° 38.351' N	016° 38.451' W	242	231	13
	P							
MSM76_180-1	RO/CTD/ADC	03.09.18 19:43	on deck	79° 38.351' N	016° 38.449' W	241		salt and oxygen sampled
	P							
MSM76_181-1	RO/CTD/ADC	03.09.18 21:07	in the water	79° 36.735' N	016° 23.900' W	281		
	P							
MSM76_181-1	RO/CTD/ADC	03.09.18 21:19	max. depth	79° 36.731' N	016° 23.880' W	281	269,4	15,3
	P							
MSM76_181-1	RO/CTD/ADC	03.09.18 21:34	on deck	79° 36.734' N	016° 23.904' W	281		
	P							
MSM76_182-1	RO/CTD/ADC	04.09.18 01:53	in the water	79° 55.681' N	015° 45.833' W	301		
	P							
MSM76_182-1	RO/CTD/ADC	04.09.18 02:06	max. depth	79° 55.682' N	015° 45.834' W	301	291	14,4
	P							
MSM76_182-1	RO/CTD/ADC	04.09.18 02:16	on deck	79° 55.682' N	015° 45.833' W	301		salt and oxygen sampled
	P							

MSM76_183-1	RO/CTD/ADC	04.09.18 06:35	in the water	80° 04.697' N	014° 11.998' W	128		
	P							
MSM76_183-1	RO/CTD/ADC	04.09.18 06:40	max. depth	80° 04.697' N	014° 11.997' W	128	117,6	14,4
	P							
MSM76_183-1	RO/CTD/ADC	04.09.18 06:49	on deck	80° 04.697' N	014° 11.998' W	128		
	P							
MSM76_184-1	RO/CTD/ADC	04.09.18 10:08	in the water	80° 03.314' N	012° 15.881' W	134		
	P							
MSM76_184-1	RO/CTD/ADC	04.09.18 10:15	max. depth	80° 03.315' N	012° 15.882' W	134	120,9	14,3
	P							
MSM76_184-1	RO/CTD/ADC	04.09.18 10:24	on deck	80° 03.314' N	012° 15.882' W	134		salt and oxygen sampled
	P							
MSM76_185-1	RO/CTD/ADC	04.09.18 13:23	in the water	79° 54.454' N	010° 32.435' W	113		
	P							
MSM76_185-1	RO/CTD/ADC	04.09.18 13:29	max. depth	79° 54.454' N	010° 32.434' W	113	102,6	14,8
	P							
MSM76_185-1	RO/CTD/ADC	04.09.18 13:38	on deck	79° 54.454' N	010° 32.435' W	113		
	P							
MSM76_186-1	RO/CTD/ADC	04.09.18 15:36	in the water	79° 46.188' N	008° 51.339' W	186		
	P							
MSM76_186-1	RO/CTD/ADC	04.09.18 15:44	max. depth	79° 46.188' N	008° 51.334' W	185	173	14,7
	P							
MSM76_186-1	RO/CTD/ADC	04.09.18 15:54	on deck	79° 46.188' N	008° 51.334' W	185		salt and oxygen sampled
	P							
MSM76_187-1	RO/CTD/ADC	04.09.18 17:32	in the water	79° 36.698' N	007° 22.792' W	230		
	P							
MSM76_187-1	RO/CTD/ADC	04.09.18 17:41	max. depth	79° 36.707' N	007° 22.777' W	229	218,8	14,6
	P							
MSM76_187-1	RO/CTD/ADC	04.09.18 17:51	on deck	79° 36.707' N	007° 22.776' W	229		
	P							
MSM76_188-1	RO/CTD/ADC	04.09.18 20:02	in the water	79° 21.810' N	006° 15.280' W	271		
	P							
MSM76_188-1	RO/CTD/ADC	04.09.18 20:12	max. depth	79° 21.810' N	006° 15.280' W	271	261	14,7
	P							

MSM76_208-1	RO/CTD/ADC	07.09.18 21:32	max. depth	79° 00.107' N	005° 18.349' E	2269	2252	14,5	
	P								
MSM76_208-1	RO/CTD/ADC	07.09.18 22:20	on deck	79° 00.248' N	005° 17.958' E	2253			salt and oxygen sampled
	P								
MSM76_209-1	RO/CTD/ADC	07.09.18 23:05	in the water	79° 00.044' N	005° 44.563' E	2033			
	P								
MSM76_209-1	RO/CTD/ADC	07.09.18 23:46	max. depth	79° 00.049' N	005° 44.581' E	2041	2024,2	13,2	
	P								
MSM76_209-1	RO/CTD/ADC	08.09.18 00:27	on deck	79° 00.049' N	005° 44.582' E	2038			
	P								
MSM76_210-1	RO/CTD/ADC	08.09.18 01:14	in the water	79° 00.012' N	006° 10.943' E	1681			
	P								
MSM76_210-1	RO/CTD/ADC	08.09.18 01:49	max. depth	79° 00.012' N	006° 10.941' E	1678	1662	12,5	
	P								
MSM76_210-1	RO/CTD/ADC	08.09.18 02:25	on deck	79° 00.012' N	006° 10.941' E	1681			salt and oxygen sampled
	P								
MSM76_211-1	RO/CTD/ADC	08.09.18 03:19	in the water	79° 00.011' N	006° 37.154' E	1322			
	P								
MSM76_211-1	RO/CTD/ADC	08.09.18 03:45	max. depth	79° 00.011' N	006° 37.153' E	1323	1310,2	13,8	
	P								
MSM76_211-1	RO/CTD/ADC	08.09.18 04:16	on deck	79° 00.011' N	006° 37.154' E	1326			
	P								
MSM76_212-1	RO/CTD/ADC	08.09.18 04:42	in the water	79° 00.011' N	006° 50.239' E	1237			
	P								
MSM76_212-1	RO/CTD/ADC	08.09.18 05:09	max. depth	79° 00.011' N	006° 50.237' E	1231	1217	14,8	
	P								
MSM76_212-1	RO/CTD/ADC	08.09.18 05:40	on deck	79° 00.011' N	006° 50.232' E	1228			salt and oxygen sampled
	P								
MSM76_213-1	MOOR	08.09.18 07:04	start	78° 59.985' N	005° 40.079' E	2091			
MSM76_213-1	MOOR	08.09.18 08:16	deployed	78° 59.985' N	005° 40.079' E	2091			F5-18
MSM76_214-1	MOOR	08.09.18 09:36	start	79° 10.010' N	006° 20.009' E	1413			
MSM76_214-1	MOOR	08.09.18 10:23	deployed	79° 09.985' N	006° 19.982' E	1414			F4-OZA, 100 m too long, mooring released again
MSM76_214-1	MOOR	08.09.18 13:03	released	79° 10.163' N	006° 21.770' E				no depth information
MSM76_214-1	MOOR	08.09.18 13:04	at surface	79° 10.159' N	006° 21.812' E				

MSM76_226-1	RO/CTD/ADC	09.09.18 15:39	on deck	80° 00.042' N	002° 44.996' E	2597		
	P							
MSM76_227-1	RO/CTD/ADC	09.09.18 15:57	in the water	80° 00.042' N	002° 44.995' E	2598		MicroCATs attached
	P							
MSM76_227-1	RO/CTD/ADC	09.09.18 16:27	max. depth	80° 00.042' N	002° 44.994' E		1497	no depth information, lowering only to 1500 m
	P							
MSM76_227-1	RO/CTD/ADC	09.09.18 17:10	on deck	80° 00.042' N	002° 44.993' E	2596		
	P							
MSM76_228-1	RO/CTD/ADC	09.09.18 18:17	in the water	79° 50.040' N	002° 45.058' E	3490		lowering only to 800 m
	P							
MSM76_228-1	RO/CTD/ADC	09.09.18 18:34	max. depth	79° 50.040' N	002° 45.059' E	3481	797	
	P							
MSM76_228-1	RO/CTD/ADC	09.09.18 18:51	on deck	79° 50.040' N	002° 45.054' E	3490		
	P							
MSM76_229-1	RO/CTD/ADC	09.09.18 19:59	in the water	79° 40.073' N	002° 45.078' E	3160		lowering only to 800 m
	P							
MSM76_229-1	RO/CTD/ADC	09.09.18 20:16	max. depth	79° 40.073' N	002° 45.073' E	3161	800,5	
	P							
MSM76_229-1	RO/CTD/ADC	09.09.18 20:34	on deck	79° 40.074' N	002° 45.071' E	3150		
	P							
MSM76_230-1	RO/CTD/ADC	09.09.18 21:37	in the water	79° 30.072' N	002° 45.159' E	2796		lowering only to 800 m
	P							
MSM76_230-1	RO/CTD/ADC	09.09.18 21:56	max. depth	79° 30.066' N	002° 45.195' E	2794	798,4	
	P							
MSM76_230-1	RO/CTD/ADC	09.09.18 22:14	on deck	79° 30.067' N	002° 45.188' E	2799		
	P							
MSM76_231-1	RO/CTD/ADC	09.09.18 23:23	in the water	79° 20.079' N	002° 44.985' E	2807		lowering only to 800 m
	P							
MSM76_231-1	RO/CTD/ADC	09.09.18 23:41	max. depth	79° 20.071' N	002° 45.022' E	2811	797,1	
	P							
MSM76_231-1	RO/CTD/ADC	09.09.18 23:59	on deck	79° 20.073' N	002° 45.017' E	2806		
	P							
MSM76_232-1	RO/CTD/ADC	10.09.18 01:08	in the water	79° 10.059' N	002° 45.233' E	5482		lowering only to 800 m
	P							

MSM76_232-1	RO/CTD/ADC	10.09.18 01:26	max. depth	79° 10.069' N	002° 45.052' E	5482	797,9	
	P							
MSM76_232-1	RO/CTD/ADC	10.09.18 01:46	on deck	79° 10.068' N	002° 45.057' E	5484		
	P							
MSM76_233-1	RO/CTD/ADC	10.09.18 02:56	in the water	79° 00.079' N	002° 45.047' E	2383		lowering only to 800 m
	P							
MSM76_233-1	RO/CTD/ADC	10.09.18 03:14	max. depth	79° 00.079' N	002° 45.046' E	2400	797,7	
	P							
MSM76_233-1	RO/CTD/ADC	10.09.18 03:33	on deck	79° 00.079' N	002° 45.047' E	2403		
	P							
MSM76_234-1	RO/CTD/ADC	10.09.18 04:36	in the water	78° 50.091' N	002° 45.040' E	2446		lowering only to 800 m
	P							
MSM76_234-1	RO/CTD/ADC	10.09.18 04:52	max. depth	78° 50.091' N	002° 45.034' E	2446	796,7	
	P							
MSM76_234-1	RO/CTD/ADC	10.09.18 05:11	on deck	78° 50.091' N	002° 45.021' E	2446		
	P							
MSM76_235-1	RO/CTD/ADC	10.09.18 06:03	in the water	78° 40.285' N	002° 45.410' E	2534		lowering only to 800 m
	P							
MSM76_235-1	RO/CTD/ADC	10.09.18 06:35	max. depth	78° 40.101' N	002° 45.027' E	2534	797	
	P							
MSM76_235-1	RO/CTD/ADC	10.09.18 06:54	on deck	78° 40.101' N	002° 45.028' E	2534		
	P							
MSM76_236-1	RO/CTD/ADC	10.09.18 08:03	in the water	78° 30.124' N	002° 44.981' E	2405		lowering only to 800 m
	P							
MSM76_236-1	RO/CTD/ADC	10.09.18 08:21	max. depth	78° 30.125' N	002° 44.950' E	2406	794,4	
	P							
MSM76_236-1	RO/CTD/ADC	10.09.18 08:40	on deck	78° 30.125' N	002° 44.949' E	2405		
	P							
MSM76_237-1	RO/CTD/ADC	10.09.18 09:52	in the water	78° 20.137' N	002° 44.931' E	2838		lowering only to 800 m
	P							
MSM76_237-1	RO/CTD/ADC	10.09.18 10:11	max. depth	78° 20.137' N	002° 44.936' E	2837	800	
	P							
MSM76_237-1	RO/CTD/ADC	10.09.18 10:31	on deck	78° 20.137' N	002° 44.935' E	2837		
	P							

MSM76_238-1	RO/CTD/ADC	10.09.18 11:41	in the water	78° 10.134' N	002° 44.988' E	2882			lowering only to 800 m
	P								
MSM76_238-1	RO/CTD/ADC	10.09.18 11:59	max. depth	78° 10.110' N	002° 44.964' E	2883	799,5		
	P								
MSM76_238-1	RO/CTD/ADC	10.09.18 12:17	on deck	78° 10.110' N	002° 44.965' E	2885			
	P								
MSM76_239-1	RO/CTD/ADC	10.09.18 13:25	in the water	78° 00.014' N	002° 44.951' E	2995			
	P								
MSM76_239-1	RO/CTD/ADC	10.09.18 14:19	max. depth	78° 00.010' N	002° 44.964' E	2992	2992,5	15,9	
	P								
MSM76_239-1	RO/CTD/ADC	10.09.18 15:28	on deck	78° 00.010' N	002° 44.964' E	2992			
	P								

8. Data and Sample Storage and Availability

Data will be processed and stored at AWI and Universities of Delaware. Data processed from the several types of investigation will be differently time-consuming. Until the post processed data is available, the preliminary data will be available to the cruise participants and external users after request to the senior scientist. The finally processed data will be submitted to the PANGAEA data library. The unrestricted availability from PANGAEA will depend on the required time and effort for processing of individual datasets and its status of scientific publication. Data will preferably be published in open access journals.

Table 8.1: Overview of data availability

Type	Database	Available	Free Access	Contact
Lowered CTD	PANGAEA	Now	Sept. 2021	torsten.kanzow@awi.de
LADCP	PANGAEA	Now	Sept. 2021	torsten.kanzow@awi.de
SADCP	PANGAEA	Now	Sept. 2021	torsten.kanzow@awi.de
Moored CTD and ADCP	PANGAEA	Now	Sept. 2022	torsten.kanzow@awi.de
Bathymetrie	PANGAEA	Now	Sept. 2022	torsten.kanzow@awi.de

9. Acknowledgements

We would like to thank Captain Ralf Schmidt his crew for their hospitality, trusting collaboration and the great atmosphere on board. We are making contributions to and received funding by the following programmes:

- RACE II (BMBF, PI K. Jochumsen)
- NAACLIM (EU, PI K. Jochumsen)
- Project T3 (Energy Transfers in Gravity Plumes) within TRR 181 (DFG, PI T. Kanzow)
- Project OGreen within SPP Regional Sea Level Change (DFG, PI T. Kanzow)
- Frontiers in Arctic Marine Monitoring (FRAM, HGF, W. von Appen)
- Greenland Ice Sheet-Ocean Interaction (GROCE, BMBF, PI T. Kanzow)

10. Reference List

Håvik, L., K. Våge, R.S. Pickart, B. Harden, W.-J. von Appen, S. Jónsson, and S. Østerhus, 2017: Structure and variability of the shelfbreak East Greenland Current north of Denmark Strait. *J. Phys. Oceanogr.*, 47, 2631-2646.

Hessner, K., El Naggar, S., Strass, V., Krägefsky, S., & Witte, H. (2017). Evaluation of X-band MR surface and ADCP subsurface currents obtained onboard the German research vessel Polarstern during ANT-XXXI expedition 2015/16. *Oceans*.

Hessner, K., El Naggar, S., von Appen, W., & Strass, V. (2018). WaMoS II: Radar-based measurements of surface waves and currents. *OceanWaveS, Wave Monitoring System: Operating Manual and Installation Guide*. Lüneburg: OceanWaveS.

Joyce, T.M., 1989: On the in situ calibration of shipboard ADCP. *J. Atmosph. Ocean. Tech.*, 6, 169-172.

Kanzow, T., Send, U., Zenk, W., Rhein, M., Chave, A., 2006. Monitoring the deep integrated meridional flow in the tropical North Atlantic: Long-term performance of a geostrophic array. *Deep-Sea Res. I*, 53 (3), 528-546

Münchow, A., K.K. Falkner, and H. Melling, 2007: Spatial continuity of measured seawater and tracer flux through Nares Strait, a dynamically wide channel bordering the Canadian Archipelago. *J. Mar. Res.*, 65, 759-788.

Pickart, R.S., M.A. Spall, D.J. Torres, K. Våge, H. Valdimarsson, C. Nobre, G.W.K. Moore, S. Jónsson, and D. Mastropole, 2017: The North Icelandic Jet and its relationship to the North Icelandic Irminger Current. *J. Mar. Res.*, 75, 605-639.

Press, W.H., S.A. Teukolsky, W.T. Vetterling, and B.P. Flannery, 2007. *Numerical Recipes 3d edition: The Art of Scientific Computing*. Cambridge University Press, Cambridge, UK, 1256 pp.